Earth-Science Reviews 232 (2022) 104099

Contents lists available at ScienceDirect

Earth-Science Reviews

journal homepage: www.elsevier.com/locate/earscirev

# The Triassic–Jurassic transition – A review of environmental change at the dawn of modern life

ARTICLE INFO

*Keywords*
Large Igneous Provinces
anoxia, euxinia
Warming
Extinction
Toarcian
Paleoceanography

ABSTRACT

The Triassic–Jurassic transition, which is here broadly defined as extending from the Late Triassic through the Early Jurassic (~237 Ma to 174 Ma), was an important interval in Earth history. The end-Triassic mass extinction (ETME), at ~201 Ma, ranks among the 'Big Five' Phanerozoic mass extinctions. It largely completed the shift from the 'Paleozoic Evolutionary Fauna' to the 'Modern Evolutionary Fauna' that had been initiated by the end-Permian mass extinction, and may have contributed to the 'Mesozoic Marine Revolution' and rise of dinosaurs to dominance in terrestrial environments. In addition, the Triassic–Jurassic transition encompasses a second-order mass extinction during the early Toarcian oceanic anoxic event (T-OAE), at ~181 Ma. The ETME was triggered by Central Atlantic Magmatic Province (CAMP) magmatism, and the T-OAE by Karoo-Ferrar Large Igneous Province (KFLIP) magmatism, both associated with the stepwise disintegration of the Pangean supercontinent. These events led to major changes in continental and marine habitats, including climatic warming, ocean acidification, and widespread watermass anoxia, that produced a cascade of lethal environmental stresses. This article undertakes a review of the ETME and T-OAE mass extinctions, the large igneous province eruptions that triggered those biotic events, and the web of environmental changes that linked them together.

## 1. Introduction

The Triassic–Jurassic (Tr-J) transition, broadly defined as extending from the Late Triassic through the Early Jurassic (~237 Ma to 174 Ma), was a critical interval in Earth history from multiple perspectives. The end-Triassic mass extinction (ETME), at ~201 Ma, was one of the 'Big Five' Phanerozoic mass extinctions (Raup and Sepkoski, 1982; Bambach, 2006), variably ranked 3rd or 4th in absolute magnitude. Although the shift from the 'Paleozoic Evolutionary Fauna' to the 'Modern Evolutionary Fauna' (cf. Sepkoski, 1981; Alroy, 2010) was initiated by the earlier end-Permian mass extinction (Erwin et al., 2002), the ETME cleaned out many of the lingering lineages of the Paleozoic Fauna, such as conodonts, conulariids, and several orders of brachiopods, setting the stage for a fuller transition to modern marine communities (Vermeij, 1977; Harper, 2003). Roughly 20 million years later (~181 Ma), Early Jurassic marine communities experienced a further, second-order extinction associated with the early Toarcian oceanic anoxic event (T-OAE) (Harries and Little, 1999). These two episodes of biotic turnover represent the closing chapters of what Wignall (2015) identified as the "the worst of times" in the Phanerozoic – the interval from the Middle Permian through the Early Jurassic during which the continental landmasses of Earth were assembled into the Pangean supercontinent, and large flood basalt eruptions predictably triggered global extinction events. (See Figs. 1–3.)

The studies in this special issue of *Earth-Science Reviews* span both major episodes of environmental disturbance: the end-Triassic mass extinction, which is strongly associated with emplacement of the Central Atlantic Magmatic Province (CAMP) (Marzoli et al., 1999), and the Toarcian Ocean Anoxic Event (T-OAE), which has been linked to the Karoo-Ferrar Large Igneous Province (KFLIP) (Pálfy and Smith, 2000). In recent years, much progress has been made in understanding the distribution of large igneous provinces in space and time (Ernst and Youbi, 2017) and their relationships to continental and marine environmental changes and to mass extinctions (Bond and Grasby, 2017). By covering both events as well as the intervening ~20-Myr time interval in a single volume, we intend to focus on their relationship to the contemporaneous, progressive breakup of Pangea. The papers in this volume apply a variety of paleontological, geochemical, and sedimentological approaches to marine and terrestrial environments across the globe. We hope that by considering them together, we can contribute to a more holistic assessment of this fascinating era of Earth history.

## 2. Framework of Triassic–Jurassic transition

### 2.1. Timescale

The time scale of the Triassic–Jurassic (Tr-J) transition has been refined in a series of recent publications (Ogg, 2012; Ogg and Hinnov, 2012; Kent et al., 2017; Lucas, 2018a; Ogg et al., 2020). The Late Triassic ranges from 237.0 Ma to 201.3 Ma and consists of the Carnian, Norian, and Rhaetian stages. The Early Jurassic ranges from 201.3 Ma to 174.1 Ma and consists of the Hettangian, Sinemurian, Pliensbachian, and Toarcian stages. The base of the Jurassic, and thus the Triassic–Jurassic boundary (TJB), has now been defined based on the first occurrence of the ammonite *Psiloceras spelae tirolicum* (von Hillebrandt et al., 2007, 2013). The Kuhjoch section, in the western Tethys Eiberg Basin, was

https://doi.org/10.1016/j.earscirev.2022.104099
Received 4 August 2021; Received in revised form 21 June 2022; Accepted 24 June 2022
Available online 2 July 2022

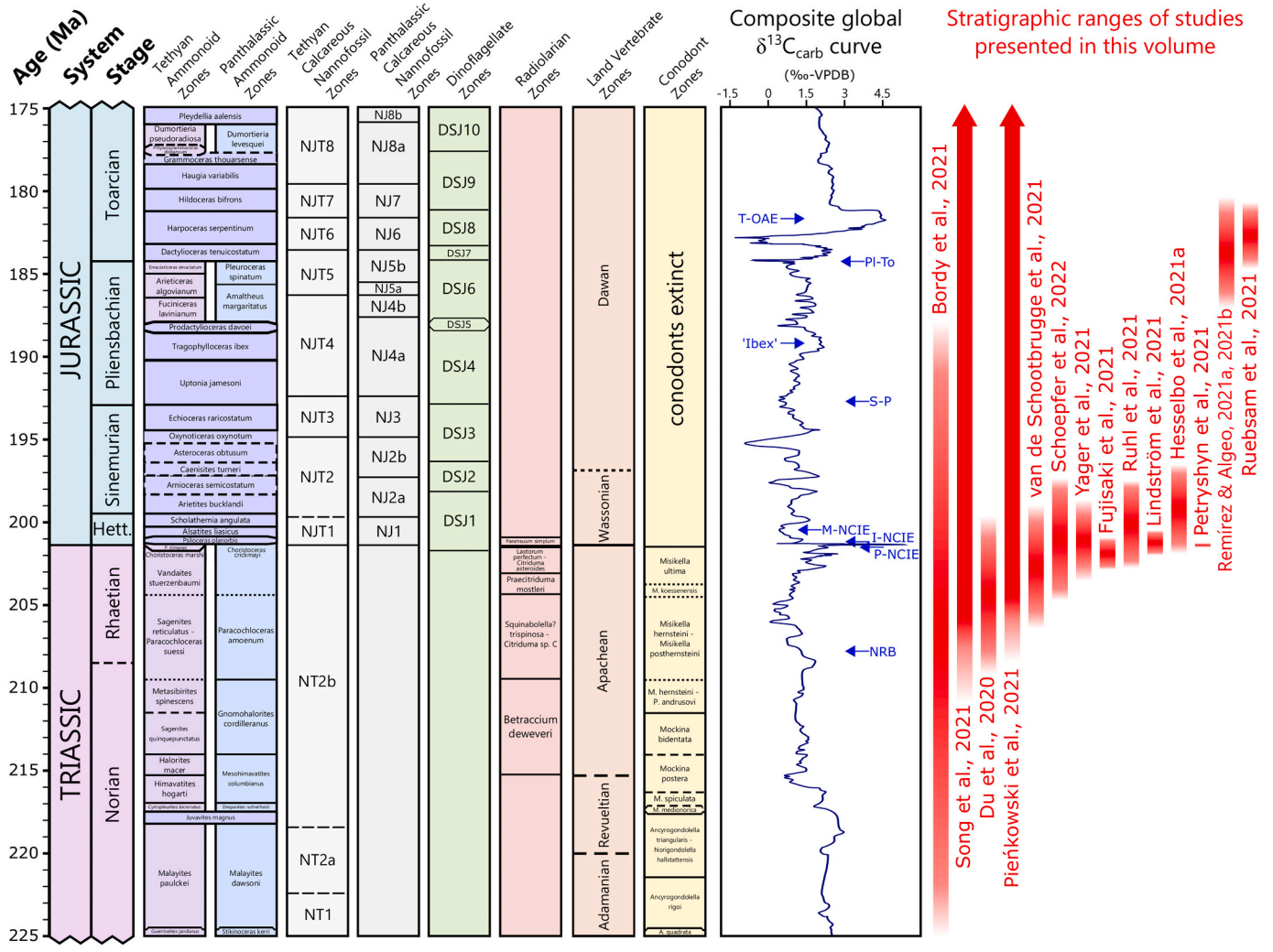


**Fig. 1.** Stratigraphic column with biostratigraphic and geochronologic data from 225 to 175 Ma. All stage boundary ages are from the Geologic Timescale 2020 (GTS20; Gradstein et al., 2020), except for the Norian-Rhaetian boundary which follows the latest date given by the International Commission on Stratigraphy (Cohen et al., 2022; <stratigraphy.org>). All biostratigraphic zonation schemes and the composite $\delta^{13}C_{carb}$ curve are from GTS20. Stratigraphic intervals of the 15 studies included the present special issue are shown.

chosen as the Global Stratotype Section and Point (GSSP) for this boundary, which is located approximately 6 m stratigraphically above the onset of the end-Triassic marine extinction (ETME). The age of the ETME can be determined by extrapolation from radioisotopically dated flood basalts overlying the ETME interval, with estimated ages for the onset of the extinction ranging from 201.51 ± 0.15 Ma (Wotzlaw et al., 2014) to 201.564 ± 0.015 Ma (Blackburn et al., 2013).

The refinement of the Tr-J transition timescale has been facilitated by recent biostratigraphic studies of many fossil groups. Key studies include analyses or syntheses of ammonoids (Balini et al., 2010; Jenks et al., 2015; Lucas, 2018b), conodonts (Rigo et al., 2018), radiolarians (O'Dogherty et al., 2010; Onoue et al., 2017), and vertebrates (Lucas, 2010; Olsen et al., 2010) for the Late Triassic, and of ammonoids (Hesselbo et al., 2000; von Hillebrandt and Krystyn, 2009; von Hillebrandt and Kment, 2015), radiolarians (Carter et al., 2010; Goričan et al., 2013; Onoue et al., 2017), and calcareous nannofossils (Ferreira et al., 2019) for the Early Jurassic.

Organic carbon isotope chemostratigraphy has proven to be an essential tool for global correlations. Three pronounced negative carbon isotopic excursions (NCIEs), herein referred to as the "precursor" (P-NCIE), "initial"(I-NCIE) and "main" (M-NCIE) in stratigraphic order, have been documented in Tr-J transition sections across Europe and the peri-Tethyan region (Pálfy et al., 2001, 2007; Hesselbo et al., 2002; Guex et al., 2004; Kürschner et al., 2007; Ruhl et al., 2009; Ruhl and Kürschner, 2011; Korte et al., 2018; Zaffani et al., 2018). Three, possibly correlative, negative carbon isotope excursions have been recognized in the Katsuyama section of central Japan (Fujisaki et al., 2018). In general, the three distinct excursions are not as easily recognized in Panthalassic sections (Ward et al., 2001, 2004, 2007; Williford et al., 2007; Lindström et al., 2021). Furthermore, carbon isotope excursions (especially in shallow peri-Tethyan sections) may have been influenced by changes in facies (Fox et al., 2020), causing ongoing difficulties in interregional correlation. Comprehensive correlations of key TJB successions have made use of a combination of biostratigraphic (palynology and ammonites), geochemical ($\delta^{13}C_{org}$), and radioisotopic (U/Pb ages) constraints (Lindström et al., 2017b, 2021; Du et al., 2020, see Appendix). Global correlations have been further refined through magnetostratigraphic studies of some Upper Triassic (Muttoni et al., 2004, 2010), TJB (Sciscio et al., 2017), and Lower Jurassic stratigraphic sections (Xu et al., 2018) as well as for the Karoo flood basalts (Moulin et al., 2011).

The highest temporal resolutions, in some cases better than 100 kyr, have been achieved through generation of astronomical time scales (ATSs) based on proxy records from both continental and marine successions that contain orbital periodicities (Muttoni et al., 2004; Huang and Hesselbo, 2014; Ikeda and Hori, 2014; Ruhl et al., 2016; Kent et al., 2017; Li et al., 2017; Ait-Itto et al., 2018; Storm et al., 2020). In

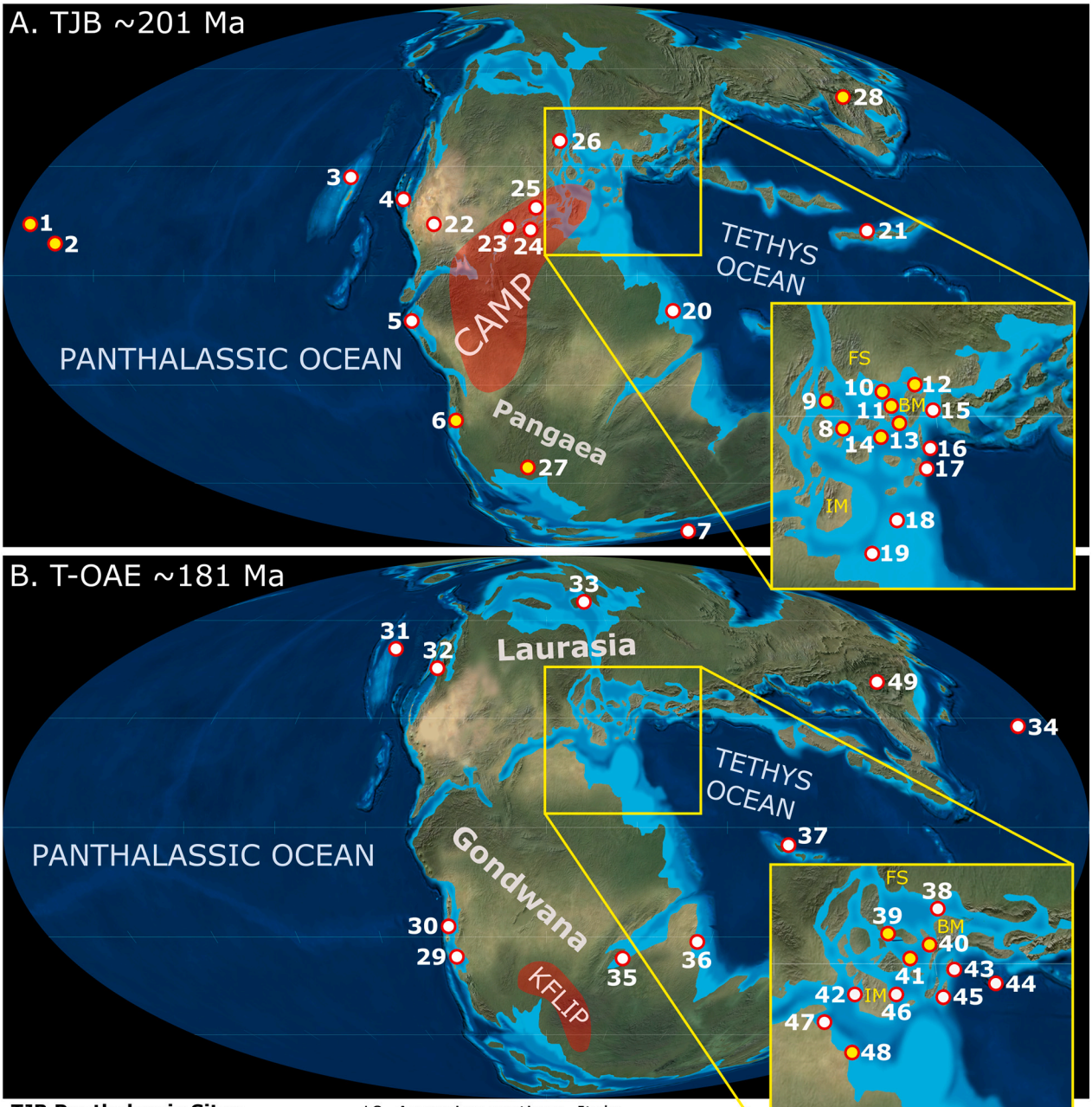


**TJB Panthalassic Sites**
1. Kurusu, Japan
2. Katsuyama, Japan
3. Kennecott Point, Canada
4. New York Canyon, USA
5. Levanto, Peru
6. Neuquén Basin, Argentina
7. North Island, New Zealand

**TJB Tethyan Sites**
8. SW Great Britain, UK
9. Hebrides Basin, UK
10. Danish Basin, Denmark
11. Polish Trough, Poland
12. North German Basin, Germany
13. South German Basin, Germany
14. Paris Basin, France
15. Csővár Basin, Hungary
16. Calcareous Alps, Austria/Italy
17. Lombardy Basin, Italy
18. Apennine sections, Italy
19. Sicilian sections, Italy
20. Ghalilah Fm., UAE
21. Southern Tibet, China

**TJB Terrestrial Sites**
22. Colorado Plateau, USA
23. Newark Basin, USA
24. Argana Basin, Morocco
25. Fundy Basin, Canada
26. East Greenland, Greenland
27. Karoo Basin, South Africa/Lesotho
28. Sichuan Basin, China

**T-OAE Panthalassic Sites**
29. Neuquén Basin, Argentina
30. El Peñon, Chile
31. Haida Gwaii, Canada
32. East Tributary, Canada
33. Siberian sections, Russia
34. Mino-Tamba sections, Japan

**T-OAE Tethyan Sites**
35. Morondava Basin, Madagascar
36. Tibetan Himalaya, China
37. Bilong County, China
38. Polish Basin, Poland
39. Cleveland Basin, UK
40. South German Basin, Germany
41. Paris Basin, France
42. Lusitanian Basin, Portugal
43. Alpine sections, Austria/Italy
44. Aegean sections, Greece
45. Adriatic sections, Croatia
46. Iberian margin, Spain
47. Moroccan Meseta, Morocco
48. Saharan Atlas, Algeria

**T-OAE Terrestrial Sites**
49. Sichuan Basin, China

*(caption on next page)*

**Fig. 2.** Global paleogeography of (a) the Triassic–Jurassic boundary (~201 Ma), and (b) the early Toarcian (~181 Ma). Red highlights show locations of CAMP and Karoo-Ferrar Large Igneous Provinces. Yellow points show sites or regions that are the focus of studies in the present special issue, white points show other important contemporaneous sites. TJB sites compiled and modified from Greene et al. (2012a) and Lindström et al. (2021, see Appendix). T-OAE sites compiled from Ruebsam et al. (2018, 2020) and Remírez and Algeo (2021a, see Appendix). Base maps from Ron Blakey, Deep Time Maps. BM = Bohemian Massif; IM = Iberian Massif; FS = Fennoscandia.

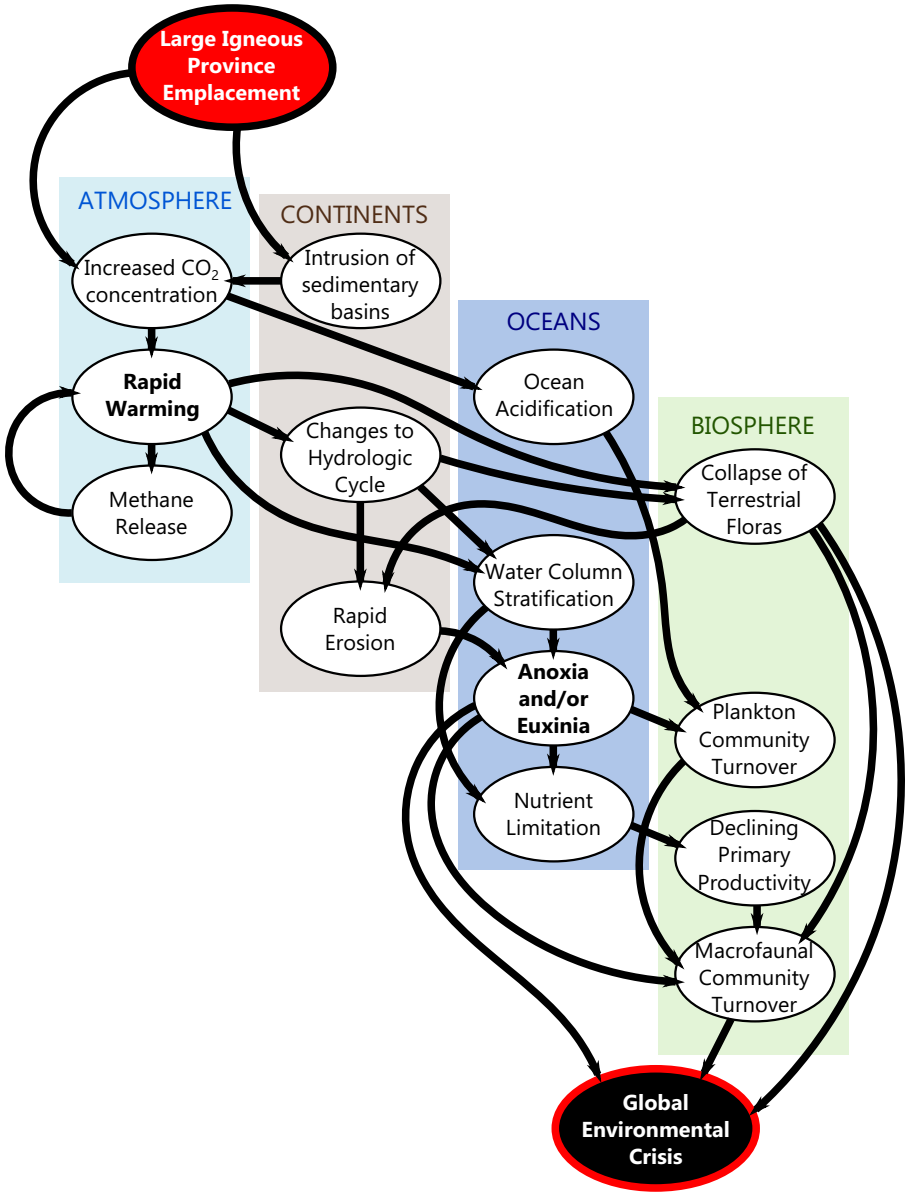


**Fig. 3.** Flow chart showing causal relationships of major changes in the atmosphere, terrestrial realm, oceans, and biosphere following CAMP and KFLIP eruptions. Factors shown in bold are potential direct kill mechanisms contributing to mass extinctions.

particular, extensive studies of continental rift basins in eastern North America have led to development of the 'Newark-Hartford astrochronostratigraphic polarity time scale' (Kent et al., 2017). The higher temporal resolution afforded by ATS studies has contributed to improved correlations of continental and marine successions (Deenen et al., 2010; Boulila et al., 2014).

### 2.2. Paleogeography and eustasy

The Pangean supercontinent, which existed through the entirety of the Triassic, began to break up in the Early Jurassic (Golonka, 2007; Seton et al., 2012; Leleu et al., 2016; Golonka et al., 2018). The Paleotethys Ocean closed during the Late Triassic, as microcontinents collided with the mainland of Laurasian Pangaea. This happened first in the Alpine-Carpathian-Mediterranean area (the Early Cimmerian Orogeny) and later in the Central and Southeast Asian areas (the Indosinian Orogeny). These orogenies resulted in the suturing of the small Indochina and Qiangtang cratons onto the margin of South China. The newly integrated Chinese-Southeast Asian assemblage, which included North and South China, Mongolia, and the eastern Cimmerian plates, emerged by the end-Triassic, leaving a large embayment of the Panthalassic Ocean, known as the Mongol-Okhotsk Ocean, between Mongolia and Laurasia.

The incipient fragmentation of Pangaea in the Late Triassic coincided

with extensional stresses that produced rift basins throughout eastern North America, northwestern Africa, and adjacent parts of Europe and South America (Golonka, 2007; Seton et al., 2012; Golonka et al., 2018). Large continental rifts originating at that time were filled with a combination of basaltic flows, lacustrine units, and continental red beds. The influence of this continental breakup on regional paleogeography has been investigated in a series of studies, e.g., of the Gulf of Mexico (Salvador, 1987), western Laurentia (Dickinson and Gehrels, 2008), the Arctic region of Laurasia (Glørstad-Clark et al., 2010), and China (Li and Huang, 2013). In the Tethyan region, the northward-dipping subduction zone along the northern margin of the Neotethys Ocean caused the formation of new spreading centers within that basin (Golonka, 2007; Golonka et al., 2018).

The eustatic record of the Triassic and Jurassic periods has been established in a series of studies (Haq et al., 1988; Haq, 2018a, 2018b). The Triassic was characterized by relatively low sea-level elevations generally, resulting from the reduced volume of mid-ocean spreading ridges at a global scale following the assembly of Pangea (Müller et al., 2013). This culminated in a global lowstand roughly coinciding with the end-Triassic extinction (Hallam and Wignall, 1999: Tanner et al., 2001, 2004) when sea levels may have fallen below the mean present-day level (Haq, 2018b), though the lowstand itself is unlikely to have been a primary extinction driver (Hesselbo et al., 2004). While third-order sea evel variations are superimposed on the generally low latest Triassic and earliest Jurassic sea level, the limited range of eustatic variation (generally 25-75 m; Haq, 2018b) implies that little or no continental ice existed in the generally warm and arid Triassic Period (Preto et al., 2010; Tanner, 2018).

Sea levels began to rise in the Early Jurassic, as sea-floor spreading accelerated with the breakup of Pangaea (Müller et al., 2013), culminating in a maximum global highstand in the mid-Cretaceous. This broad rise was punctuated by several short-term peaks in the Early Jurassic, first at the mid-Pliensbachian, and then more notably in the Toarcian. Starting from a lowstand at the Pliensbachian-Toarcian boundary, sea levels rose 30-90 meters (Hallam, 1997), reaching a peak as high as high as 75 m above their mean present-day level by the mid-Toarcian (Haq, 2018b). A study by Ruebsam et al. (2019) constrains the duration of this transgression to as little as 300 kyr, which may imply the collapse of a continental ice sheet (Korte and Hesselbo, 2011), though regional factors may also have played a role in driving third-order sea-level changes (Haq, 2018b).

### 2.3. Major events

The ETME has long been recognized as one of the largest Phanerozoic mass extinctions (Raup and Sepkoski, 1982). It has been strongly linked to Central Atlantic Magmatic Province (CAMP) volcanic activity and associated intrusive magmatism (Marzoli et al., 1999, 2004; Deenen et al., 2010; Blackburn et al., 2013; Panfili et al., 2019). The metastudy of Lindström et al. (2021) presents a comprehensive review of radioisotopic ages of CAMP intrusives and extrusives, and a compilation of potential proxy records for volcanism, including $\delta^{13}C$, $pCO_2$, iridium and other platinum group elements, mercury, polycyclic aromatic hydrocarbons (PAH), charcoal, and $SO_2$, and an analysis of their relationship to the timing of biotic decline and extinctions among multiple clades, including ammonoids, radiolarians, conodonts, cyst-producing dinoflagellates, and plants. Based on the observation that the onset of the I-NCIE (i.e., *Spelae* CIE) coincides with PAHs derived from incomplete combustion of sedimentary organic matter, and evidence of $SO_2$ damage to plants, the authors interpret the isotopic record to reflect a massive release of isotopically light carbon and sulfur, driven by igneous sill intrusions in the Trans-Amazonian basins, which contain both evaporite- and organic-rich sediments. However, while this negative CIE can be recognized globally, its magnitude varies regionally, with $\delta^{13}C_{org}$ declining to a greater extent in the Tethyan interior (~3-6 ‰) compared to Panthalassic sections (~2-5 ‰), which may reflect the extent to which the ETME coincided with a collapse of terrestrial productivity in different environments (Ruhl et al., 2021, see Appendix). Furthermore, the compound-specific and biomarker analysis of Fox et al. (2020) suggests a local source of light carbon to southwestern UK sections, suggesting that the "initial" CIE in this setting may not have required the input of thermogenic light carbon.

The Early Jurassic interval between the TJB (201.3 Ma) and the T-OAE (181.5 Ma) witnessed several smaller carbon-cycle perturbations (Cramer and Jarvis, 2020, and references therein). The Sinemurian–Pliensbachian boundary, at 190.8 Ma, is characterized by a negative CIE (the "S-P Event") reported from multiple European carbonate successions (Franceschi et al., 2014, 2019). The S-P Event and its aftermath were possibly due to a reorganization of ocean circulation linked to the opening of the 'Hispanic Corridor' connecting the interior Tethys Ocean to the tropical East Pacific. The Ibex Zone of the lower Pliensbachian is characterized by a positive CIE and warming, a pattern that reflects an influx of warm, saline water from the equatorial ocean into the western Tethys (Armendáriz et al., 2012). The Pliensbachian-Toarcian (Pl-To) boundary, at 182.7 Ma, was marked by a 2–3‰ negative CIE, and paleoenvironmental changes that have been attributed to an early phase of Karoo-Ferrar LIP magmatism (Percival et al., 2015, 2016).

The Toarcian oceanic anoxic event (T-OAE; sometimes referred to as the 'Jenkyns Event'), at 181.5 Ma, is characterized by a global negative CIE of ~2 to 7 ‰ in both carbonate and organic carbon isotope records, peaking during the *exaratum* subzone of the *Falciferum* Zone of the early Toarcian (Jenkyns, 1988; Hesselbo et al., 2000; Suan et al., 2008b; Boulila et al., 2014; Suan et al., 2015; Boulila and Hinnov, 2017; Ikeda et al., 2018; Rosales et al., 2018; Remírez and Algeo, 2021b, see Appendix). The magnitude of this excursion makes it the largest carbon cycle perturbation of the Early Jurassic (Müller et al., 2017). The trigger for the T-OAE is thought to have been the emplacement of the Karoo-Ferrar Large Igneous Province in southern Gondwana (Courtillot and Renne, 2003; Svensen et al., 2007; Them et al., 2017a). Estimates of the duration of the T-OAE are highly variable, ranging from 120 kyr to 2.4 Myr. The various approaches to this question are reviewed in detail in Remírez and Algeo (2021b, see Appendix).

In many restricted basins, the early Toarcian CIE coincided with deposition of laminated, lipid-rich (high-hydrogen index) black shales containing abundant green algal organic matter. Some of these units have yielded biomarker evidence for water column stratification and photic-zone euxinia (Schouten et al., 2000; Frimmel et al., 2004; Ruebsam et al., 2018; Suan et al., 2018; Xu et al., 2018). The T-OAE coincided with global climatic warming (Bailey et al., 2003; Rosales et al., 2004; McElwain et al., 2005; van de Schootbrugge et al., 2005a, 2005b; Suan et al., 2008a; Korte et al., 2015; Arabas et al., 2017), marine mass extinctions (Little and Benton, 1995; Harries and Little, 1999), and the collapse of neritic and pelagic carbonate production (Blomeier and Reijmer, 1999; Mattioli et al., 2009; Caswell and Frid, 2017; Caswell and Dawn, 2019; Vasseur et al., 2021). This event has been widely studied, especially in Europe, where it is characterized by high extinction rates (Harries and Little, 1999; Wignall et al., 2005; Caruthers et al., 2013; Danise et al., 2015). However, some taxa proliferated during this event, e.g., the brachiopod *Soaresirhynchia*, a slow-growing, deep-sea taxon whose success in the western Tethys Ocean at this time has been attributed to its low metabolic rate (Ullmann et al., 2020).

There is considerable regional variation in the expression of the Toarcian OAE, even within the relatively limited area represented by Europe and the Mediterranean region. The T-OAE has been extensively investigated in northern Europe, including the UK (Hesselbo et al., 2000; Palliani et al., 2002; Cohen et al., 2004; Pearce et al., 2008; McArthur et al., 2008; Kemp et al., 2011; Caswell and Coe, 2012; French et al., 2014; Thibault et al., 2018), Germany (Schouten et al., 2000; Röhl et al., 2001; Schmid-Röhl et al., 2002; Berner et al., 2013; Suan et al., 2015; Song et al., 2017), and France (Hermoso et al., 2009a, 2009b, 2012; Harazim et al., 2013; Boulila et al., 2014; Fonseca et al., 2018). In these areas, the T-OAE is characterized by the widespread deposition of anoxic

black shales (with TOC typically 5-10 %, but as high as 20 % in some settings) and a large negative excursion in $\delta^{13}C_{org}$ profiles (–5 to –7 ‰) within the early Toarcian *semicelatum* and *exaratum* subzones (Wignall et al., 2005; van de Schootbrugge et al., 2005a; McArthur et al., 2008). In contrast, southern Europe and northern Africa show weaker expressions of the T-OAE (Bodin et al., 2010; da Rocha et al., 2016), with peak TOC values generally in the 0.5-3 % range (Reolid et al., 2020). Sections from Hungary (Raucsik and Varga, 2008; Baranyi et al., 2016; Müller et al., 2017), also deposited in the interior Tethys region are also characterized by lower TOC content (0.5-3.5 %) and a smaller negative $\delta^{13}C_{org}$ excursion (–2 to –7 ‰).

The expression of the T-OAE outside of Europe is spatially complex. Sections from Tibet, which were deposited in the eastern Tethys basin, show TOC values above 10% during the early Toarcian, though the $\delta^{13}C_{org}$ excursion is muted relative to European sections (–1 ‰; Fu et al., 2016). In the Panthalassic realm, as represented by sections from western Canada (Caruthers et al., 2011, 2014; Them et al., 2017b), the Mino-Tamba accretionary complex of Japan (Gröcke et al., 2011; Ikeda et al., 2018), and the Neuquén Basin of Argentina (Mazzini et al., 2010; Al-Suwaidi et al., 2016), the T-OAE is consistently associated with a negative organic carbon isotope excursion of 2-5 ‰, though accumulations of organic carbon are not seen in all sections.

## 3. Large Igneous Provinces associated with the Triassic–Jurassic transition

### 3.1. Central Atlantic Magmatic Province (CAMP)

The ETME has been linked to Central Atlantic Magmatic Province (CAMP) volcanism and associated intrusive magmatism (e.g., Marzoli et al., 1999, 2004, 2018; Verati et al., 2007; Deenen et al., 2010; Blackburn et al., 2013; Panfili et al., 2019). Extending over an expanse of ~5,000 km north-to-south and ~2,000 km east-to-west, and covering areas of northwestern Europe, West Africa, eastern North America, and Brazil, the CAMP was one the largest continental large igneous provinces in Earth history (Marzoli et al., 1999; McHone, 2003). The tectonic framework and emplacement history of the CAMP have been reviewed in several studies (Hames et al., 2003; Jourdan et al., 2009; Davies et al., 2017, 2021). Intrusive magmatic activity began at least 100 kyr before the main flood basalt stage (Davies et al., 2017; Heimdal et al., 2020), predating the ETME by a similar amount of time (Jourdan et al., 2009). Emplacement of the CAMP magmas was rapid, due to exsolution of large quantities of mantle- and lower-crust derived $CO_2$ in crustal magma-conduit systems, leading to discrete individual eruptive episodes lasting possibly just a few centuries each (Capriolo et al., 2020, 2022). As a result of CAMP volcanism, massive quantities of carbon dioxide ($CO_2$), sulfur dioxide ($SO_2$), hydrogen sulfide, and other volatiles were released into the atmosphere during the Tr-J transition (McHone, 2003) in at least three major pulses over ~600 kyr (Schaller et al., 2012).

Mercury (Hg) concentrations and isotopes are now widely applied as volcanic proxies (Shen et al., 2020). Although a number of complicating factors, such as mercury host phases and non-volcanogenic Hg sources, must be considered when interpreting this proxy (Shen et al., 2019; Them et al., 2019), normalized Hg enrichments and isotope ratios show little to no mass-independent fractionation in both marine and terrestrial TJB sections provide further evidence of the CAMP as the cause of the ETME and concurrent environmental changes (Thibodeau et al., 2016; Percival et al., 2017; Fantasia et al., 2019a; Lindström et al., 2019; Kovács et al., 2020; Schoepfer et al., 2022; Yager et al., 2021, see Appendix). In a deep-ocean TJB succession from Japan, pyrite is the dominant host of mercury, and a spike in Hg/sulfur ratios at the TJB (within dating uncertainties) is likely to record Hg inputs from CAMP volcanism in a location almost antipodal to the centers of CAMP eruption (Schoepfer et al., 2022, see Appendix). Terrestrial successions have also yielded increased levels of mercury—a highly genotoxic element. Hg spikes are associated with an increased frequency of abnormal fern spores, suggesting that mercury (or co-emitted volcanic gases) caused severe environmental stresses and genetic damage to land plants during the Tr-J transition Lindström et al., 2019).

Bolide impacts have also been proposed to explain the ETME, as an alternative mechanism to the CAMP eruptions. The discovery of an iridium anomaly in co-occurrence with a fern spike (trilete spores) in the eastern US was the basis for advocating a bolide impact scenario (Olsen et al., 2002a, 2002b). However, there have been only limited reports of other potentially bolide-related features, such as shocked quartz grains, impact craters, and seismites (Bice et al., 1992; Simms, 2003; Lucas and Tanner, 2007; Tanner et al., 2008, 2016, 2020), and their connection to a bolide impact remains uncertain. Platinum-group element data from CAMP volcanic rocks in Morocco show Pd/Ir, Pt/Ir and Pt/Rh ratios similar to those of marine and terrestrial TJB successions, and very different from those of known bolides (Tegner et al., 2020; Whiteside et al., 2020). Thus, the hypothesis that the ETME was caused by one or more bolide impacts is poorly supported, if not yet fully falsified (Cohen et al., 2017). Evidence of bolide impact is present elsewhere within Upper Triassic successions, most notably in the middle Norian, where it is associated with a turnover of marine fauna. This event likely relects the impact that formed the Manicouagan crater in Quebec, at approximately 214 Ma (Walkden et al., 2002; Onoue et al., 2016), and is not directly associated with the ETME.

### 3.2. Karoo-Ferrar Large Igneous Province (KFLIP)

The Toarcian OAE has been linked to activity of the Karoo-Ferrar LIP (KFLIP), another large magmatic province associated with the breakup of Pangea. The KFLIP extended about 5,000 km north-to-south and 1,200-2,000 km east-to-west, covering parts of South Africa, Antarctica, and southern Australia (Duncan et al., 1997; Ivanov et al., 2017). The origin of the KFLIP remains controversial, with hypotheses centered on subduction (Cox, 1978), mantle plumes (Ellam et al., 1992), and heated asthenosphere (Heinonen and Luttinen, 2010).

The Karoo LIP was originally dated using the $^{40}Ar/^{39}Ar$ technique, yielding a wide range of ages from ~184 to ~174 Ma (Duncan et al., 1997; Jourdan et al., 2005, 2008). These studies argued that the long duration of magmatism in this province was due to slow lithospheric extension preceding continental crustal rupture, and that the relatively modest magnitude of the Toarcian extinction event was consonant with this extended period of magmatism. The more recently developed single-crystal zircon, chemical abrasion U–Pb ID-TIMS method has demonstrated that most magmatism occurred over a far shorter interval (Sell et al., 2014; Burgess et al., 2015; Ivanov et al., 2017). Burgess et al. (2015) reported a starting age of 182.779 ± 0.033 Ma for the Ferrar LIP with a duration of just 349±49 kyr. The same study made a single age determination for the Karoo LIP (183.246 ± 0.045 Ma) but inferred that it had a longer magmatic history than the Ferrar LIP.

The Pliensbachian-Toarcian (Pl-To) boundary, at 182.7 Ma, may record an early phase of magmatic activity in the KFLIP (Pálfy and Smith, 2000; Jourdan et al., 2009; Suan et al., 2008a). This inference is supported by elevated mercury (Hg) concentrations at that time (Percival et al., 2015). The Pl-To boundary event is marked by a 2-3‰ negative CIE accompanied by paleoenvironmental changes, faunal and floral extinctions, and enhanced continental weathering (Hesselbo et al., 2000; Dera et al., 2009a; Littler et al., 2010; Suan et al., 2010; Caruthers et al., 2013; Brazier et al., 2015; Percival et al., 2016; Schöllhorn et al., 2020).

## 4. Paleoclimate during the Triassic–Jurassic transition

### 4.1. Paleotemperatures

Global climate conditions likely became increasingly unstable during the Late Triassic, compared to the Early and Middle Triassic (Tanner,

2018). Isotopes of paleosol carbonates imply large temperature swings in continental settings during the late Norian to Rhaetian, with multiple transient warming events of 7-9 °C (Cleveland et al., 2008), although these estimates have significant error bars related to uncertainties in soil moisture levels and the low temporal resolution of the paleosol database. The ETME was accompanied by a major rise in global temperatures (Korte et al., 2009; Ruhl et al., 2011). Oxygen isotopes of calcitic oyster shells from southwestern Britain suggest warming on the order of 8 °C in the earliest Jurassic, following a brief cooling episode in the latest Rhaetian Langport Member (Korte et al., 2009). Stomatal density analysis of plant fossils suggests a rapid warming of 3-4 °C during the ETME, coupled to increased atmospheric $CO_2$ (McElwain et al., 1999; Bonis et al., 2010; Steinthorsdottir et al., 2011), which is consistent with modeling of pulsed CAMP volcanism (Landwehrs et al., 2020).

Clumped carbonate isotopes have been applied in a study examining a stratigraphically thin interval of the Cotham Marble (part of the Lilstock Formation, near Bristol, UK), believed to represent $\leq$80 kyr coincident with the ETME (Petryshyn et al., 2021, see Appendix). This study identified mild to warm ocean temperatures marked by repeated, short-term swings of ~16 °C. These are interpreted as a signature of local seasonality, but represent too little time to draw inferrences about climatic warming or cooling linked to the ETME.

A novel approach to paleotemperature reconstruction based on the carbon isotopic composition of wood and continental organic matter fluxes ($TOC_{cont}$), and conversion of these proxies to palaeotemperature estimates using an independently calibrated (stomatal) $pCO_2$ record, was undertaken by Pieńkowski et al. (2021, see Appendix). Despite the novel proxy approach, these authors were able to recognize significant warming events, with effects on terrestrial ecosystems, during both the ETME crisis and the Toarcian OAE.

Climate stabilized somewhat through the Early Jurassic. Isotope data from belemnites indicates that the Pliensbachian was characterized by a long cooling trend, followed by a sharp warming at the Pl-To boundary, coupled with a sharp positive CIE (Gómez et al., 2016). Some evidence indicates minor cooling in the earliest Toarcian Polymorphum-Tenuicostatum ammonoid zone, prior to the T-OAE (Ruebsam et al., 2019, 2020, 2021). This cooling has been linked to a transient eustatic sea level fall, lasting perhaps only ~100 kyr, presumably due to global cooling linked to aerosol emissions at the start of the Karoo-Ferrar LIP eruptions (Krencker et al., 2019).

The T-OAE represents the second major warming episode of the Tr-J transition. (Suan et al., 2008a, 2008b, 2010; Korte and Hesselbo, 2011; Dera et al., 2011a, 2011b; Silva and Duarte, 2015; Gómez et al., 2008, 2016; Peti and Thibault, 2017). The magnitude of warming has been estimated via oxygen isotopic analyses of belemnites, with conventional measurements yielding temperature changes of 5-8 °C (Gómez et al., 2008, 2016), while clumped isotope measurements suggest even more dramatic temperature swings (Fernandez et al., 2021). A study employing organic molecular thermometry stressed the dynamism of Toarcian temperatures, with temperature changes as large as 10 °C within 100 kyr intervals, and peak tropical sea surface temperatures as high as 32 °C (Ruebsam et al., 2020).

### 4.2. Atmospheric $CO_2$

The main driver of higher temperatures during the Tr-J transition is considered to have been increases in atmospheric greenhouse gas concentrations. Elevated atmospheric $pCO_2$ levels have been inferred based on plant stomatal data (McElwain et al., 1999; Retallack, 2001; Beerling and Berner, 2002; Bonis et al., 2010; Steinthorsdottir et al., 2011; Slodownik et al., 2021) and soil carbonate carbon isotopes (Schaller et al., 2011, 2012, 2015). These studies suggest a doubling to tripling of $CO_2$ (from 600-1,000 ppm in the latest Triassic to 2,000-3,000 ppm in the earliest Jurassic, with the soil carbonate proxy running higher than 5,000 uatm (Schaller et al., 2011; Hönisch et al., 2012). Large increases in atmospheric $CO_2$ levels have also been inferred during the T-OAE (Courtillot, 1994; Duncan et al., 1997; Pálfy and Smith, 2000; Jourdan et al., 2009; Svensen et al., 2012; Moulin et al., 2017).

The most commonly cited source of excess $CO_2$ to the atmosphere during the ETME and T-OAE is volcanic outgassing. For the ETME, this would be from the basaltic rocks of the CAMP, as directly evidenced from the abundant $CO_2$ preserved in melt inclusions (Capriolo et al., 2020). For the T-OAE, the main source of $CO_2$ is likely to have been the KFLIP. However, $CO_2$ sourced directly from magmas may have been supplemented by several other sources of excess carbon to the atmosphere. Methane, a more powerful greenhouse gas than $CO_2$, might have been released either through destabilization of seafloor hydrates (Hesselbo et al., 2000; Pálfy et al., 2001; Galli et al., 2005; Ruhl et al., 2011; Them et al., 2017b), or via generation of thermogenic methane as igneous sills intruded organic-rich sedimentary deposits (McElwain et al., 2005; Svensen et al., 2007).

The volume of released greenhouse gases necessary to achieve the inferred rise in atmospheric $CO_2$ levels (or the measured shift in carbon-cycle $\delta^{13}C$ values) has been estimated in several studies. Beerling and Berner (2002) calculated that a release of 8,000-9,000 Gt of carbon as $CO_2$ or 5,000 Gt of carbon as $CH_4$ would have been necessary. Pálfy et al., 2001 concluded that volcanic $CO_2$ outgassing was insufficient to fully account for this rise, and that a positive feedback loop in which volcanically induced warming destabilized seafloor methane hydrates must have developed. A recent modeling study by Capriolo et al. (2022) concluded that, while methane destabilization may help to explain the observed isotope excursions, direct emission of $CO_2$ from sequential CAMP eruptions would be sufficient to drive catastrophic environmental change.

### 4.3. Hydrological cycle and weathering intensity

Warmer climates generally lead to more humid conditions, owing to greater evaporation and the higher saturation point of warmer air (Huntington, 2006). Intensification of the hydrological cycle has been inferred for both the TJB and Pliensbachian-Toarcian transition (Cohen et al., 2004; Steinthorsdottir et al., 2012; Brazier et al., 2015; Percival et al., 2016; Fu et al., 2017; Them et al., 2017a; Iqbal et al., 2019; Schöllhorn et al., 2020). During the T-OAE, global weathering may have transiently increased by an overall factor of six (Kemp et al., 2020). The most common type of evidence for an enhanced hydrologic cycle is a shift toward higher values of geochemical indices for subaerial weathering, such as the chemical index of alteration (CIA). However, enhanced weathering is also evidenced by shifts toward greater clay content and larger proportions of kaolinite in the clay fraction, as well as by bedforms indicative of mass wasting (Xu et al., 2018) or high-energy sediment transport and enhanced fluvial discharge (Fantasia et al., 2018a, 2018b, 2019a). In some shallow-marine T-OAE sections, an increase in turbidites and tempestites may be the product of increased humidity and storm intensity (Han et al., 2018; Fantasia et al., 2019a, 2019b).

Evidence for enhanced soil erosion during the ETME event was reported by van de Schootbrugge et al. (2021, see Appendix). They examined the palynomorph content of four Upper Triassic-Lower Jurassic sections in France, Germany, and Denmark, identifying a spike in reworked Paleozoic and Neoproterozoic palynomorphs within uppermost Rhaetian sediments that coincided with the disappearance of dominant Triassic pollen taxa and a proliferation of fern spores. The inverted stratigraphy of the reworked palynomorphs indicates a sequential process of deforestation, soil loss, and deep erosion. A similar increase in reworked phytoclast abundance occurred during the T-OAE event (Kemp et al., 2019). Many nearshore sections, especially those on the southern margin of the European Epicontinental Sea, contain an abundance of wood in the Lower Toarcian (Polgári et al., 2005; Hesselbo et al., 2007; Rodrigues et al., 2019).

Isotopic evidence supports increases in subaerial weathering intensity during the ETME. The seawater $^{87}Sr/^{86}Sr$ record shows a long-

term decline from the Late Triassic (late Norian) through the Early Jurassic (early Toarcian), consistent with a long-term increase in non-radiogenic Sr, linked to an increase in the activity of mid-ocean ridges globally (Müller et al., 2013). Local minima corresponding with the Tr-J and Pl-To transitions likely represent short-term loadings of non-radiogenic Sr from the CAMP and Karoo-Ferrar LIPs, while the shift to more positive values in the Toarcian represents enhanced continental weathering (Jones et al., 1994; Korte et al., 2003; Cohen and Coe, 2007; Callegaro et al., 2012; Lindström et al., 2021). Accelerated weathering at the TJB is also indicated by latest-Rhaetian reversal in osmium isotopic trends, with a shift toward more radiogenic values punctuating the longer-term Rhaetian trend toward unradiogenic values (Cohen and Coe, 2002, 2007; Kuroda et al., 2010). While the shift toward radiogenic values coinciding with the onset of the ETME likely reflects enhanced continental weathering, the Rhaetian trend toward unradiogenic values begins well before the earliest dated CAMP rocks, and cannot be directly attributed to CAMP emplacement (Lindström et al., 2021). High-resolution osmium-isotope data also reveal an increase in chemical weathering intensity during the T-OAE, with inputs of non-radiogenic Os from KFLIP basalts (van Acken et al., 2019).

Intensification of the hydrological cycle and increased weathering intensity are observed during both the ETME and T-OAE (Cohen et al., 2004; van de Schootbrugge et al., 2009; Steinthorsdottir et al., 2012; Lindström et al., 2012; Brazier et al., 2015; Percival et al., 2016; Fu et al., 2017; Them et al., 2017a; Iqbal et al., 2019; Kemp et al., 2020; Schöllhorn et al., 2020). The evidence discussed above supports the hypothesis of a sudden strengthening of the global hydrological cycle as a rapid, direct response to carbon release and atmospheric warming by the CAMP and KFLIP eruptions (Izumi et al., 2018a).

Although both the TJB and T-OAE are widely associated with wetter conditions, aridification did occur in some regions, notably South China (Li et al., 2020a). One example is provided by the study of Song et al. (2021, see Appendix), which shows peaks in polycyclic aromatic hydrocarbons (PAHs) of probable wildfire origin, both at the TJB and at several other levels in the Upper Triassic. The temporal distribution of these peaks suggests that the pre-TJB episodes represent aridification due to southward shifts of the paleo-Intertropical Convergence Zone (ITCZ), although the TJB episode itself is likely to represent CAMP-related effects. Increased charcoal concentrations, evidencing increasing wildfire activity, have been detected from the TJB interval in multiple sections (Marynowski and Simoneit, 2009; Belcher et al., 2010; Petersen and Lindström, 2012), and may reflect regional aridification or increased lightning activity as a source of ignition. Recent studies of fluviolacustrine environments from the Sichuan Basin (Li et al., 2020b) suggests intense aridification, leading to evaporite deposition, during the T-OAE, despite an overall rise in lake levels that may reflect intensification of the monsoonal climate (Xu et al., 2021).

## 5. Paleoceanography of the Triassic–Jurassic transition

### 5.1. Global carbon cycle

Upper Triassic sections are characterized by generally gradual variations in $\delta^{13}C_{carb}$, including a 2-3 ‰ decrease from the Carnian into the Norian, and an increase of similar magnitude from the Norian to the Rhaetian (Muttoni et al., 2014). However, the Norian/Rhaetian boundary (NRB) records a major carbon-cycle perturbation, as recorded by $\delta^{13}C_{org}$ in sections from Italy, Greece, Australia, New Zealand, USA, and Canada (Rigo et al., 2020).

A series of negative excursions in carbon isotopes characterize the latest Triassic through earliest Jurassic (Hesselbo et al., 2002). The earliest negative excursion in carbon isotopes is in the late Rhaetian. It is correlated with the ETME by some authors (e.g., Lindström et al., 2017b) and as preceeding it by others (Hesselbo et al., 2002), and is typically described as the “Precursor CIE”, or P-NCIE. The very latest Rhaetian features a positive excursion in carbon isotopes, more pronounced in some sections than others, followed by a negative CIE immediately preceding or coinciding with the TJB (the so-called “Initial CIE”, or I-NCIE (Hesselbo et al., 2002; Lindström et al., 2017b, 2021; Ruhl et al., 2021, see Appendix).

While there have been multiple attempts at high-resolution correlations between marine and terrestrial sections exhibiting these shifts (Jenkyns et al., 2001; Kemp et al., 2005; van de Schootbrugge et al., 2008; Whiteside et al., 2010, Hesselbo and Pieńkowski, 2011; Hermoso et al., 2012; Ruebsam et al., 2014; Suan et al., 2015; Bodin et al., 2016; Yager et al., 2017, Lindström et al., 2017b, 2021), the extent to which these early carbon isotope shifts reflect global processes (such as exogenous carbon input via the emplacement of the CAMP) vs. local changes in carbon sources and depositional environments remains unclear (Schobben et al., 2019; Fox et al., 2020, 2022; Beith et al., 2021; Ruhl et al., 2021; Lindström et al., 2021, see Appendix). Profiles from both Boreal and Tethyan sections often show that the overall shift to minimum values was stepped, comprising at least two rapid negative shifts in $\delta^{13}C$ superimposed on a more protracted decrease, with the younger events more likely to be directly related to the CAMP emplacement (e.g., Whiteside et al., 2010; Lindström et al., 2017b, 2021).

Carbon isotope profiles in the southwest UK exhibit a ~3 ‰ positive CIE in the interval correlated to the tilmanni ammonite biozone, just above the initial CIE, followed by another negative shift (the so-called ‘Main CIE’, or M-NCIE) spanning essentially the entire Hettangian Stage (Hesselbo et al., 2021a, see Appendix). The Hettangian-Sinemurian boundary in this area is characterized by a positive shift that peaks in the lower Sinemurian at values of ca +4 ‰. This long-term positive CIE may reflect prolonged enhanced organic carbon burial within an extensive system of rift basins in the fragmenting Pangea supercontinent, although patterns in other basins are not entirely consistent.

The Sinemurian-Pliensbachian boundary was marked by a negative CIE (the “S-P Event”), recognized in European carbonate successions (Hesselbo et al., 2007; Littler et al., 2010; Bodin et al., 2016; Franceschi et al., 2019; Schöllhorn et al., 2020). The Ibex Zone of the lower Pliensbachian is characterized by a positive CIE associated with climatic warming (Armendáriz et al., 2012). The Pliensbachian-Toarcian (Pl-To) boundary coincided with a 2-3‰ negative CIE that marked the initial eruptive phase of the KFLIP (Hesselbo et al., 2000; Dera et al., 2009a; Littler et al., 2010; Suan et al., 2010; Caruthers et al., 2013; Brazier et al., 2015; Percival et al., 2016; Schöllhorn et al., 2020).

The T-OAE is characterized by a large negative CIE at the base of the Serpentinum (= Falciferum, = Levisoni) ammonite Zone, briefly interrupting a broader early Toarcian positive CIE, as recorded in carbonates, fossil wood, and bulk organic matter (Hesselbo et al., 2000, 2007; Cohen et al., 2004; van de Schootbrugge et al., 2005a, 2005b; Suan et al., 2008a; Hermoso et al., 2009a, 2009b, 2012; Gröcke et al., 2011; Hesselbo and Pieńkowski, 2011; Al-Suwaidi et al., 2016; Müller et al., 2017; Izumi et al., 2018a, 2018b; Fantasia et al., 2019a; Ruebsam et al., 2020). At a global scale, it is the most characteristic feature of the T-OAE (Remírez and Algeo, 2021a, see Appendix). The T-OAE exhibits significant interregional variation in its expression, being particularly pronounced in the Northwest European Shelf (NWES) region, where T-OAE strata exhibit a CIE of –5 to –7 ‰ and TOC content up to ~10 %. This suggests that the NWES was subject to factors favoring regional development of watermass stratification, deepwater anoxia, and organic matter accumulation. Some lacustrine facies also accumulated organic-rich black shales with negative CIEs at the T-OAE (Xu et al., 2017). However, the negative CIE is not a universal signature of the T-OAE—in the Bachental Basin of the Northern Calcareous Alps, this signature was distorted by local processes, with transient development of suboxic zones in which Mn-oxide reduction yielded strongly negative CIEs located above and below the T-OAE (Neumeister et al., 2015, 2016, 2020).

### 5.2. Oceanic redox conditions

Redox changes may have occurred as early as the mid-Rhaetian in the European Epicontinental Sea (EES), although their linkage to CAMP is uncertain (Blumenberg et al., 2016). Strongly reducing conditions developed across the EES during the Tr-J transition, although some shallow marginal-marine areas did not experience anoxia at the TJB (e.g., Boomer et al., 2021). Biomarker and S-isotope data indicate the existence of shallow (photic-zone) euxinia, probably linked to strong water-column stratification, though this postdates the I-NCIE, which is often interpreted to coincide with most intense episodes of extinction in shallow water settings (Richoz et al., 2012; Jaraula et al., 2013; Luo et al., 2018; Beith et al., 2021). Lower Jurassic black shales of the South German Basin feature enrichment in $\delta^{15}N$ coincident with high redox-sensitive element concentrations, indicating an increase in water-column denitrification and decreased oxygen concentrations (Quan et al., 2008). The geographic distribution of such anoxia, and its continuation for a significant interval into the Early Jurassic, suggest that it may have been related to long-term incursions of reduced salinity watermasses, e.g., via the Viking Corridor (Jaraula et al., 2013).

Redox conditions and nitrogen cycling within the central Panthalassic Ocean during the Tr-J transition have been investigated in studies of deep-ocean abyssal chert sections in Japan, examining depletion of hematite (Ikeda et al., 2015), redox-sensitive trace-elements and bulk-nitrogen $\delta^{15}N$ (Fujisaki et al., 2016, 2021;Schoepfer et al., 2022, see Appendix), and pyrite framboid sizes (Izumi et al., 2018b). These studies broadly concur in recognizing a vertically expanded OMZ and decreased primary productivity due to global warming caused by CAMP volcanism, as well as low $\delta^{15}N$ values due to ocean stratification and incomplete nitrate utilization. Even larger redox shifts occurred in the northeastern Panthalassic Ocean, where contemporaneous photic-zone euxinia developed (Kasprak et al., 2015) in response to water column stratification (Schoepfer et al., 2016), and thick phosphorite deposits accumulated (Larina et al., 2019).

In contrast, the Toarcian OAE was a widespread, though not global, phenomenon (Cohen et al., 2004; Dera et al., 2009a, 2009b; Brazier et al., 2015; Fantasia et al., 2018a; Them et al., 2017a, 2017b; McArthur, 2019; see review in Remírez and Algeo, 2021a, see Appendix). Estimates of paleoseawater $\delta^{98/95}Mo$ suggest the T-OAE had an intensity equal to or greater than that of Cretaceous and Early Cenozoic OAEs (Dickson, 2017). Ocean deoxygenation was regionally exacerbated by elevated rates of marine organic matter production, mainly driven by green algae, cyanobacteria, and microbes such as green sulfur bacteria, leading to bottom water anoxia and photic-zone euxinia (Palliani et al., 2002; van de Schootbrugge et al., 2013).

Redox conditions during the T-OAE were highly variable geographically. Marine anoxia and black shale deposition were particularly widespread in the epicontinental basins of northwestern and central Europe (Baudin et al., 1990; Jenkyns, 2010). The reasons for this regional pattern have been intensely debated (e.g., Remírez and Algeo, 2021b, 2021c; Hesselbo et al., 2021b, see Appendix), with evidence to support development of warm and humid conditions that invigorated the hydrological cycle and enhanced water-column stratification, especially in marginal-marine basins. These climatic changes may have also contributed to enhanced marine productivity (Jenkyns, 2010; Monteroo-Serrano et al., 2015; Them et al., 2017a; Xu et al., 2018). The Panthalassic region also experienced a pronounced shift toward more reducing conditions during the T-OAE, as shown by trace-metal enrichment patterns in Japanese deep-ocean sections (Fujisaki et al., 2016). A recent study using thallium (Tl) isotopes, which are potentially more sensitive to redox shifts in the suboxic range, inferred that this shift began around the Pliensbachian/Toarcian boundary, ~600 kyr before the T-OAE, a timing that is consistent with eruptions of the KFLIP as its trigger (Them et al., 2018). The same study also recorded perturbed Tl isotopes during the T-OAE interval, reflecting a second deoxygenation event that coincided with the main phase of KFLIP volcanism.

OAEs are thought to be terminated by rising oxygen levels due to organic carbon burial, at a characteristic timescale of ~1 Myr (Algeo and Ingall, 2007). This increase in atmospheric oxygen is evidenced by charcoal and PAH evidence for wildfire activity in the latest Triassic and earliest Jurassic (Marynowski and Simoneit, 2009; van de Schootbrugge et al., 2009; Belcher et al., 2010; Petersen and Lindström, 2012; Williford et al., 2014). The same mechanism is also proposed to have terminated the T-OAE (Baker et al., 2017), supported by charcoal and phytoclast abundance data from sections in Portugal and Wales that show a peak coinciding with the termination of the OAE. This suggests that fire intensity may serve as a negative climatic feedback, limiting increases in $O_2$.

### 5.3. Marine productivity

Most studies that have addressed primary productivity trends across the TJB have identified decreased productivity during the ETME crisis (Ward et al., 2001; Richoz et al., 2012; Schoepfer et al., 2016; van de Schootbrugge et al., 2013), although episodes of high productivity may have occurred in the Early Jurassic, driven by a resumption of ocean circulation or a rapid flux of nutrients into the European epicontinental seaway (van de Schootbrugge et al., 2013). Organic biomarkers (e.g., pristane/phytane ratio, gammacerane index), coupled with palynology and geochemical proxies, suggest both enhanced stratification and major changes in phytoplankton community composition, with dinoflagellates declining in importance as prasinophytes, diazotrophs, methanotrophs, and green sulfur bacteria played an increasingly important ecological role (Richoz et al., 2012; Kasprak et al., 2015).

Changes in productivity, especially in open marine settings, may be related to changes in nutrient cycles. The Kennecott Point section (Canada) preserves evidence for increased nitrogen fixation, likely reflecting stratification of the water column, in the 400–800 kyr immediately preceding the biostratigraphic Triassic–Jurassic boundary. This change in the nitrogen cycle corresponds with a minimum in primary or export productivity in the photic zone, and euxinic conditions in the bottom water (Kasprak et al., 2015; Schoepfer et al., 2016). Similar disturbances to the nitrogen cycle can be recognized at the Katsuyama section, deposited in the central Panthalassic Ocean (Fujisaki et al., 2021, see Appendix), where an initial period of nitrogen limitation prior to the TJB leads to a period of nutrient availability in the earliest Jurassic. This resumption of productivity shortly after the ETME is also seen at Kennecott Point and may be due to enhanced nutrient delivery from the continents or vertical mixing of nutrient-replete deep water (Schoepfer et al., 2016, Fujisaki et al., 2021, see Appendix). An even longer interval of apparent stratification, coupled with decreased productivity and reducing conditions in the thermocline, can be recognized at the Kurusu section, (also deposited in the Panthalassic Ocean), where stratification appears to have become significant as much as 1 million years prior to the TJB (Schoepfer et al., 2022, see Appendix).

Much like carbon isotope signals and redox conditions, patterns of primary productivity during the T-OAE were geographically complex, and may have interacted with oceanographic and redox conditions in multiple ways (Jenkyns, 2010). Changes in nannofossil fluxes and in the body sizes of benthic invertebrates in northwestern European sections have been interpreted to reflect an initial stage of high productivity during deoxygenation, followed by an interval of low productivity as anoxia impacted nutrient cycles (Caswell and Coe, 2013; Caswell and Dawn, 2019; Menini et al., 2021). Data from other Tethyan sections suggests elevated productivity where the nutrient flux from adjacent landmasses was sufficient, or where local stratification led to phosphorus regeneration, while more southerly locations in the western Tethys experienced declining productivity (Vetö et al., 1997; Fantasia et al., 2018b; Reolid et al., 2019b; Ruebsam et al., 2020). A flourishing of algal and bacterioplanktonic organisms appears to have contributed to the significant increase in TOC content during the T-OAE (Neumeister et al., 2015, 2016, 2020), though carbon preservation was likely also

enhanced by salinity stratification in the European epicontinental seaway (van de Schootbrugge et al., 2013; Remírez and Algeo, 2021a, 2021b). There is also biomarker evidence for a shift to greater microbial productivity in lacustrine facies during the T-OAE (Liu et al., 2020).

### 5.4. Oceanic acidification

Ocean acidification is most easily observed in deep-ocean areas, where the depth of the lysocline may shift substantially in response to such events. Such a shift during the Tr-J transition may be attested by changes in the mineralogy of deep-ocean sediments, e.g., loss of authigenic hematite (Ikeda et al., 2015). However, a sparse deep-ocean record for the pre-Cretaceous makes it necessary to search for evidence of the effects of acidification in shallow-marine sections, e.g., reductions in carbonate accumulation rates and selection biases against calcifying and other acid-sensitive organisms (Greene et al., 2012a; Corsetti et al., 2015; Ritterbush et al., 2015). Such features developed in some shallow-marine areas during the Tr-J transition, including a strong reduction of carbonate sediments, loss of the more soluble components such as aragonite and high-Mg calcite (Črne et al., 2011), rarer appearance of calcareous taxa (Hautmann, 2004; van de Schootbrugge et al., 2007; Kiessling and Simpson, 2011), and a transient elimination of coral reefs (Greene et al., 2012a). However, modern experiments have shown that organismal responses to lowered pH can vary strongly (Findlay et al., 2011), and there is evidence from the fossil record that calcification of some bivalves actually increased during the Tr-J transition (Mander et al., 2008). Furthermore, oceanic acidification can account for only a fraction (~20%) of the observed shifts in Ca isotopic compositions ($\delta^{44/40}Ca$) of marine carbonates, with other factors (e.g., increased aragonite precipitation) accounting for the remainder (Jost et al., 2017).

The ability of CAMP volcanic gas emissions to generate ocean acidification was tested by Berner and Beerling (2007), who used a carbon-cycle model to infer that only extreme conditions of massive and shortlived degassing of $CO_2$ and $SO_2$ from CAMP volcanism could have caused the entire ocean to become undersaturated with respect to calcium carbonate. With total degassing of 21,000 GtC as $CO_2$ and 57,000 GtS as $SO_2$, an undersaturated ocean with respect to all calcium carbonate minerals could have persisted for 20-40 kyr, but only if the volcanic degassing lasted for no longer than 50-100 kyr. A more recent modeling study by Landwehrs et al. (2020) found that pulsed emissions of up to 7500 GtC and 500 GtS, in 1-6 kyr intervals, led to reduced oceanic pH and calcium carbonate saturation, particularly in the Tethys Ocean, but did not cause undersaturation with respect to calcium carbonate on a global scale.

Ocean acidification has been inferred during the T-OAE as well, using boron isotopes of brachiopod shells (Müller et al., 2020b). This acidification had pronounced effects on carbonate platform development in some shallow areas (Trecalli et al., 2012; Han et al., 2018; Ettinger et al., 2021). Condensed shale intervals in carbonate successions have often been interpreted as evidence of sediment starvation as a result of sea-level rise (Pittet et al., 2014; Thibault et al., 2018), but it is an open question as to whether such intervals might represent changes in carbonate saturation levels (Müller et al., 2020a). High Sr concentrations in lower Hettangian units may reflect a global-scale change in carbonate saturation state, with a reduction of biological aragonite precipitation and increased continental weathering (Ge et al., 2018, 2019). Fluctuations in carbonate saturation levels are supported by evidence of seafloor carbonate dissolution and precipitation of synsedimentary fan cements (Greene et al., 2012b). Both benthic and pelagic carbonate production was significantly reduced during the T-OAE (Mattioli et al., 2009; Trecalli et al., 2012; Ettinger et al., 2021; Krencker et al., 2020).

### 5.5. Ocean circulation

Environmental changes in the NWES during the Tr-J transition have been linked to large-scale changes in ocean circulation as a result of the breakup of Pangea and opening of new oceanic gateways. The S-P Event, which was accompanied by a rapid migration of unusual bivalves (the *Lithiotis* Fauna) into the Tethyan region, is hypothesized to have been triggered by opening of the Hispanic Corridor, connecting the western Tethys with the proto-Gulf of Mexico and, possibly, the Panthalassic Ocean (Franceschi et al., 2014, 2019). The changes associated with the Ibex Zone of the lower Pliensbachian, i.e., a positive CIE, apparent warming, and lower seawater $^{87}Sr/^{86}Sr$ values, have been attributed to an influx of warm, saline waters from the equatorial Tethys (Armendáriz et al., 2012).

Changes in ocean circulation have been inferred for the T-OAE as well, specifically, the opening of the Viking Corridor to the Arctic Ocean (Harazim et al., 2013; Correia et al., 2017; Ruvalcaba Baroni et al., 2018), which was probably related to plate tectonic movements in the North Atlantic region (Korte et al., 2015). While large negative CIEs characterize lower Toarcian strata across the entire western Tethyan region, a strong north-south gradient in redox conditions and organic matter accumulation rates is consistent with such a mechanism. Specifically, southern areas closer to the paleo-equator, and further from the Viking Corridor, e.g., in Portugal (da Rocha et al., 2016), Spain (Reolid et al., 2018, 2019a, 2019b; Silva et al., 2021), and Morocco (Bodin et al., 2010), did not accumulate organic-rich facies during the T-OAE, suggesting relatively well-oxygenated conditions on the seafloor, despite some evidence for dysoxia in the water column and sediments (Reolid et al., 2020). More northern basins, e.g., in France (Harazim et al., 2013) and Germany (van de Schootbrugge et al., 2019), experienced anoxia and black shale deposition well beyond the end of the Toarcian negative CIE.

This pattern is consistent with an influx of low-salinity Arctic waters via the Viking Corridor, leading to density stratification within the NWES. This interpretation is supported by a shift in favor of algal types with an affinity for cold-water, low-salinity conditions (e.g., prasinophytes; Prauss and Riegel, 1989; Dera and Donnadieu, 2012). However, a recent palynological study inferred that an influx of oxygenated, low-salinity Arctic waters through the Viking Corridor led to the termination of the T-OAE in the NWES, rather than its strengthening (van de Schootbrugge et al., 2020a, 2020b), so the relationship between proposed ocean circulation changes to other events of the Tr-J transition remains in doubt.

Although the eruptions of large igneous provinces frequently have global effects (Courtillot and Renne, 2003; Ernst and Youbi, 2017; Johansson et al., 2018), the T-OAE is more strongly expressed as a distinct event in the NWES than in other regions. The reason for this exceptional expression of the T-OAE in the NWES has been a matter of debate. McArthur et al. (2008) and McArthur (2019) used Mo concentration data to link this event to extreme restriction of the Cleveland Basin (UK), related to pycnoclinal deepening triggered by heavy freshwater runoff that prevented deepwater exchange with the open ocean. This model was subsequently supported by a study based on organic geochemical proxies and stable isotopes that inferred development of a seasonally stratified water column during the T-OAE (French et al., 2014), as well as a $\delta^{98/95}Mo$ study that inferred stronger watermass restriction in the Cleveland Basin relative to other NWES basins (Dickson et al., 2017). However, a conflicting model based on sea-level rise during the T-OAE was presented by Thibault et al. (2018). Remírez and Algeo (2021b, see Appendix) tested these competing hypotheses for formation of the laminated, organic-rich 'Jet Rock' black shales using the recently proposed elemental paleosalinity proxies of Wei and Algeo (2020), concluding that a sharp decline in watermass salinity, probably due to low-brackish conditions, occurred during the peak of the T-OAE, a finding that favors the McArthur et al. (2008) model. In this context, Hesselbo et al. (2021b) and Remírez and Algeo (2021c) offer an in-depth discussion on the interpretation of marine fossils in shales containing geochemical evidence for brackish depositional conditions.

## 6. Paleobiology of the Triassic–Jurassic transition

### 6.1. Terrestrial biotas

Terrestrial ecosystems were severely affected by the Tr-J transition, as shown by major turnovers in floral assemblages at the ETME globally, which to a permanent change in the composition of global floras at many sites (Zhang and Grant-Mackie, 2001; McElwain et al., 2007, 2009; van de Schootbrugge et al., 2009; Bonis et al., 2010; Mander et al., 2010; Bonis and Kürschner, 2012; de Jersey and McKellar, 2013; Lindström, 2016; Lindström et al., 2017a; van Eldijk et al., 2018; Gravendyck et al., 2020; Zhang et al., 2020). A phase of 'mass-rarity' of the abundant Rhaetian palynomorph *Ricciisporites* is characteristic of the onset of the extinction, with the extinction interval itself dominated by spores, which may reflect the dominance of ferns relative to seed plants (van de Schootbrugge et al., 2009; Lindström, 2016, 2021). In the rift basins of eastern North America and northern Africa, the Triassic-Jurassic boundary is marked by the disappearance of *Ovalipollis ovalis*, *Vallasporites ignacii*, and *Patinasporites densus*, among other sporomorphs (Whiteside et al., 2007). Cheirolepid conifers originated prior to the TJB, and were affected by the extinction, but become markedly dominant in the Early Jurassic, up to >90% in many assemblages (Whiteside et al., 2007; Lindström, 2016). The appearance of aberrant palynomorph types is suggestive of the mutagenic effects of environmental pollutants (Steinthorsdottir et al., 2018), potentially including volcanic mercury, (Lindström et al., 2019; Gravendyck et al., 2020) on terrestrial vegetation. In East Greenland, the replacement of Late Triassic forests comprised of low-LMA (leaf mass per area) taxa by Early Jurassic forests comprised of high-LMA taxa is consistent with the influence of extreme climatic warming, which selected for taxa that had a stress-tolerant strategy and adaptive plasticity in leaf functional traits such as LMA (Soh et al., 2017). The findings of these studies argue against the conclusion of Barbacka et al. (2017), based on a metastudy of European palynomorph data for the Anisian to Toarcian interval, that there was no significant turnover in terrestrial vegetation at the TJB.

During the T-OAE, terrestrial floras shifted from a high-diversity mixture of conifers, seed ferns, wet-adapted ferns, and lycophytes to a low-diversity assemblage dominated by cheirolepid conifers, cycads, and *Cerebropollenites*-producers, which were able to survive in warm, drought-like conditions (Slater et al., 2019). Despite a rapid recovery of vegetation after the T-OAE, the overall community composition remained notably different than that prior to the event. Significant changes in terrestrial floras across the Pliensbachian/Toarcian boundary demonstrate that the effects of the early stages of volcanogenic warming events were more severe for continental than for marine ecosystems (Slater et al., 2019). Despite major changes in terrestrial vegetation, the Tr-J transition did not have any apparent effect on insects and other terrestrial invertebrates, e.g., as reported for the Lepidoptera (moths and butterflies) (van Eldijk et al., 2018). However, the fossil record of terrestrial invertebrates is sparse, and it is possible that new data will necessitate a revision of this inference in the future.

Terrestrial vertebrates were variously affected by the Tr-J transition. Well-studied formations, particularly the Karoo Basin of South Africa, continue to yield new findings regarding dinosaur paleobiogeography (McPhee et al., 2017; Bordy et al., 2021, see Appendix). Late Triassic terrestrial tetrapod assemblages were characterized by strong provinciality despite a lack of geographic barriers, probably due to strong climatic influences, and cosmopolitanism prevailed only in the aftermath of massive ecological disruptions (Whiteside et al., 2011, 2015). Almost all pseudosuchians as well as other reptile lineages died out at the ETME, including previously abundant clades such as the aetosaurs, phytosaurs, and rauisuchids, along with many therapsids and large temnospondyl amphibians, leaving dinosaurs, pterosaurs, and protomammals comparatively unscathed (Tanner et al., 2004; Kustatscher et al., 2018). Although the replacement of pseudosuchians by dinosaurs in large continental niches has long been recognized as a feature of the Tr-J transition (Olsen et al., 2002a), the role of the extinction in the dynamics of this changeover is now better understood. Dinosaurian diversity increased slowly through the Late Triassic (Brusatte et al., 2008a, 2008b), but the extinctions of pseudosuchians occurred abruptly, after which dinosaurian global hegemony was fully established. The vertebrate ichnological record also supports this inference—the frequency of tracks of medium- and large-sized theropods increases during the Late Triassic (Bernardi et al., 2016). Late Triassic formations contain a mixture of dinosaur, dinosauromorph, pseudosuchian, and non-mammalian therapsid tracks, whereas Early Jurassic assemblages are dominated by saurischian dinosaur tracks (Bernardi et al., 2016; Lucas, 2018c), and include the first appearance of ornithischian tracks and skeletons (Olsen et al., 2022).

### 6.2. Marine biotas

The Tr-J transition affected nearly all components of contemporaneous marine ecosystems. The base of the marine food chain, phytoplankton, was strongly impacted. Dinoflagellates and coccolithophorids, taxa that had originated during the Carnian-Norian, experienced a severe diversity reduction (van de Schootbrugge et al., 2007). Only two cyst-producing dinoflagellate genera are known from the earliest Jurassic (*Dapcodinium* and *Beaumontella*), and only one calcareous nannoplankton taxon survived through the Tr-J transition (*Crucirhabdus primulus*). The reduction of these clades appears to have been ecologically exploited by green algae, including the prasinophytes and acritarchs, which had been in decline since the Late Paleozoic but underwent a transient rebound as 'disaster species' in the immediate aftermath of the ETME (van de Schootbrugge et al., 2007; Richoz et al., 2012; Kasprak et al., 2015). Their proliferation may have been due to the rapid rise of $pCO_2$ related to the CAMP eruptions, which impeded calcification by calcareous phytoplankton, allowing other forms, especially those adapted to high $pCO_2$, to proliferate (van de Schootbrugge et al., 2007). Dinoflagellates and coccolithophorids did not recover until the late Pliensbachian, when both groups underwent a marked diversification. The T-OAE is marked by a similar pattern, with a pronounced decline of dinoflagellates during the peak of that event (Prauss and Riegel, 1989; Slater et al., 2019).

Zooplankton were also affected by the ETME, with significant losses of radiolarians (Carter and Hori, 2005; Kocsis et al., 2014) and the complete extinction of conulariids (Lucas, 2012) and conodonts (Karádi et al., 2020). The disappearance of conodonts was shown to have been asynchronous at a global scale, by comparing last occurrence records with integrated high-resolution bio- and chemostratigraphic correlations (Du et al., 2020, see Appendix). This analysis revealed that conodonts disappeared prior to the M-NCIE in the Tethys and eastern Panthalassic regions, but survived to NCIE3 (believed to be equivalent to the M-NCIE) in the mid-Panthalassic Ocean, suggesting conodonts survived for another ~150 kyr in open ocean settings.

Among marine invertebrates, the ETME resulted in the disappearance of ~20-25% of families, 40-50% of genera, and ~60-70% of species (Raup and Sepkoski, 1982; Kiessling et al., 2007). The hardest-hit clades included ammonites, bivalves, and corals, which experienced a combination of elevated extinction and depressed origination rates (McElwain et al., 2007; Kiessling and Simpson, 2011). The ETME was characterized by a degree of ecological selectivity: higher extinction rates are reported among reef dwellers relative to level-bottom dwellers, inshore taxa relative to offshore taxa, organisms favoring carbonate substrate over siliciclastic substrates, and low-latitude forms relative to intermediate- and high-latitude forms (Kiessling et al., 2007). Among corals, which exhibited a 96% decline at the genus level, ecological selectivity was manifested as preferential survival of taxa having low levels of corallite integration (Stanley et al., 2018). There were further losses among marine invertebrates during the late Pliensbachian and early Toarcian (Bambach, 2006). At the same time, certain taxa prospered during these crises, e.g., epifaunal bivalve of the genera *Agerchlamys*, *Pseudolima*, and

*Meleagrinella* are found in dense concentrations within the TJB crisis interval, especially in organic rich deposits that may reflect anoxic conditions (McRoberts et al., 2012).

Ammonites were strongly affected by the ETME (Guex et al., 2004), with ceratitids, the most prominent order of ammonites in the Triassic, going completely extinct. Other orders such as the Ammonitina, Lytoceratina, and Phylloceratina diversified from the Early Jurassic onward. Ammonites continued to suffer extinctions during the Early Jurassic, when diversity declines may have occurred in as many as six steps, beginning at the Pliensbachian-Toarcian boundary and extending into the late Toarcian, although the main decline was correlative with the early Toarcian T-OAE (i.e., the Tenuicostatum/Serpentinum Zone boundary; Dera et al., 2015; Caruthers et al., 2013, 2014). Belemnites experienced a modest decline during the T-OAE, but recovered their loss of diversity by the late Toarcian, before undergoing a more serious decline in the Aalenian through Kimmeridgian (Dera et al., 2016).

Brachiopod diversity declined slowly during the Late Triassic, even prior to losses at the ETME, then increased somewhat in the Early Jurassic before suffering further losses during the Toarcian. Two out of four orders, the spiriferinids and athyridids, were more strongly affected by the ETME, and were confined to the western Tethys during the Early Jurassic before ultimately going extinct at the T-OAE (Vörös, 2002; Vörös et al., 2016). In contrast, the two surviving orders, the rhynchonellids and terebratulids, maintained a cosmopolitan distribution through both of these events. The spiriferinids and athyridids differed in having a spiral brachidium and lophophore, linked to a passive feeding strategy, and their preferential loss during the Tr-J transition reflects ecological selectivity against this trophic mode. Their temporary survival following the ETME is an example of the "dead clades walking" phenomenon (Jablonski, 2002; Vörös et al., 2016; Barnes et al., 2021).

Other marine invertebrate groups suffered diversity losses during the ETME, including bivalves (Mander et al., 2008; Wignall and Atkinson, 2020), scleractinian corals (Kiessling and Simpson, 2011), and sphinctozoan sponges (Hautmann, 2012). Reef communities collapsed, as corals nearly disappeared from the Tethys Ocean at the end of the Triassic and did not return to their previous abundance until the late Sinemurian (Stanley et al., 2018). Bioeroders typical of modern reefs, such as endolithic bivalves and clionaid sponges, were uncommon prior to the Late Triassic, and increased in size, abundance, and ecological importance throughout the Jurassic (Bertling, 1999; Bromley, 2004; Buatois et al., 2016). Transient decreases in body size (i.e., the Lilliput Effect) occurred among belemnites, brachiopods, ammonites, and bivalves (Morten and Twitchett, 2009; Ros-Franch et al., 2019; Piazza et al., 2020).

The relationship of the TJB to ichnofaunal assemblages has been examined in several studies, with declines in bioturbation generally linked to local environmental controls, e.g., more reducing conditions, although possibly driven by global changes (e.g., Barras and Twitchett, 2007). There are well-documented changes in trace-fossil size and diversity through the interval—both in continental and in shallow marine environments (Barras and Twitchett, 2016). Although reduction or loss of trace fossils is expected in anoxic facies, a similar pattern is observed in non-anoxic, shallow-marine facies, where ichnoassemblages may be limited to abundant but monogeneric assemblages, e.g., those dominated by *Thalassinoides* (Miguez-Salas et al., 2017). Recovery from the end-Triassic mass extinction is characterized by a gradual increase in burrow size and the reappearance of deep-tier trace fossils, suggesting the return to "normal" environmental conditions by the end of the Hettangian (Barras and Twitchett, 2007).

Detailed paleoecological analyses of benthic invertebrate communities, and their changes across the Tr-J transition, have been undertaken in some areas. In the United Arab Emirates, the ETME is marked by an abrupt transition from a lagoonal community rich in corals, calcareous sponges, and large bivalves to a fossiliferous substrate of oolitic grainstones and thrombolitic microbialites, recording a shift from biotic to abiotic calcification (Ge et al., 2018). Microbialites have been reported at the TJB in several studies (Ibarra et al., 2016; Ge et al., 2018), suggesting that the loss of so many marine invertebrate taxa during the ETME opened a niche for microbes, a pattern documented also at the Permian-Triassic boundary (e.g., Baud et al., 2007). At Ya Ha Tinda Ranch in Alberta, Canada, the T-OAE is marked by a change from a diverse pre-event community to one dominated by opportunistic, low-oxygen-tolerant taxa, with limited diversity (mainly bivalves and brachiopods) and significant reductions in body size (Martindale and Aberhan, 2017). At Ratnek El Kahla, Algeria, the T-OAE succession yielded evidence that oxygen deficiency affected even shallow benthic marine communities, and that, in view of a concurrent decline in primary productivity rates, lower aqueous $O_2$ levels were the product of rising seawater temperatures and slower ocean circulation rather than elevated marine productivity and aerobic respiration (Ruebsam et al., 2021, see Appendix).

Marine vertebrate diversity was also strongly affected by the ETME. Ichthyosaurs experienced an evolutionary bottleneck that reduced this clade to just four lineages, and it remained at low diversity through the remainder of the Mesozoic (Thorne et al., 2011). In contrast, the T-OAE appears to have had little effect on ichthyosaur diversity, and these large predators remained abundant throughout the interval of anoxia (Maxwell and Vincent, 2016). Following the T-OAE, a rapid invasion of the European Epicontinental Sea by large forms may reflect opportunistic feeding behavior and exploitation of ephemeral resources in response to rapid environmental change.

Biodiversity declines among both marine and terrestrial clades may have begun as early as the start of the Late Triassic (Rigo et al., 2020), although such declines, if real, were triggered by some mechanism other than the CAMP eruptions, which did not begin for another ~30 million years. Conventionally, the ETME has been thought to be multi-phased, with elevated extinction rates associated with each major perturbation of the global carbon cycle (Wignall and Atkinson, 2020; but see Fox et al., 2020). In western Sicily, the first negative CIE marks the disappearance of the large megalodontids, which were replaced by small and thin-shelled specimens, while the "Main" CIE corresponds to the last occurrence (LO) of the megalodontids and, approximately 50 m upsection, to the total demise of the Rhaetian benthic foraminifer community (Todaro et al., 2018). In the British Isles, the first extinction (in the lower Cotham Member) eliminated many bivalves and ostracods, whereas the second extinction (top of the Langport Member) caused the loss of further bivalves, ostracods, the last of the conodonts (Wignall and Atkinson, 2020) and phytosaurs (Fox et al., 2020). The two phases of marine extinction coincided with marked turnovers in palynofloral assemblages, with the interlude between them being dominated by fern spores (Bonis et al., 2010; Lindström, 2021). However, the palynological records of the St. Audries Bay section and the GSSP in Austria are not easily reconciled, as the order of sporomorph last occurrences relative to the invertebrate last occurrence is reversed.

The Early Toarcian mass extinction also had two stages: (i) at the onset of anoxia, with the extinction of most benthic species and the survival of a few adapted to thrive in low-oxygen conditions (Rodríguez-Tovar et al., 2017; Ros-Franch et al., 2019), and (ii) at the end of the anoxic interval, when newly evolved species colonized the re-oxygenated soft sediments, with the recovery fauna not resembling that which came before (Caruthers et al., 2013, 2014; Danise et al., 2013; Rodríguez-Tovar et al., 2019).

### 6.3. Extinction mechanisms

The climatic and environmental effects of the CAMP eruptions are thought to have been the primary cause of the ETME (Marzoli et al., 1999, 2004, 2018; Deenen et al., 2010; Whiteside et al., 2010; Lindström et al., 2021). Although CAMP activity commenced prior to the onset of the extinction event (Davies et al., 2017), the main extinction episode coincided with intensified magmatism and peak global warming, coincident with the I-NCIE. In Europe, there appear to be two extinction

levels, the first coinciding with regression (and closely associated with disruption of terrestrial floras, see Lindström, 2021), whilst the second occurred at a flooding surface marked by the spread of marine anoxia (Wignall and Atkinson, 2020; Fox et al., 2020). As CAMP eruptions gradually became less voluminous during the Hettangian, terrestrial ecosystems began to stabilize and marine clades such as ammonoids began to rediversify (Lindström et al., 2021).

The terminal Triassic crisis shares features with other extinction events (i.e., the Permian-Triassic boundary and early Toarcian), suggesting a common response to a common driver, i.e., large igneous province eruptions (Wignall and Atkinson, 2020). In this 'greenhouse extinction' scenario (cf. Kidder and Worsley, 2010), rapid warming of the oceans and atmosphere drove a cascade of environmental and ecological effects, including ocean stratification leading to deepwater anoxia (Kump et al., 2005; Richoz et al., 2012), enhanced terrestrial erosion and sediment flux to the oceans (Algeo and Twitchett, 2010), methane clathrate destabilization driving a positive warming feedback (Kidder and Worsley, 2010), ocean acidification (Črne et al., 2011), and prolonged instability in marine nutrient cycles, productivity rates, and organic carbon burial fluxes (Whiteside and Ward, 2011). Biomarker studies have documented water-column stratification and euxinia in many sections globally (Richoz et al., 2012; van de Schootbrugge et al., 2013; Kasprak et al., 2015), although the specific mechanisms by which greenhouse warming disturbed marine biogeochemical cycles are not yet clear.

The immediate causes of mass extinction remain in debate. In the terrestrial realm, deposition of volcanic pollutants that harmed vegetation has been identified as a major factor (van de Schootbrugge et al., 2009; Steinthorsdottir et al., 2018; Lindström et al., 2019; Gravendyck et al., 2020), although elevated $CO_2$ levels (i.e., lower $[O_2]/[CO_2]$) in the atmosphere and volcanic winters may also have been important (Yiotis et al., 2017). Despite the extraordinarily high $pCO_2$ of most of the Late Triassic and Early Jurassic, the recent discovery of lake-ice-rafted debris and dinosaur tracks in the Pangean arctic (Olsen et al., 2022) shows that wintertime freezing occurred in these high latitudes. Based on these discoveries, a major factor in dinosaurian survival through the ETME may have been that they were insulated, and therefore pre-adapted, to the intense volcanic winters of the CAMP eruptions, which overwhelmed the effects of global warming (Landwehrs et al., 2020) for a short but consequential interval of time. In the marine realm, ocean acidification has been implicated in several studies (Črne et al., 2011; Greene et al., 2012a, 2012b; Hönisch et al., 2012; Ikeda et al., 2015), although watermass anoxia (Martindale and Aberhan, 2017) and temperature changes were likely co-factors. These factors, or combinations of these factors, are similar to those that may have influenced other Phanerozoic extinction events.

## 7. Summary

A broad transition in the Earth system took place between the Late Triassic and the Middle Jurassic, with the most significant changes concentrated around the end-Triassic mass extinction and early Toarcian. The ultimate cause of this transition was the emplacement of two Large Igneous Provinces, associated with the progressive breakup of the Pangaean supercontinent and, later, its Gondwanan component.

While important questions remain in developing a mechanistic understanding of this transition, the contributions in this special issue show that progress is being made on a number of fronts. Combinations of carbon isotope stratigraphy, biostratigraphy, and astronomical chronology are solving longstanding questions of interregional correlation, allowing for stronger integration of the Tethyan and Panthalassic records. At the same time, it is becoming better understood that the Triassic-Jurassic transition was a complex event, expressed differently on the increasingly fragmented continents, and increasingly fragmented oceans, of the post-Pangaean world. New records of change in continental environments, and in a wide variety of marine settings, provide tremendous potential to reconstruct the progress of these linked crises across the globe.

## Declaration of Competing Interest

The authors declare that they have no conflicts of interest.

## Acknowledgments

The authors would like to thank the editors and editorial staff of *Earth Science Reviews* for their patience and help in putting together this special issue. We would also like to thank Sofie Lindström and Micha Ruhl for their constructive reviews that significantly improved this manuscript.

## Appendix 1 Summary of submissions to this special issue

Bordy et al. (2021) undertake a metastudy of the geochronology and fossil assemblages of the well-known upper Stormberg Group (Elliot and Clarens formations), in the main Karoo Basin in South Africa. Based on zircon U-Pb dating, magnetostratigraphy, and biostratigraphic correlations, they revise the stratigraphic framework of this group. Their analysis infers a mid-Norian through Rhaetian age for the lower Elliot Formation and a Hettangian–Sinemurian age for the upper Elliot Formation. This confirms the presence of the TJB within the Elliot Formation, making it one of the few fossiliferous continental units that records the ETME. A mainly Pliensbachian age was obtained for the overlying Clarens Formation. The authors show that sauropodomorphs, but not ornithischian or theropod, dinosaurs, were well-established in the main Karoo Basin by ~220 million years ago.

Du et al., (2020) study the demise of the conodont animal during the end-Triassic mass extinction (ETME). Establishing the timeline of its disappearance requires the use of an independent time marker for stratigraphic correlation, one that is not reliant on biostratigraphy. The interval prior to the ETME contains three negative CIEs, referred to as the "precursor" (P-NCIE), "initial" (I-NCIE) and "main" (M-NCIE) negative carbon isotope excursions. The authors integrate these carbon isotope excursions with existing biostratigraphy to correlate nine TJB sections, including both carbonate-dominated sections in the Tethys Ocean and abyssal chert sections from the central Panthalassic Ocean. In addition to their wide geographic distribution, the sections also represent a range of depositional water depths. Using this stratigraphic correlation, the authors chart the progressive disappearance of the conodont animal in sediments spanning the TJB. Their results show the final extinction of the taxon Conodonta to have been diachronous, with conodonts disappearing prior to the M-NCIE in most sections but persisting into the M-NCIE equivalent in the central Panthalassic Ocean, far from the CAMP eruptions. The one exception to this general pattern is the Csővár section in Hungary, where conodonts have been recovered from lowermost Jurassic strata, despite the section's location in the interior of the Tethys Ocean, which may reflect local paleoceanographic conditions.

Fujisaki et al. (2021) investigate redox conditions and nitrogen cycling within the central Panthalassic Ocean, based on redox-sensitive trace-element concentrations and bulk-nitrogen $\delta^{15}N$ data from the abyssal cherts of the Katsuyama section, SW Japan. The authors identify a negative nitrogen isotope excursion (NNIE) beginning in the earliest Jurassic, which can be divided into two phases based on organic carbon isotope stratigraphy. The authors infer that during the first phase of the NNIE, declining nitrogen isotope values were caused decreased nitrate utilization, as CAMP-driven global warming caused stratification and decreased primary productivity. In the second phase, continental weathering and upwelling of nitrate rich dep water led to eutrophic conditions. Trace element data indicates that the deep waters of the central Panthalassic Ocean remained oxic throughout the TJB interval, though the water column oxygen minimum zone likely expanded

significantly during the extinction interval. Likewise, nitrate remained the predominant form of dissolved inorganic nitrogen in the global ocean. This paper is among the first to identify an expanded water column oxygen minimum in the pelagic ocean, showing that expansion of oceanic oxygen minima and changes to the marine nitrogen cycle may have been key factors contributing to the end-Triassic mass extinction.

Hesselbo et al. (2021a) present an extensive carbon and oxygen isotope dataset from Lower Jurassic (Hettangian and lower Sinemurian) mollusks and brachiopods collected from biostratigraphically well-calibrated coastal outcrops in the Bristol Channel and Hebrides basins (UK). These sections represent the southern part of the Laurasian Seaway, connecting the Tethys and Boreal oceans. The authors document a positive (~3 ‰) CIE immediately above the TJB (in the *tilmanni* ammonite Biozone), followed by a pronounced negative CIE (the 'Main Negative CIE') spanning the Hettangian Stage. A shift toward higher values is seen at the Hettangian-Sinemurian boundary and throughout the lower Sinemurian, with peak values of +4.3 ‰ near the top of the lower Sinemurian. This long-term positive trend is evidence of prolonged period of enhanced organic carbon burial that is inferred to have occurred in the extensive system of lacustrine and marine rifts that traversed a fragmenting Pangea after emplacement of the Central Atlantic Magmatic Province. In parallel, oxygen-isotope values of the skeletal carbonate show a continuous downward trend from the lower part of the Hettangian (~ −1 ‰ $\delta^{18}O_{carb}$ in the *planorbis* Zone) to the top of the lower Sinemurian (~ −2.5 ‰ $\delta^{18}O_{carb}$ in the higher *turneri* Zone), recording a gradual temperature rise and/or addition of a meteoric or cryospheric water component. Consequently, any atmospheric carbon-dioxide drawdown effect on global palaeotemperatures, as suggested by progressively increasing $\delta^{13}C_{carb}$ values and assuming a constant silicate weathering sink, was more than counterbalanced in the seaway by regional processes that led to significantly warmer bottom water temperatures.

Lindström et al. (2021) offer a metastudy of the relationship of CAMP magmatism to the Triassic–Jurassic biotic crisis. This study presents a comprehensive review of radioisotopic ages of CAMP intrusives and extrusives, a compilation of potentially volcanically related proxy records including $\delta^{13}C$, $pCO_2$, iridium and other platinum group elements, mercury, polycyclic aromatic hydrocarbons (PAH), charcoal, and $SO_2$, and an analysis of their relationship to the timing of biotic declines and extinctions among multiple biotic clades including ammonoids, radiolarians, conodonts, dinocysts, and spores and pollen. The authors conclude that: (1) CAMP activity commenced prior to the onset of the marine extinctions, (2) an initial negative $\delta^{13}C$ excursion (the Marshi CIE) was due to emission of isotopically light carbon linked to eruption of Tiourjdal and Prevalent group lavas, (3) pedogenic carbonates provide evidence of a more than twofold increase in atmospheric $pCO_2$ at that time, and (4) a temporary cooling occurred after the Marshi CIE. They further find that the main extinction interval coincided with intensified magmatism and peak global warming, coincident with the Spelae CIE. The extinction interval coincided with increased subaerial weathering, and the devastation of terrestrial plant communities by excess sulfur dioxide deposition. Isotopic records provide evidence for the massive release of isotopically light carbon and sulfur at this time, which the authors speculate may be derived from sill intrusions into the organic- and evaporite-rich Trans-Amazonian basins. Finally, they infer that CAMP eruptions became progressively voluminous during the Hettangian, as indicated by cooling following the Spelae CIE, a stabilization of terrestrial ecosystems, and incipient rediversification of ammonoids.

Petryshyn et al. (2021) generate sea-surface temperature and $\delta^{18}O_{water}$ values based on clumped isotope (Δ47) measurements of a ~20-cm-thick, shallow-marine microbialite horizon from the Cotham Member of the Lilstock Formation near Bristol, UK. This horizon, although of limited duration (estimated to be 1-80 kyr), is considered to be correlative with the TJB extinction horizon and, thus, has the potential to test competing hypotheses regarding the pattern of temperature change during the TJB event and its relationship to contemporaneous extinctions—both short-term cooling (~100s of years) related to sulfur aerosols and longer-term warming (~10,000 yr) related to $CO_2$ emissions have been proposed. This study identified mild to warm ocean temperatures during the extinction event marked by repeated short-term swings of ~16 °C, which is interpreted as a signature of strong local seasonality, but no apparent evidence for short-term cooling or initial warming through the study interval, implying that the initial onset of the biodiversity crisis may necessitate another mechanism. These results are significant in constituting the oldest non-biomineralized marine seasonal temperature record.

Pieńkowski et al. (2021) focus on the relationships between the carbon isotopic composition of wood, continental organic matter fluxes ($TOC_{cont}$), and ambient air temperatures. They report an empirical positive relationship between $\delta^{13}C_{wood}$ and $TOC_{cont}$ in Rhaetian/Lower Jurassic strata from Kaszewy, Poland, that is inferred to be related to the efficiency of terrestrial biodegradation of woody material. Specifically, warming triggered by a flux of $^{12}C$-enriched methane enhances fungal-bacterial decomposition of wood, reducing the flux of woody debris to marine environments and decreasing its $\delta^{13}C$. This relationship can be converted to palaeotemperature estimates using an independently calibrated (stomatal) $pCO_2$ record. Based on the $\delta^{13}C_{wood}/TOC_{cont}$ relationship, qualitative trends in air temperature can be reconstructed for c. 40°N paleolatitude (i.e., the warm temperate climatic zone). The authors note that deposits from coastal/deltaic facies are most suitable for studying these relationships because they contain organic material that is delivered from a large catchment area, and thus represent a broad spatial average. This study also reports a detailed chemostratigraphic correlation of these marginal/non-marine Polish deposits with the biostratigraphically well-constrained Llanbedr (Mochras Farm) core in N. Wales and other marine succession, supported by sequence stratigraphic correlation and biostratigraphic markers.

Remírez and Algeo (2021a) undertake a metastudy of the global carbon cycle during the Early Jurassic T-OAE, which was characterized by widespread deposition of organic-rich sediments and a large negative CIE. The T-OAE exhibits significant interregional variation in its expression, being particularly pronounced in the Northwest European Shelf (NWES) region, where sediments exhibit a CIE of –5 to –7 ‰ and TOC content as high as ~10 %. Its more limited expression in other regions suggests that the NWES was subject to regional oceanographic factors that led to strong development of watermass stratification, deepwater anoxia, and organic matter accumulation. At a global scale, the most characteristic feature of the T-OAE is its negative CIE, rather than a shift to reducing redox conditions. The available data are consistent with Karoo-Ferrar Large Igneous Province magmatism as the trigger of the T-OAE.

Remírez and Algeo (2021b) examine the nature of the T-OAE in the classic coastal exposures of the Cleveland Basin (UK), where the peak of the T-OAE is marked by laminated, pyritic, organic-rich black shales called the Jet Rock. Several competing hypotheses have been advanced to account for this deposit: (1) McArthur et al. (2008) proposed that increased freshwater runoff caused a low-salinity surface layer to expand, preventing deepwater exchange with the open ocean, intensifying water-column stratification and deep-water anoxia, whereas (2) Thibault et al. (2018) proposed that sea-level rise caused deepening within the Cleveland Basin that promoted anoxia. A key point of contention was interpretation of Mo/TOC ratios, which are exceptionally low within the Jet Rock: Hypothesis 1 regarded the low values as evidence of deep-water restriction within the Cleveland Basin, with enhanced removal of aqueous Mo to the sediment under euxinic conditions and a lack of Mo resupply from the open ocean due to reduced deepwater exchange. Hypothesis 2 inferred that the low values were due to regional (i.e., across the Northwest European Shelf) or global drawdown of seawater Mo, due to a massive flux of Mo to euxinic sediments. A key difference was that Hypothesis 1 predicted freshening of the Cleveland Basin watermass, whereas Hypothesis 2 predicted a shift

toward more saline conditions or, possibly, maintenance of fully marine conditions. Remírez and Algeo (2021b) tested these competing models using newly proposed shale paleosalinity proxies. Their dataset showed a decline in B/Ga from ~6 (fully marine) in the pre-T-OAE interval to ~1 (strongly reduced salinity) at the peak of this event, followed by a return to ~6 (fully marine) in its aftermath, strongly supporting the McArthur et al. (2008) model. The possible implications of marine fossils in the Jet Rock and other issues pertaining to Cleveland Basin paleosalinity interpretations were debated in Hesselbo et al. (2021b) and Remírez and Algeo (2021c).

Ruebsam et al. (2021) investigate environmental controls on a shallow-marine faunal community in the Toarcian section at Ratnek El Kahla, Algeria, located on the northern Gondwana paleomargin. The development of a 'benthic barren interval' in this section, and other oxygenated shelf sections in the region, indicates that even shallow water environments lacking black shales experienced a Toarcian crisis. The barren interval at Ratnek El Kahla coincides with the climax of the T-OAE and correlates with its characteristic negative CIE. Compared to background values, sediments in the benthic barren interval are enriched in organic matter and redox-sensitive metals, and they contain better-preserved bacterial lipids and more highly sulfurized organic matter, attesting to a decline in pore water $O_2$ and increased $H_2S$ concentrations. While these observations suggest that shallow benthic communities suffered from prolonged oxygen-deficient conditions, lowered oxygen levels cannot have resulted from increased aerobic decomposition of organic matter, in view of the concurrent decline in primary productivity. Rather, seafloor anoxia was driven by rising seawater temperatures and slowed ocean circulation linked to a hyper-greenhouse climate.

Ruhl et al. (2021) present a detailed study of the Triassic–Jurassic transition in the Neuquén Basin of Argentina. The authors report total organic carbon content, pyrolysis analysis, organic carbon isotopes, elemental mercury concentrations, and other elemental data from this Southern Hemisphere basin on the margin of the eastern Panthalassic Ocean. They find that the end-Triassic mass extinction coincided with a minor negative CIE in bulk organic matter, with the small magnitude of the excursion (2–3‰) possibly related to the extreme aridity of the adjacent Pangean landmass, which may have led to a limited flux of terrestrial organic matter to the basin. Increased mercury deposition can be detected in the basin prior to the negative CIE associated with the end-Triassic mass extinction, and thus cannot be directly related to extrusive CAMP activity. Intrusive CAMP activity, and interactions with the intruded rock, may have been a major source of Hg to the atmosphere. Low-oxygen conditions, coinciding with enhanced organic matter preservation, developed in the basin during the Triassic–Jurassic transition. The authors present mass-balance calculations showing that changes in carbon burial are sufficient to explain observed fluctuation in the global exogenic carbon cycle across the TJB.

Schoepfer et al. (2022) investigate the flux of mercury (Hg) as a proxy for volcanic inputs to a site in the central Panthalassic Ocean (Kurusu, Japan). Hg concentrations are strongly correlated with sedimentary sulfide content in this radiolarian chert section, indicating that pyrite is the dominant host of mercury. However, a distinct increase in the Hg/sulfur ratio near the TJB may record enhanced Hg inputs from CAMP volcanism. The rhythmically bedded nature of the sediments allowed construction of a floating astronomical age model tied to the radiolarian-defined Triassic–Jurassic boundary. A series of discrete spikes in sulfide concentration up to ~1 Myr before the ETME record precursor environmental stresses, also correlating with changes in plankton community composition. The authors infer that these changes reflect the development of stratification in the water column, with reducing conditions developing in the thermocline below the surface mixed layer. Comparing the evidence from Kurusu to other Panthalassic sections, the authors propose a model in which water-column stratification began to develop in the open Panthalassic Ocean as much as ~1 Myr before the Triassic–Jurassic boundary. By ~400 kyr before the boundary, this rising chemocline was impinging on slopes of island arcs and the South American continental margin. In this interpretation, the end-Triassic extinction coincided with both the main phase of CAMP eruptions and the irruption of reducing deep waters into photic zone and shelf environments.

Song et al. (2021) investigate secular variation in wildfire frequency during the Late Triassic (late Norian) to early Middle Jurassic (Aalenian) in two terrestrial sections from the Sichuan Basin of South China. The proxies used in this study are polycyclic aromatic hydrocarbons (PAHs) of probable wildfire origin, including pyrene, benzofluoranthene, benzo[e]pyrene, indeno[1,2,3-cd]pyrene, benzo[ghi]perylene, and coronene. They identify sharp increases in the abundances of both pyrolytic PAHs (related to wildfire) and oxygenated PAHs with furan structure (related to enhanced soil erosion or weathering) at two horizons within the Rhaetian Stage (R1 and R2), and at the TJB. They infer that, although CAMP-induced climate changes set the stage for more frequent wildfires in South China, the immediate trigger was probably a southward shift of the paleo-Intertropical Convergence Zone (ITCZ). These observations suggest a complex feedback involving climatic warming, precipitation and evapotranspiration, vegetation density, and wildfire prevalence during the Tr-J transition.

van de Schootbrugge et al. (2021) examine the palynomorph content of four Upper Triassic-Lower Jurassic sections in France, Germany, and Denmark. They find strong evidence for intense soil erosion on continental landmasses at the TJB, coinciding with the emplacement of the CAMP. Latest Rhaetian sediments, deposited in different basins across NW Europe, record a dramatic increase in the incidence of reworked Palaeozoic and Neoproterozoic palynomorphs derived from eroded soil and regolith. Increased erosion coincided with the disappearance of dominant Triassic pollen taxa and a proliferation in fern spores. The underlying cause of these changes was deforestation, soil loss, and deep erosion, which is revealed by an inverted stratigraphy, whereby the age of the reworked material increases upsection. These changes were due to volcanism, climatic change, and forest fires during the Tr-J transition.

Yager et al. (2021) focus on mercury and mercury isotopes as proxies for large igneous province magmatism. To assess the degree to which depositional environment controls the accumulation of mercury, the authors compare Hg records and other geochemical data from five TJB sections, including Tethyan carbonate sections from southern Europe and Panthalassic sections from the western Pangean shelf. Measurements of organic carbon and carbonate content, mercury content, and mercury stable isotopes show that sedimentary environments and depositional mechanisms exercise a strong control on the appearance of mercury anomalies in marine sedimentary strata. Hg/TOC increases around the TJB are observed in all sections, corresponding well with the timing of CAMP emplacement at St. Audries Bay (UK) and New York Canyon (Nevada). However, other sections show a prolonged interval of elevated Hg/TOC ratios extending into the Hettangian. While Hg isotope values were influenced by depositional water depth, all sections show a decrease in mass-independent mercury isotope fractionation during the end-Triassic mass extinction, indicating a large influx of exogenous mercury that can be attributed to CAMP magmatism.

## References

Ait-Itto, F.Z., Martinez, M., Price, G.D., Addi, A.A., 2018. Synchronization of the astronomical time scales in the Early Toarcian: a link between anoxia, carbon-cycle perturbation, mass extinction and volcanism. Earth Planet. Sci. Lett. 493, 1–11.

Algeo, T.J., Ingall, E., 2007. Sedimentary $C_{org}$:P ratios, paleocean ventilation, and phanerozoic atmospheric $pO_2$. Palaeogeogr. Palaeoclimatol. Palaeoecol. 256 (3-4), 130–155.

Algeo, T.J., Twitchett, R.J., 2010. Anomalous early triassic sediment fluxes due to elevated weathering rates and their biological consequences. Geology 38 (11), 1023–1026.

Alroy, J., 2010. The shifting balance of diversity among major marine animal groups. Science 329 (5996), 1191–1194.

Al-Suwaidi, A.H., Hesselbo, S.P., Damborenea, S.E., Manceñido, M.O., Jenkyns, H.C., Riccardi, A.C., Angelozzi, G.N., Baudin, F., 2016. The Toarcian Oceanic Anoxic Event

(Early Jurassic) in the Neuquén Basin, Argentina: a reassessment of age and carbon isotope stratigraphy. J. Geol. 124 (2), 171–193.
Arabas, A., Schlögl, J., Meister, C., 2017. Early Jurassic carbon and oxygen isotope records and seawater temperature variations: insights from marine carbonate and belemnite rostra (Pieniny Klippen Belt, Carpathians). Palaeogeogr. Palaeoclimatol. Palaeoecol. 485, 119–135.
Armendáriz, M., Rosales, I., Bádenas, B., Aurell, M., García-Ramos, J.C., Piñuela, L., 2012. High-resolution chemostratigraphic records from Lower Pliensbachian belemnites: palaeoclimatic perturbations, organic facies and water mass exchange (Asturian basin, northern Spain). Palaeogeogr. Palaeoclimatol. Palaeoecol. 333, 178–191.
Bailey, T.R., Rosenthal, Y., McArthur, J.M., Van de Schootbrugge, B., Thirlwall, M.F., 2003. Paleoceanographic changes of the Late Pliensbachian-Early Toarcian interval: a possible link to the genesis of an Oceanic Anoxic Event. Earth Planet. Sci. Lett. 212 (3-4), 307–320.
Baker, S.J., Hesselbo, S.P., Lenton, T.M., Duarte, L.V., Belcher, C.M., 2017. Charcoal evidence that rising atmospheric oxygen terminated Early Jurassic ocean anoxia. Nat. Commun. 8 (1), 1–7.
Balini, M., Lucas, S.G., Jenks, J.F., Spielmann, J.A., 2010. Triassic ammonoid biostratigraphy: an overview. In: Lucas, S.G. (Ed.), Triassic Timescale, Geological Society of London Special Publication, 334, pp. 221–262.
Bambach, R.K., 2006. Phanerozoic biodiversity mass extinctions. Annu. Rev. Earth Planet. Sci. 34, 127–155.
Baranyi, V., Pálfy, J., Görög, Á., Riding, J.B., Raucsik, B., 2016. Multiphase response of palynomorphs to the Toarcian oceanic anoxic event (Early Jurassic) in the Réka Valley section, Hungary. Rev. Palaeobot. Palynol. 235, 51–70.
Barbacka, M., Pacyna, G., Kocsis, Á.T., Jarzynka, A., Ziaja, J. and Bodor, E., 2017. Changes in terrestrial floras at the Triassic–Jurassic Boundary in Europe. Palaeogeogr. Palaeoclimatol. Palaeoecol. 480, 80-93.
Barnes, B.D., Sclafani, J.A., Zaffos, A., 2021. Dead clades walking are a pervasive macroevolutionary pattern. Proc. Natl. Acad. Sci. 118 (15).
Barras, C.G., Twitchett, R.J., 2007. Response of the marine infauna to Triassic–Jurassic environmental change: ichnological data from southern England. Palaeogeogr. Palaeoclimatol. Palaeoecol. 244 (1-4), 223–241.
Barras, C.G., Twitchett, R.J., 2016. The late Triassic mass extinction event. In: Mángano, M.G., Buatois, L.A. (Eds.), The Trace-Fossil Record of Major Evolutionary Events, v. 2. Springer, Dordrecht, pp. 1–17. Mesozoic and Cenozoic.
Baud, A., Richoz, S., Pruss, S., 2007. The lower Triassic anachronistic carbonate facies in space and time. Glob. Planet. Chang. 55 (1-3), 81–89.
Baudin, F., Herbin, J.P., Vandenbroucke, M., 1990. Mapping and geochemical characterization of the Toarcian organic matter in the Mediterranean Tethys and Middle East. Org. Geochem. 16 (4–6), 677–687.
Beerling, D.J., Berner, R.A., 2002. Biogeochemical constraints on the Triassic-Jurassic boundary carbon cycle event. Glob. Biogeochem. Cycles 16 (3), 10–11.
Beith, S.J., Fox, C.P., Marshall, J.E., Whiteside, J.H., 2021. Recurring photic zone euxinia in the northwest Tethys impinged end-Triassic extinction recovery. Palaeogeogr. Palaeoclimatol. Palaeoecol. 584, 110680.
Belcher, C.M., Mander, L., Rein, G., Jervis, F.X., Haworth, M., Hesselbo, S.P., Glasspool, I. J., McElwain, J.C., 2010. Increased fire activity at the Triassic/Jurassic boundary in Greenland due to climate-driven floral change. Nat. Geosci. 3 (6), 426–429.
Bernardi, M., Petti, F.M., Piñuela, L., García-Ramos, J.C., Avanzini, M., Lockley, M.G., 2016. The Mesozoic vertebrate radiation in terrestrial settings. In: Mángano, M.G., Buatois, L.A. (Eds.), The Trace-Fossil Record of Major Evolutionary Events, *Volume 2:* Mesozoic and Cenozoic. Springer, Dordrecht, pp. 135–177.
Berner, R.A., Beerling, D.J., 2007. Volcanic degassing necessary to produce a CaCO3 undersaturated ocean at the Triassic–Jurassic boundary. Palaeogeogr. Palaeoclimatol. Palaeoecol. 244 (1–4), 368–373.
Berner, Z.A., Puchelt, H., Noeltner, T., Kramar, U.T.Z., 2013. Pyrite geochemistry in the Toarcian Posidonia Shale of south-west Germany: evidence for contrasting trace-element patterns of diagenetic and syngenetic pyrites. Sedimentology 60 (2), 548–573.
Bertling, M., 1999. Late Jurassic reef bioerosion–the dawning of a new era. Geology 45, 173–176.
Bice, D.M., Newton, C.R., McCauley, S., Reiners, P.W., McRoberts, C.A., 1992. Shocked quartz at the Triassic–Jurassic boundary in Italy. Science 255 (5043), 443–446.
Blackburn, T.J., Olsen, P.E., Bowring, S.A., McLean, N.M., Kent, D.V., Puffer, J., McHone, G., Rasbury, E.T., Et-Touhami, M., 2013. Zircon U-Pb geochronology links the end-Triassic extinction with the Central Atlantic Magmatic Province. Science 340 (6135), 941–945.
Blomeier, D.P., Reijmer, J.J., 1999. Drowning of a Lower Jurassic carbonate platform: Jbel Bou Dahar, High Atlas, Morocco. Facies 41 (1), 81–110.
Blumenberg, M., Heunisch, C., Lückge, A., Scheeder, G., Wiese, F., 2016. Photic zone euxinia in the central Rhaetian Sea prior the Triassic–Jurassic boundary. Palaeogeogr. Palaeoclimatol. Palaeoecol. 461, 55–64.
Bodin, S., Krencker, F.N., Kothe, T., Hoffmann, R., Mattioli, E., Heimhofer, U., Kabiri, L., 2016. Perturbation of the carbon cycle during the late Pliensbachian–early Toarcian: new insight from high-resolution carbon isotope records in Morocco. J. Afr. Earth Sci. 116, 89–104.
Bodin, S., Mattioli, E., Fröhlich, S., Marshall, J.D., Boutib, L., Lahsini, S., Redfern, J., 2010. Toarcian carbon isotope shifts and nutrient changes from the Northern margin of Gondwana (High Atlas, Morocco, Jurassic): palaeoenvironmental implications. Palaeogeogr. Palaeoclimatol. Palaeoecol. 297 (2), 377–390.
Bond, D.P., Grasby, S.E., 2017. On the causes of mass extinctions. Palaeogeogr. Palaeoclimatol. Palaeoecol. 478, 3–29.
Bonis, N.R., Kürschner, W.M., 2012. Vegetation history, diversity patterns, and climate change across the Triassic/Jurassic boundary. Paleobiology 38, 240–264.
Bonis, N.R., Van Konijnenburg-Van Cittert, J.H.A., Kürschner, W.M., 2010. Changing $CO_2$ conditions during the end-Triassic inferred from stomatal frequency analysis on *Lepidopteris ottonis* (Goeppert) Schimper and *Ginkgoites taeniatus* (Braun) Harris. Palaeogeogr. Palaeoclimatol. Palaeoecol. 295, 146–161.
Boomer, I., Copestake, P., Raine, R., Azmi, A., Fenton, J.P., Page, K.N., O'Callaghan, M., 2021. Stratigraphy, palaeoenvironments and geochemistry across the Triassic–Jurassic boundary transition at Carnduff, County Antrim, Northern Ireland. Proceedings of the Geologist Association 132 (6), 667–687.
Bordy, E.M., Abrahams, M., Sharman, G.R., Viglietti, P.A., Benson, R.B., McPhee, B.W., Barrett, P.M., Sciscio, L., Condon, D., Mundil, R., Rademan, Z., 2021. A chronostratigraphic framework for the upper Stormberg Group: Implications for the Triassic–Jurassic boundary in southern Africa. Earth Sci. Rev. 103120 in press.
Boulila, S., Galbrun, B., Huret, E., Hinnov, L.A., Rouget, I., Gardin, S., Bartolini, A., 2014. Astronomical calibration of the Toarcian Stage: implications for sequence stratigraphy and duration of the early Toarcian OAE. Earth Planet. Sci. Lett. 386, 98–111.
Boulila, S., Hinnov, L.A., 2017. A review of tempo and scale of the early Jurassic Toarcian OAE: implications for carbon cycle and sea level variations. Newsl. Stratigr. 50 (4), 363–389.
Brazier, J.M., Suan, G., Tacail, T., Simon, L., Martin, J.E., Mattioli, E., Balter, V., 2015. Calcium isotope evidence for dramatic increase of continental weathering during the Toarcian oceanic anoxic event (Early Jurassic). Earth Planet. Sci. Lett. 411, 164–176.
Bromley, R.G., 2004. A stratigraphy of marine bioerosion. In: McIlroy, D. (Ed.), The Application of Ichnology to Palaeoenvironmental and Stratigraphic Analysis, 228, pp. 455–479. Geological Society of London Special Publication.
Brusatte, S.L., Benton, M.J., Ruta, M., Lloyd, G.T., 2008a. Superiority, competition, and opportunism in the evolutionary radiation of dinosaurs. Science 321 (5895), 1485–1488.
Brusatte, S.L., Benton, M.J., Ruta, M., Lloyd, G.T., 2008b. The first 50 Myr of dinosaur evolution: macroevolutionary pattern and morphological disparity. Biol. Lett. 4 (6), 733–736.
Buatois, L.A., Carmona, N.B., Curran, H.A., Netto, R.G., Mángano, M.G., Wetzel, A., 2016. The Mesozoic marine revolution. In: The trace-fossil record of major evolutionary events. Springer, Dordrecht, pp. 19–134.
Burgess, S.D., Bowring, S.A., Fleming, T.H., Elliot, D.H., 2015. High-precision geochronology links the Ferrar large igneous province with early-Jurassic ocean anoxia and biotic crisis. Earth Planet. Sci. Lett. 415, 90–99.
Callegaro, S., Rigo, M., Chiaradia, M., Marzoli, A., 2012. Latest Triassic marine Sr isotopic variations, possible causes and implications. Terra Nova 24 (2), 130–135.
Capriolo, M., Marzoli, A., Aradi, L.E., Callegaro, S., Dal Corso, J., Newton, R.J., Mills, B. J., Wignall, P.B., Bartoli, O., Baker, D.R., Youbi, N., 2020. Deep $CO_2$ in the end-Triassic Central Atlantic Magmatic Province. Nat. Commun. 11 (1), 1670, 11 pp.
Capriolo, M., Mills, B.J., Newton, R.J., Dal Corso, J., Dunhill, A.M., Wignall, P.B., Marzoli, A., 2022. Anthropogenic-scale CO2 degassing from the Central Atlantic Magmatic Province as a driver of the end-Triassic mass extinction. Glob. Planet. Chang. 209, 103731.
Carter, E.S., Hori, R.S., 2005. Global correlation of the radiolarian faunal change across the Triassic–Jurassic boundary. Can. J. Earth Sci. 42 (5), 777–790.
Carter, E.S., Goričan, Š., Guex, J., O'Dogherty, L., De Wever, P., Dumitrica, P., Hori, R.S., Matsuoka, A., Whalen, P.A., 2010. Global radiolarian zonation for the Pliensbachian, Toarcian and Aalenian. Palaeogeogr. Palaeoclimatol. Palaeoecol. 297 (2), 401–419.
Caruthers, A.H., Gröcke, D.R., Smith, P.L., 2011. The significance of an Early Jurassic (Toarcian) carbon-isotope excursion in Haida Gwaii (Queen Charlotte Islands), British Columbia, Canada. Earth Planet. Sci. Lett. 307 (1–2), 19–26.
Caruthers, A.H., Smith, P.L., Gröcke, D.R., 2013. The Pliensbachian–Toarcian (Early Jurassic) extinction, a global multi-phased event. Palaeogeogr. Palaeoclimatol. Palaeoecol. 386, 104–118.
Caruthers, A.H., Smith, P.L., Gröcke, D.R., 2014. The Pliensbachian-Toarcian (Early Jurassic) extinction: a North American perspective. In: Keller, G., Kerr, A.C. (Eds.), Volcanism, Impacts, and Mass Extinctions: Causes and Effects, Geol. Soc. Am. Spec. Pap., 505, pp. 225–243.
Caswell, B.A., Coe, A.L., 2012. A high-resolution shallow marine record of the Toarcian (Early Jurassic) Oceanic Anoxic Event from the East Midlands Shelf, UK. Palaeogeogr. Palaeoclimatol. Palaeoecol. 365-366, 124–135.
Caswell, B.A., Coe, A.L., 2013. Primary productivity controls on opportunistic bivalves during Early Jurassic oceanic deoxygenation. Geology 41, 1163–1166.
Caswell, B.A., Dawn, S.J., 2019. Recovery of benthic communities following the Toarcian oceanic anoxic event in the Cleveland Basin, UK. Palaeogeogr. Palaeoclimatol. Palaeoecol. 521, 114–126.
Caswell, B.A., Frid, C.L., 2017. Marine ecosystem resilience during extreme deoxygenation: the Early Jurassic oceanic anoxic event. Oecologia 183 (1), 275–290.
Cleveland, D.M., Nordt, L.C., Dworkin, S.I., Atchley, S.C., 2008. Pedogenic carbonate isotopes as evidence for extreme climatic events preceding the Triassic–Jurassic boundary: Implications for the biotic crisis? Pedogenic carbonate isotopes as evidence for Late Triassic climate changes. GSA Bull. 120 (11-12), 1408–1415.
Cohen, A.S., Coe, A.L., 2002. New geochemical evidence for the onset of volcanism in the Central Atlantic magmatic province and environmental change at the Triassic–Jurassic boundary. Geology 30 (3), 267–270.
Cohen, A.S., Coe, A.L., 2007. The impact of the Central Atlantic Magmatic Province on climate and on the Sr-and Os-isotope evolution of seawater. Palaeogeogr. Palaeoclimatol. Palaeoecol. 244 (1-4), 374–390.
Cohen, A.S., Coe, A.L., Harding, S.M., Schwark, L., 2004. Osmium isotope evidence for the regulation of atmospheric CO2 by continental weathering. Geology 32 (2), 157–160.
Cohen, B.E., Mark, D.F., Lee, M.R., Simpson, S.L., 2017. A new high-precision $^{40}Ar/^{39}Ar$ age for the Rochechouart impact structure: At least 5 Ma older than the Triassic–Jurassic boundary. Meteorit. Planet. Sci. 52 (8), 1600–1611.

Cohen, K.M., Harper, D.A.T., Gibbard, P.L., 2022. ICS International Chronostratigraphic Chart 2021/05. International Commission on Stratigraphy. IUGS. www.stratigraphy.org (visited: 7/8/2021).
Correia, V.F., Riding, J.B., Duarte, L.V., Fernandes, P., Pereira, Z., 2017. The palynological response to the Toarcian Oceanic Anoxic Event (Early Jurassic) at Peniche, Lusitanian Basin, western Portugal. Mar. Micropaleontol. 137, 46–63.
Corsetti, F.A., Ritterbush, K.A., Bottjer, D.J., Greene, S.E., Ibarra, Y., Yager, J.A., West, A. J., Berelson, W.M., Rosas, S., Becker, T.W., Levine, N.M., 2015. Investigating the paleoecological consequences of supercontinent breakup: sponges clean up in the early Jurassic. The Sediment. Rec. 13 (2), 4–10.
Courtillot, V., 1994. Mass extinctions in the last 300 million years: one impact and seven flood basalts. Israel J. Earth Sci. 43 (255), 66.
Courtillot, V.E., Renne, P.R., 2003. On the ages of flood basalt events. C. R. Geosci. 335 (1), 113–140.
Cox, K.G., 1978. Flood basalts, subduction and the break-up of Gondwanaland. Nature 274, 47–49.
Cramer, B.D., Jarvis, I., 2020. Carbon isotope stratigraphy. In: Geologic Time Scale 2020. Elsevier, pp. 309–343.
Črne, A.E., Weissert, H., Goričan, S., Bernasconi, S.M., 2011. A biocalcification crisis at the Triassic–Jurassic boundary recorded in the Budva Basin (Dinarides, Montenegro). GSA Bull. 123, 40–50.
da Rocha, R.B., Mattioli, E., Duarte, L.V., Pittet, B., Elmi, S., Mouterde, R., Cabral, M.C., Comas-Rengifo, M.J., Gómez, J.J., Goy, A., Hesselbo, S.P., 2016. Base of the Toarcian stage of the lower Jurassic defined by the global boundary stratotype section and point (GSSP) at the Peniche section (Portugal). Episodes J. Int. Geosci. 39 (3), 460–481.
Danise, S., Twitchett, R.J., Little, C.T., 2015. Environmental controls on Jurassic marine ecosystems during global warming. Geology 43 (3), 263–266.
Danise, S., Twitchett, R.J., Little, C.T.S., Clemence, M.E., 2013. The impact of global warming and anoxia on marine benthic community dynamics: an example from the Toarcian (Early Jurassic). PLoS One 8, e56255.
Davies, J.H.F.L., Marzoli, A., Bertrand, H., Youbi, N., Ernesto, M., Greber, N.D., Ackerson, M., Simpson, G., Bouvier, A.S., Baumgartner, L., Pettke, T., 2021. Zircon petrochronology in large igneous provinces reveals upper crustal contamination processes: new U–Pb ages, Hf and O isotopes, and trace elements from the Central Atlantic magmatic province (CAMP). Contrib. Mineral. Petrol. 176 (1), 1–24.
Davies, J.H.F.L., Marzoli, A., Bertrand, H., Youbi, N., Ernesto, M., Schaltegger, U., 2017. End-Triassic mass extinction started by intrusive CAMP activity. *Nature.* Communications *8* (1), 15596, 8 pp.
de Jersey, N.J., McKellar, J.L., 2013. The palynology of the Triassic–Jurassic transition in southeastern Queensland, Australia, and correlation with New Zealand. Palynology 37 (1), 77–114.
Deenen, M.H., Ruhl, M., Bonis, N.R., Krijgsman, W., Kürschner, W.M., Reitsma, M., Van Bergen, M.J., 2010. A new chronology for the end-Triassic mass extinction. Earth Planet. Sci. Lett. 291 (1-4), 113–125.
Dera, G., Pellenard, P., Neige, P., Deconinck, J.F., Pucéat, E., Dommergues, J.L., 2009a. Distribution of clay minerals in Early Jurassic Peritethyan seas: palaeoclimatic significance inferred from multiproxy comparisons. Palaeogeogr. Palaeoclimatol. Palaeoecol. 271 (1-2), 39–51.
Dera, G., Pucéat, E., Pellenard, P., Neige, P., Delsate, D., Joachimski, M.M., Reisberg, L., Martinez, M., 2009b. Water mass exchange and variations in seawater temperature in the NW Tethys during the Early Jurassic: evidence from neodymium and oxygen isotopes of fish teeth and belemnites. Earth Planet. Sci. Lett. 286 (1-2), 198–207.
Dera, G., Donnadieu, Y., 2012. Modeling evidences for global warming, Arctic seawater freshening, and sluggish oceanic circulation during the Early Toarcian anoxic event. Paleoceanography 27 (2).
Dera, G., Neige, P., Dommergues, J.L., Brayard, A., 2011a. Ammonite paleobiogeography during the Pliensbachian-Toarcian crisis (Early Jurassic) reflecting paleoclimate, eustasy, and extinctions. Glob. Planet. Chang. 78 (3-4), 92–105.
Dera, G., Brigaud, B., Monna, F., Laffont, R., Pucéat, E., Deconinck, J.F., Pellenard, P., Joachimski, M.M., Durlet, C., 2011b. Climatic ups and downs in a disturbed Jurassic world. Geology 39 (3), 215–218.
Dera, G., Prunier, J., Smith, P.L., Haggart, J.W., Popov, E., Guzhov, A., Rogov, M., Delsate, D., Thies, D., Cuny, G., Pucéat, E., 2015. Nd isotope constraints on ocean circulation, paleoclimate, and continental drainage during the Jurassic breakup of Pangea. Gondwana Res. 27 (4), 1599–1615.
Dera, G., Toumoulin, A., De Baets, K., 2016. Diversity and morphological evolution of Jurassic belemnites from South Germany. Palaeogeogr. Palaeoclimatol. Palaeoecol. 457, 80–97.
Dickinson, W.R., Gehrels, G.E., 2008. U-Pb ages of detrital zircons in relation to paleogeography: Triassic paleodrainage networks and sediment dispersal across southwest Laurentia. J. Sediment. Res. 78 (12), 745–764.
Dickson, A.J., 2017. A molybdenum-isotope perspective on Phanerozoic deoxygenation events. Nat. Geosci. 10 (10), 721–726.
Dickson, A.J., Gill, B.C., Ruhl, M., Jenkyns, H.C., Porcelli, D., Idiz, E., Lyons, T.W., van den Boorn, S.H., 2017. Molybdenum-isotope chemostratigraphy and paleoceanography of the Toarcian Oceanic Anoxic Event (Early Jurassic). Paleoceanography 32 (8), 813–829.
Du, Y., Chiari, M., Karádi, V., Nicora, A., Onoue, T., Pálfy, J., Roghi, G., Tomimatsu, Y., Rigo, M., 2020. The asynchronous disappearance of conodonts: New constraints from Triassic- Jurassic boundary sections in the Tethys and Panthalassa. Earth Sci. Rev. 103176 in press.
Duncan, R.A., Hooper, P.R., Rehacek, J., Marsh, J., Duncan, A.R., 1997. The timing and duration of the Karoo igneous event, southern Gondwana. J. Geophys. Res. Solid Earth 102 (B8), 18127–18138.
Ellam, R.M., Carlson, R.W., Shirey, S.B., 1992. Evidence from Re-Os isotopes for plume-lithosphere mixing in Karoo flood basalt genesis. Nature 359, 718–721.
Ernst, R.E., Youbi, N., 2017. How Large Igneous Provinces affect global climate, sometimes cause mass extinctions, and represent natural markers in the geological record. Palaeogeogr. Palaeoclimatol. Palaeoecol. 478, 30–52.
Erwin, D.H., Bowring, S.A., Yugan, J., 2002. End-Permian mass extinctions: a review. In: Koeberl, C., MacLeod, K.G. (Eds.), Catastrophic Events and Mass Extinctions: Impacts and Beyond, Geological Society of America Special Paper, 356, pp. 363–384.
Ettinger, N.P., Larson, T.E., Kerans, C., Thibodeau, A.M., Hattori, K.E., Kacur, S.M., Martindale, R.C., 2021. Ocean acidification and photic-zone anoxia at the Toarcian Oceanic Anoxic Event: Insights from the Adriatic Carbonate Platform. Sedimentology 68, 63–107.
Fantasia, A., Föllmi, K.B., Adatte, T., Bernárdez, E., Spangenberg, J.E., Mattioli, E., 2018a. The Toarcian oceanic anoxic event in southwestern Gondwana: An example from the Andean basin, northern Chile. J. Geol. Soc. Lond. 175 (6), 883–902.
Fantasia, A., Föllmi, K.B., Adatte, T., Spangenberg, J.E., Montero-Serrano, J.C., 2018b. The Early Toarcian oceanic anoxic event: Paleoenvironmental and paleoclimatic change across the Alpine Tethys (Switzerland). Glob. Planet. Chang. 162, 53–68.
Fantasia, A., Föllmi, K.B., Adatte, T., Spangenberg, J.E., Mattioli, E., 2019a. Expression of the Toarcian Oceanic Anoxic Event: new insights from a Swiss transect. Sedimentology 66 (1), 262–284.
Fantasia, A., Adatte, T., Spangenberg, J.E., Font, E., Duarte, L.V., Föllmi, K.B., 2019b. Global versus local processes during the Pliensbachian–Toarcian transition at the Peniche GSSP, Portugal: A multi-proxy record. Earth Sci. Rev. 198, 102932.
Fernandez, A., Korte, C., Ullmann, C.V., Looser, N., Wohlwend, S., Bernasconi, S.M., 2021. Reconstructing the magnitude of Early Toarcian (Jurassic) warming using the reordered clumped isotope compositions of belemnites. Geochim. Cosmochim. Acta 293, 308–327.
Ferreira, J., Mattioli, E., Suchéras-Marx, B., Giraud, F., Duarte, L.V., Pittet, B., Suan, G., Hassler, A., Spangenberg, J.E., 2019. Western Tethys Early and Middle Jurassic calcareous nannofossil biostratigraphy. Earth Sci. Rev. 197, 102908.
Findlay, H.S., Wood, H.L., Kendall, M.A., Spicer, J.I., Twitchett, R.J., Widdicombe, S., 2011. Comparing the impact of high CO2 on calcium carbonate structures in different marine organisms. Mar. Biol. Res. 7 (6), 565–575.
Fonseca, C., Mendonça Filho, J.G., Lézin, C., Duarte, L.V., Fauré, P., 2018. Organic facies variability during the Toarcian Oceanic Anoxic Event record of the Grands Causses and Quercy basins (southern France). Int. J. Coal Geol. 190, 218–235.
Fox, C.P., Cui, X., Whiteside, J.H., Olsen, P.E., Summons, R.E., Grice, K., 2020. Molecular and isotopic evidence reveals the end-Triassic carbon isotope excursion is not from massive exogenous light carbon. Proc. Natl. Acad. Sci. 117 (48), 30171–30178.
Fox, C.P., Whiteside, J.H., Olsen, P.E., Cui, X., Summons, R.E., Idiz, E., Grice, K., 2022. Two-pronged kill mechanism at the end-Triassic mass extinction. Geology 50, 448–453.
Franceschi, M., Dal Corso, J., Posenato, R., Roghi, G., Masetti, D., Jenkyns, H.C., 2014. Early Pliensbachian (Early Jurassic) C-isotope perturbation and the diffusion of the Lithiotis Fauna: Insights from the western Tethys. Palaeogeogr. Palaeoclimatol. Palaeoecol. 410, 255–263.
Franceschi, M., Corso, J.D., Cobianchi, M., Roghi, G., Penasa, L., Picotti, V., Preto, N., 2019. Tethyan carbonate platform transformations during the Early Jurassic (Sinemurian–Pliensbachian, Southern Alps): Comparison with the Late Triassic Carnian Pluvial Episode. GSA Bull. 131 (7-8), 1255–1275.
French, K.L., Sepúlveda, J., Trabucho-Alexandre, J., Gröcke, D.R., Summons, R.E., 2014. Organic geochemistry of the early Toarcian oceanic anoxic event in Hawsker Bottoms, Yorkshire, England. Earth Planet. Sci. Lett. 390, 116–127.
Frimmel, A., Oschmann, W., Schwark, L., 2004. Chemostratigraphy of the Posidonia Black Shale, SW Germany: I. Influence of sea-level variation on organic facies evolution. Chem. Geol. 206 (3–4), 199–230.
Fu, X., Wang, J., Feng, X., Wang, D., Chen, W., Song, C., Zeng, S., 2016. Early Jurassic carbon-isotope excursion in the Qiangtang Basin (Tibet), the eastern Tethys: Implications for the Toarcian Oceanic anoxic event. Chem. Geol. 442, 62–72.
Fu, X., Wang, J., Zeng, S., Feng, X., Wang, D., Song, C., 2017. Continental weathering and palaeoclimatic changes through the onset of the Early Toarcian oceanic anoxic event in the Qiangtang Basin, eastern Tethys. Palaeogeogr. Palaeoclimatol. Palaeoecol. 487, 241–250.
Fujisaki, W., Sawaki, Y., Yamamoto, S., Sato, T., Nishizawa, M., Windley, B.F., Maruyama, S., 2016. Tracking the redox history and nitrogen cycle in the pelagic Panthalassic deep ocean in the Middle Triassic to Early Jurassic: Insights from redox-sensitive elements and nitrogen isotopes. Palaeogeogr. Palaeoclimatol. Palaeoecol. 449, 397–420.
Fujisaki, W., Matsui, Y., Asanuma, H., Sawaki, Y., Suzuki, K., Maruyama, S., 2018. Global perturbations of carbon cycle during the Triassic–Jurassic transition recorded in the mid-Panthalassa. Earth Planet. Sci. Lett. 500, 105–116.
Fujisaki, W., Fukami, Y., Matsui, Y., Sato, T., Sawaki, Y., Suzuki, K., 2021. Redox conditions and nitrogen cycling during the Triassic–Jurassic transition: A new perspective from the mid-Panthalassa. Earth Sci. Rev. 103173.
Galli, M.T., Jadoul, F., Bernasconi, S.M., Weissert, H., 2005. Anomalies in global carbon cycling and extinction at the Triassic/Jurassic boundary: evidence from a marine C-isotope record. Palaeogeogr. Palaeoclimatol. Palaeoecol. 216 (3-4), 203–214.
Ge, Y., Shi, M., Steuber, T., Al-Suwaidi, A.H., Suarez, M.B., 2018. Environmental change during the Triassic–Jurassic boundary interval of an equatorial carbonate platform: Sedimentology and chemostratigraphy of the Ghalilah Formation, United Arab Emirates. Palaeogeogr. Palaeoclimatol. Palaeoecol. 502, 86–103.
Ge, Y., Al-Suwaidi, A.H., Shi, M., Li, Q., Morad, S., Steuber, T., 2019. Short-term variation of ooid mineralogy in the Triassic–Jurassic boundary interval and its environmental implications: Evidence from the equatorial Ghalilah Formation, United Arab Emirates. Glob. Planet. Chang. 182, 103006.

Glørstad-Clark, E., Faleide, J.I., Lundschien, B.A., Nystuen, J.P., 2010. Triassic seismic sequence stratigraphy and paleogeography of the western Barents Sea area. Mar. Pet. Geol. 27 (7), 1448–1475.
Golonka, J., 2007. Late Triassic and Early Jurassic palaeogeography of the world. Palaeogeogr. Palaeoclimatol. Palaeoecol. 244 (1-4), 297–307.
Golonka, J., Embry, A., Krobicki, M., 2018. Late Triassic global plate tectonics. In: Tanner, L.H. (Ed.), The Late Triassic World. Springer, Cham, Switzerland, pp. 27–58.
Gómez, J.J., Goy, A., Canales, M.L., 2008. Seawater temperature and carbon isotope variations in belemnites linked to mass extinction during the Toarcian (Early Jurassic) in Central and Northern Spain. Comparison with other European sections. Palaeogeogr. Palaeoclimatol. Palaeoecol. 258 (1-2), 28–58.
Gómez, J.J., Comas-Rengifo, M.J., Goy, A., 2016. Palaeoclimatic oscillations in the Pliensbachian (early Jurassic) of the Asturian Basin (northern Spain). Clim. Past 12 (5), 1199–1214.
Goričan, Š., Carter, E.S., Guex, J., O'Dogherty, L., De Wever, P., Dumitrica, P., Hori, R.S., Matsuoka, A., Whalen, P.A., 2013. Evolutionary patterns and palaeobiogeography of Pliensbachian and Toarcian (Early Jurassic) radiolaria. Palaeogeogr. Palaeoclimatol. Palaeoecol. 386, 620–636.
Gradstein, F.M., Ogg, J.G., Schmitz, M.D., 2020. In: Ogg, G.M. (Ed.), Geologic Time Scale 2020. Elsevier.
Gravendyck, J., Schobben, M., Bachelier, J.B., Kürschner, W.M., 2020. Macroecological patterns of the terrestrial vegetation history during the end-Triassic biotic crisis in the central European Basin: A palynological study of the Bonenburg section (NW-Germany) and its supra-regional implications. Glob. Planet. Chang. 194, 103286.
Greene, S.E., Martindale, R.C., Ritterbush, K.A., Bottjer, D.J., Corsetti, F.A., Berelson, W. M., 2012a. Recognising ocean acidification in deep time: An evaluation of the evidence for acidification across the Triassic–Jurassic boundary. Earth Sci. Rev. 113 (1-2), 72–93.
Greene, S.E., Bottjer, D.J., Corsetti, F.A., Berelson, W.M., Zonneveld, J.P., 2012b. A subseafloor carbonate factory across the Triassic–Jurassic transition. Geology 40 (11), 1043–1046.
Gröcke, D.R., Hori, R.S., Trabucho-Alexandre, J., Kemp, D.B., Schwark, L., 2011. An open ocean record of the Toarcian oceanic anoxic event. Solid Earth 2 (2), 245–257.
Guex, J., Bartolini, A., Atudorei, V., Taylor, D., 2004. High-resolution ammonite and carbon isotope stratigraphy across the Triassic–Jurassic boundary at New York Canyon (Nevada). Earth Planet. Sci. Lett. 225 (1-2), 29–41.
Hallam, A., 1997. Estimates of the amount and rate of sea-level change across the Rhaetian—Hettangian and Pliensbachian—Toarcian boundaries (latest Triassic to early Jurassic). J. Geol. Soc. 154 (5), 773–779.
Hallam, A., Wignall, P.B., 1999. Mass extinctions and sea-level changes. Earth Sci. Rev. 48 (4), 217–250.
Hames, W., McHone, J.G., Renne, P., Ruppel, C., 2003. The Central Atlantic Magmatic Province: Insights from Fragments of Pangea. American Geophysical Union, Geophysical Monograph 136.
Han, Z., Hu, X., Kemp, D.B., Li, J., 2018. Carbonate-platform response to the Toarcian Oceanic Anoxic Event in the southern hemisphere: Implications for climatic change and biotic platform demise. Earth Planet. Sci. Lett. 489, 59–71.
Haq, B.U., 2018a. Jurassic sea-level variations: a reappraisal. GSA Today 28 (1), 4–10.
Haq, B.U., 2018b. Triassic eustatic variations reexamined. GSA Today 28 (12), 4–9.
Haq, B.U., Hardenbol, J., Vail, P.R., 1988. Mesozoic and Cenozoic chronostratigraphy and cycles of sea-level change. In: Wilgus, C.K., Hastings, B.S., Ross, C.A., Posamentier, H., Van Wagoner, J., Kendall, C.G.St.C. (Eds.), Sea-Level Changes: An Integrated Approach, SEPM Special Publication, 42, pp. 71–108.
Harazim, D., Van De Schootbrugge, B.A.S., Sorichter, K., Fiebig, J., Weug, A., Suan, G., Oschmann, W., 2013. Spatial variability of watermass conditions within the European Epicontinental Seaway during the Early Jurassic (Pliensbachian–Toarcian). Sedimentology 60 (2), 359–390.
Harper, E.M., 2003. The Mesozoic marine revolution. In: Kelley, P.H., Kowalewski, M., Hansen, T.A. (Eds.), Predator—Prey Interactions in the Fossil Record. Springer, pp. 433–455.
Harries, P.J., Little, C.T., 1999. The early Toarcian (Early Jurassic) and the Cenomanian–Turonian (Late Cretaceous) mass extinctions: similarities and contrasts. Palaeogeogr. Palaeoclimatol. Palaeoecol. 154 (1-2), 39–66.
Hautmann, M., 2004. Effect of end-Triassic CO2 maximum on carbonate sedimentation and marine mass extinction. Facies 50 (2), 257–261.
Hautmann, M., 2012. Extinction: end-Triassic mass extinction (eLS). John Wiley, Chichester.
Heimdal, T.H., Jones, M.T., Svensen, H.H., 2020. Thermogenic carbon release from the Central Atlantic magmatic province caused major end-Triassic carbon cycle perturbations. Proceed. Nat. Acad. Sci. 117 (22), 11968–11974.
Heinonen, J.S., Luttinen, A.V., 2010. Mineral chemical evidence for extremely magnesian subalkaline melts from the Antarctic extension of the Karoo large igneous province. Mineral. Petrol. 99 (3-4), 201–217.
Hesselbo, S.P., Pieńkowski, G., 2011. Stepwise atmospheric carbon-isotope excursion during the Toarcian oceanic anoxic event (Early Jurassic, Polish Basin). Earth Planet. Sci. Lett. 301 (1-2), 365–372.
Hermoso, M., Le Callonnec, L., Minoletti, F., Renard, M., Hesselbo, S.P., 2009a. Expression of the Early Toarcian negative carbon-isotope excursion in separated carbonate microfractions (Jurassic, Paris Basin). Earth Planet. Sci. Lett. 277 (1–2), 194–203.
Hermoso, M., Minoletti, F., Le Callonnec, L., Jenkyns, H.C., Hesselbo, S.P., Rickaby, R.E., Renard, M., De Rafélis, M., Emmanuel, L., 2009b. Global and local forcing of Early Toarcian seawater chemistry: A comparative study of different paleoceanographic settings (Paris and Lusitanian basins). Paleoceanography 24 (4).
Hermoso, M., Minoletti, F., Rickaby, R.E., Hesselbo, S.P., Baudin, F., Jenkyns, H.C., 2012. Dynamics of a stepped carbon-isotope excursion: ultra high-resolution study of Early Toarcian environmental change. Earth Planet. Sci. Lett. 319, 45–54.
Hesselbo, S.P., Gröcke, D.R., Jenkyns, H.C., Bjerrum, C.J., Farrimond, P., Bell, H.S.M., Green, O.R., 2000. Massive dissociation of gas hydrate during a Jurassic oceanic anoxic event. Nature 406 (6794), 392–395.
Hesselbo, S.P., Robinson, S.A., Surlyk, F., Piasecki, S., 2002. Terrestrial and marine extinction at the Triassic–Jurassic boundary synchronized with major carbon-cycle perturbation: A link to initiation of massive volcanism? Geology 30 (3), 251–254.
Hesselbo, S.P., Robinson, S.A., Surlyk, F., 2004. Sea-level change and facies development across potential Triassic–Jurassic boundary horizons, SW Britain. J. Geol. Soc. 161 (3), 365–379.
Hesselbo, S.P., Jenkyns, H.C., Duarte, L.V., Oliveira, L.C., 2007. Carbon-isotope record of the Early Jurassic (Toarcian) Oceanic Anoxic Event from fossil wood and marine carbonate (Lusitanian Basin, Portugal). Earth Planet. Sci. Lett. 253 (3-4), 455–470.
Hesselbo, S.P., Korte, C., Ullmann, C.V., Ebbesen, A.L., 2021a. Carbon and oxygen isotope records from the southern Eurasian Seaway following the Triassic–Jurassic boundary: Parallel long-term enhanced carbon burial and seawater warming. Earth Sci. Rev. 103131.
Hesselbo, S.P., Little, C.T., Ruhl, M., Thibault, N., Ullmann, C.V., 2021b. Comments on "Paleosalinity determination in ancient epicontinental seas: A case study of the T-OAE in the Cleveland Basin (UK)" by Remírez, M.N. and Algeo, T.J. Earth-Sci. Rev. *208*, 103290.
Hönisch, B., Ridgwell, A., Schmidt, D.N., Thomas, E., Gibbs, S.J., Sluijs, A., Zeebe, R., Kump, L., Martindale, R.C., Greene, S.E., Kiessling, W., 2012. The geological record of ocean acidification. Science 335 (6072), 1058–1063.
Huang, C., Hesselbo, S.P., 2014. Pacing of the Toarcian Oceanic Anoxic Event (Early Jurassic) from astronomical correlation of marine sections. Gondwana Res. 25, 1348–1356.
Huntington, T.G., 2006. Evidence for intensification of the global water cycle: review and synthesis. J. Hydrol. 319 (1-4), 83–95.
Ibarra, Y., Corsetti, F.A., Greene, S.E., Bottjer, D.J., 2016. A microbial carbonate response in synchrony with the end-Triassic mass extinction across the SW UK. Sci. Rep. 6 (1), 1–8.
Ikeda, M., Hori, R.S., 2014. Effects of Karoo–Ferrar volcanism and astronomical cycles on the Toarcian Oceanic Anoxic Events (Early Jurassic). Palaeogeogr. Palaeoclimatol. Palaeoecol. 410, 134–142.
Ikeda, M., Hori, R.S., Ikehara, M., Miyashita, R., Chino, M., Yamada, K., 2018. Carbon cycle dynamics linked with Karoo-Ferrar volcanism and astronomical cycles during Pliensbachian-Toarcian (Early Jurassic). Glob. Planet. Chang. 170, 163–171.
Ikeda, M., Hori, R.S., Okada, Y., Nakada, R., 2015. Volcanism and deep-ocean acidification across the end-Triassic extinction event. Palaeogeogr. Palaeoclimatol. Palaeoecol. 440, 725–733.
Iqbal, S., Wagreich, M., Kürschner, W.M., Gier, S., Bibi, M., 2019. Hot-house climate during the Triassic/Jurassic transition: The evidence of climate change from the southern hemisphere (Salt Range, Pakistan). Glob. Planet. Chang. 172, 15–32.
Ivanov, A.V., Meffre, S., Thompson, J., Corfu, F., Kamenetsky, V.S., Kamenetsky, M.B., Demonterova, E.I., 2017. Timing and genesis of the Karoo-Ferrar large igneous province: New high precision U-Pb data for Tasmania confirm short duration of the major magmatic pulse. Chem. Geol. 455, 32–43.
Izumi, K., Kemp, D.B., Itamiya, S., Inui, M., 2018a. Sedimentary evidence for enhanced hydrological cycling in response to rapid carbon release during the early Toarcian oceanic anoxic event. Earth Planet. Sci. Lett. 481, 162–170.
Izumi, K., Endo, K., Kemp, D.B., Inui, M., 2018b. Oceanic redox conditions through the late Pliensbachian to early Toarcian on the northwestern Panthalassa margin: Insights from pyrite and geochemical data. Palaeogeogr. Palaeoclimatol. Palaeoecol. 493, 1–10.
Jablonski, D., 2002. Survival without recovery after mass extinctions. Proc. Natl. Acad. Sci. 99 (12), 8139–8144.
Jaraula, C.M., Grice, K., Twitchett, R.J., Böttcher, M.E., LeMetayer, P., Dastidar, A.G., Opazo, L.F., 2013. Elevated $pCO_2$ leading to Late Triassic extinction, persistent photic zone euxinia, and rising sea levels. Geology 41 (9), 955–958.
Jenks, J.F., Monnet, C., Balini, M., Brayard, A., Meier, M., 2015. Biostratigraphy of Triassic ammonoids. In: Klug, C., Korn, D., De Baets, K., Kruta, I., Mapes, R.H. (Eds.), Ammonoid Paleobiology: From Macroevolution to Paleogeography. Springer, Dordrecht, pp. 329–388.
Jenkyns, H.C., 1988. The early Toarcian (Jurassic) anoxic event: stratigraphic, sedimentary, and geochemical evidence. Am. J. Sci. 288, 101–151.
Jenkyns, H.C., 2010. Geochemistry of oceanic anoxic events. Geochem. Geophys. Geosyst. 11 (3).
Jenkyns, H.C., Gröcke, D.R., Hesselbo, S.P., 2001. Nitrogen isotope evidence for water mass denitrification during the early Toarcian (Jurassic) oceanic anoxic event. Paleoceanography 16 (6), 593–603.
Johansson, L., Zahirovic, S., Müller, R.D., 2018. The interplay between the eruption and weathering of large igneous provinces and the deep-time carbon cycle. Geophys. Res. Lett. 45 (11), 5380–5389.
Jones, C.E., Jenkyns, H.C., Hesselbo, S.P., 1994. Strontium isotopes in Early Jurassic seawater. Geochim. Cosmochim. Acta 58 (4), 1285–1301.
Jost, A.B., Bachan, A., van de Schootbrugge, B., Brown, S.T., DePaolo, D.J., Payne, J.L., 2017. Additive effects of acidification and mineralogy on calcium isotopes in Triassic/Jurassic boundary limestones. Geochem. Geophys. Geosyst. 18 (1), 113–124.
Jourdan, F., Féraud, G., Bertrand, H., Kampunzu, A.B., Tshoso, G., Watkeys, M.K., Le Gall, B., 2005. Karoo large igneous province: Brevity, origin, and relation to mass extinction questioned by new $^{40}Ar/^{39}Ar$ age data. Geology 33 (9), 745–748.

Jourdan, F., Féraud, G., Bertrand, H., Watkeys, M.K., Renne, A.P., 2008. The $^{40}Ar/^{39}Ar$ ages of the sill complex of the Karoo large igneous province: Implications for the Pliensbachian-Toarcian climate change. Geochem. Geophys. Geosyst. 9 (6).
Jourdan, F., Marzoli, A., Bertrand, H., Cirilli, S., Tanner, L., Kontak, D., McHone, G., Renne, P., Bellieni, G., 2009. 40Ar/39Ar ages of CAMP in North America: implications for the Triassic–Jurassic boundary and the 40K decay constant bias. Lithos 110 (1-4), 167–180.
Karádi, V., Cau, A., Mazza, M., Rigo, M., 2020. The last phase of conodont evolution during the Late Triassic: Integrating biostratigraphic and phylogenetic approaches. Palaeogeogr. Palaeoclimatol. Palaeoecol. 549, 109144.
Kasprak, A.H., Sepúlveda, J., Price-Waldman, R., Williford, K.H., Schoepfer, S.D., Haggart, J.W., Ward, P.D., Summons, R.E., Whiteside, J.H., 2015. Episodic photic zone euxinia in the northeastern Panthalassic Ocean during the end-Triassic extinction. Geology 43 (4), 307–310.
Kemp, D.B., Coe, A.L., Cohen, A.S., Schwark, L., 2005. Astronomical pacing of methane release in the Early Jurassic period. Nature 437 (7057), 396–399.
Kemp, D.B., Coe, A.L., Cohen, A.S., Weedon, G.P., 2011. Astronomical forcing and chronology of the early Toarcian (Early Jurassic) oceanic anoxic event in Yorkshire, UK. Paleoceanography 26 (4).
Kemp, D.B., Baranyi, V., Izumi, K., Burgess, R.D., 2019. Organic matter variations and links to climate across the early Toarcian oceanic anoxic event (T-OAE) in Toyora area, southwest Japan. Palaeogeogr. Palaeoclimatol. Palaeoecol. 530, 90–102.
Kemp, D.B., Selby, D., Izumi, K., 2020. Direct coupling between carbon release and weathering during the Toarcian oceanic anoxic event. Geology 48 (10), 976–980.
Kent, D.V., Olsen, P.E., Muttoni, G., 2017. Astrochronostratigraphic polarity time scale (APTS) for the Late Triassic and Early Jurassic from continental sediments and correlation with standard marine stages. Earth Sci. Rev. 166, 153–180.
Kidder, D.L., Worsley, T.R., 2010. Phanerozoic large igneous provinces (LIPs), HEATT (haline euxinic acidic thermal transgression) episodes, and mass extinctions. Palaeogeogr. Palaeoclimatol. Palaeoecol. 295 (1-2), 162–191.
Kiessling, W., Simpson, C., 2011. On the potential for ocean acidification to be a general cause of ancient reef crises. Glob. Chang. Biol. 17, 56–67.
Kiessling, W., Aberhan, M., Brenneis, B., Wagner, P.J., 2007. Extinction trajectories of benthic organisms across the Triassic–Jurassic boundary. Palaeogeogr. Palaeoclimatol. Palaeoecol. 244 (1-4), 201–222.
Kocsis, Á.T., Kiessling, W., Pálfy, J., 2014. Radiolarian biodiversity dynamics through the Triassic and Jurassic: implications for proximate causes of the end-Triassic mass extinction. Paleobiology 40 (4), 625–639.
Korte, C., Hesselbo, S.P., 2011. Shallow marine carbon and oxygen isotope and elemental records indicate icehouse-greenhouse cycles during the Early Jurassic. Paleoceanography 26 (4).
Korte, C., Kozur, H.W., Bruckschen, P., Veizer, J., 2003. Strontium isotope evolution of Late Permian and Triassic seawater. Geochim. Cosmochim. Acta 67 (1), 47–62.
Korte, C., Hesselbo, S.P., Jenkyns, H.C., Rickaby, R.E.M., Spötl, C., 2009. Palaeoenvironmental significance of carbon- and oxygen-isotope stratigraphy of marine Triassic Jurassic boundary sections in SW Britiain. J. Geol. Soc. Lond. 166, 431–445.
Korte, C., Hesselbo, S.P., Ullmann, C.V., Dietl, G., Ruhl, M., Schweigert, G., Thibault, N., 2015. Jurassic climate mode governed by ocean gateway. Nat. Commun. 6 (1), 1–7.
Korte, C., Ruhl, M., Pálfy, J., Ullmann, C.V., Hesselbo, S.P., 2018. Chemostratigraphy across the Triassic–Jurassic boundary. In: Sial, A.N., Gaucher, C., Ramkumar, M., Ferreira, V.P. (Eds.), Chemostratigraphy Across Major Chronological Boundaries, American Geophysical Union, Geophysical Monograph, 240, pp. 183–210.
Kovács, E.B., Ruhl, M., Demény, A., Fórizs, I., Hegyi, I., Horváth-Kostka, Z.R., Móricz, F., Vallner, Z., Pálfy, J., 2020. Mercury anomalies and carbon isotope excursions in the western Tethyan Csővár section support the link between CAMP volcanism and the end-Triassic extinction. Glob. Planet. Chang. 194, 103291.
Krencker, F.N., Fantasia, A., Danisch, J., Martindale, R., Kabiri, L., El Ouali, M., Bodin, S., 2020. Two-phased collapse of the shallow-water carbonate factory during the late Pliensbachian–Toarcian driven by changing climate and enhanced continental weathering in the Northwestern Gondwana Margin. Earth-Sci. Rev. 208, 103254.
Krencker, F.N., Lindström, S., Bodin, S., 2019. A major sea-level drop briefly precedes the Toarcian oceanic anoxic event: implication for Early Jurassic climate and carbon cycle. Sci. Rep. 9 (1), 1–12.
Kump, L.R., Pavlov, A., Arthur, M.A., 2005. Massive release of hydrogen sulfide to the surface ocean and atmosphere during intervals of oceanic anoxia. Geology 33 (5), 397–400.
Kuroda, J., Hori, R.S., Suzuki, K., Gröcke, D.R., Ohkouchi, N., 2010. Marine osmium isotope record across the Triassic–Jurassic boundary from a Pacific pelagic site. Geology 38 (12), 1095–1098.
Kürschner, W.M., Bonis, N.R., Krystyn, L., 2007. Carbon-isotope stratigraphy and palynostratigraphy of the Triassic–Jurassic transition in the Tiefengraben section-Northern Calcareous Alps (Austria). Palaeogeogr. Palaeoclimatol. Palaeoecol. 244 (1-4), 257–280.
Kustatscher, E., Ash, S.R., Karasev, E., Pott, C., Vajda, V., Yu, J.X., McLoughlin, S., 2018. Flora of the Late Triassic. In: Tanner, L.H. (Ed.), The Late Triassic World. Springer, Cham, Switzerland, pp. 545–622.
Landwehrs, J.P., Feulner, G., Hofmann, M., Petri, S., 2020. Climatic fluctuations modeled for carbon and sulfur emissions from end-Triassic volcanism. Earth Planet. Sci. Lett. 537, 116174.
Larina, E., Bottjer, D.J., Corsetti, F.A., Zonneveld, J.P., Celestian, A.J., Bailey, J.V., 2019. Uppermost Triassic phosphorites from Williston Lake, Canada: link to fluctuating euxinic-anoxic conditions in northeastern Panthalassa before the end-Triassic mass extinction. Sci. Rep. 9 (1), 1–9.
Leleu, S., Hartley, A.J., van Oosterhout, C., Kennan, L., Ruckwied, K., Gerdes, K., 2016. Structural, stratigraphic and sedimentological characterisation of a wide rift system: The Triassic rift system of the Central Atlantic Domain. Earth-Sci. Rev. 158, 89–124.
Li, H.Y., Huang, X.L., 2013. Constraints on the paleogeographic evolution of the North China Craton during the Late Triassic–Jurassic. J. Asian Earth Sci. 70, 308–320.
Li, M., Zhang, Y., Huang, C., Ogg, J., Hinnov, L., Wang, Y., Zou, Z., Li, L., 2017. Astronomical tuning and magnetostratigraphy of the Upper Triassic Xujiahe Formation of South China and Newark Supergroup of North America: implications for the Late Triassic time scale. Earth Planet. Sci. Lett. 475, 207–223.
Li, L., Wang, Y., Kürschner, W.M., Ruhl, M., Vajda, V., 2020a. Palaeovegetation and palaeoclimate changes across the Triassic–Jurassic transition in the Sichuan Basin, China. Palaeogeogr. Palaeoclimatol. Palaeoecol. 556, 109891.
Li, X., Wang, J., Rasbury, T., Zhou, M., Wei, Z., Zhang, C., 2020b. Early Jurassic climate and atmospheric CO 2 concentration in the Sichuan paleobasin, southwestern China. Clim. Past 16 (6), 2055–2074.
Lindström, S., 2016. Palynofloral patterns of terrestrial ecosystem change during the end-Triassic event–a review. Geol. Mag. 153 (2), 223–251.
Lindström, S., 2021. Two-phased mass rarity and extinction in land plants during the end-Triassic climate crisis. Front. Earth Sci. 9, 1079.
Lindström, S., Erlström, M., Piasecki, S., Nielsen, L.H., Mathiesen, A., 2017a. Palynology and terrestrial ecosystem change of the Middle Triassic to lowermost Jurassic succession of the eastern Danish Basin. Rev. Palaeobot. Palynol. 244, 65–95.
Lindström, S., van De Schootbrugge, B., Dybkjær, K., Pedersen, G.K., Fiebig, J., Nielsen, L.H., Richoz, S., 2012. No causal link between terrestrial ecosystem change and methane release during the end-Triassic mass extinction. Geology 40 (6), 531–534.
Lindström, S., van de Schootbrugge, B., Hansen, K.H., Pedersen, G.K., Alsen, P., Thibault, N., Dybkjær, K., Bjerrum, C.J., Nielsen, L.H., 2017b. A new correlation of Triassic–Jurassic boundary successions in NW Europe, Nevada and Peru, and the Central Atlantic Magmatic Province: A time-line for the end-Triassic mass extinction. Palaeogeogr. Palaeoclimatol. Palaeoecol. 478, 80–102.
Lindström, S., Sanei, H., van de Schootbrugge, B., Pedersen, G.K., Lesher, C.E., Tegner, C., Heunisch, C., Dybkjær, K., Outridge, P.M., 2019. Volcanic mercury and mutagenesis in land plants during the end-Triassic mass extinction. *Science*. Advances 5 (10), eaaw4018.
Lindström, S., Callegaro, S., Davies, J., Tegner, C., van de Schootbrugge, B., Pedersen, G. K., Youbi, N., Sanei, H., Marzoli, A., 2021. Tracing volcanic emissions from the Central Atlantic Magmatic Province in the sedimentary record. Earth Sci. Rev. 103444.
Little, C.T., Benton, M.J., 1995. Early Jurassic mass extinction: a global long-term event. Geology 23 (6), 495–498.
Littler, K., Hesselbo, S.P., Jenkyns, H.C., 2010. A carbon-isotope perturbation at the Pliensbachian-Toarcian boundary: evidence from the Lias Group, NE England. Geol. Mag. 147 (2), 181–192.
Liu, M., Sun, P., Them II, T.R., Li, Y., Sun, S., Gao, X., Huang, X., Tang, Y., 2020. Organic geochemistry of a lacustrine shale across the Toarcian Oceanic Anoxic Event (Early Jurassic) from NE China. Glob. Planet. Chang. 103214.
Lucas, S.G., 2010. The Triassic timescale based on nonmarine tetrapod biostratigraphy and biochronology. In: Lucas, S.G. (Ed.), Triassic Timescale, Geological Society of London Special Publication, 334, pp. 447–500.
Lucas, S.G., 2012. The extinction of the conulariids. Geosciences 2 (1), 1–10.
Lucas, S.G., 2018a. The Late Triassic Timescale. In: Tanner, L.H. (Ed.), The Late Triassic World. Springer, Cham, Switzerland, pp. 1–26.
Lucas, S.G., 2018b. Late Triassic ammonoids: Distribution, biostratigraphy and biotic events. In: Tanner, L.H. (Ed.), The Late Triassic World. Springer, Cham, Switzerland, pp. 237–262.
Lucas, S.G., 2018c. Late Triassic terrestrial tetrapods: Biostratigraphy, biochronology and biotic events. In: Tanner, L.H. (Ed.), The Late Triassic World. Springer, Cham, Switzerland, pp. 351–406.
Lucas, S.G., Tanner, L.H., 2007. The nonmarine Triassic–Jurassic boundary in the Newark Supergroup of eastern North America. Earth Sci. Rev. 84, 1–20.
Luo, G., Richoz, S., van de Schootbrugge, B., Algeo, T.J., Xie, S., Ono, S., Summons, R.E., 2018. Multiple sulfur-isotopic evidence for a shallowly stratified ocean following the Triassic–Jurassic boundary mass extinction. Geochim. Cosmochim. Acta 231, 73–87.
Mander, L., Twitchett, R.J., Benton, M.J., 2008. Palaeoecology of the Late Triassic extinction event in the SW UK. J. Geol. Soc. Lond. 165, 319–332.
Mander, L., Kürschner, W.M., McElwain, J.C., 2010. An explanation for conflicting records of Triassic–Jurassic plant diversity. Proceed. Nat. Acad. Sci. (U.S.A.) *107* (35), 15351–15356.
Martindale, R.C., Aberhan, M., 2017. Response of macrobenthic communities to the Toarcian Oceanic Anoxic Event in northeastern Panthalassa (Ya Ha Tinda, Alberta, Canada). Palaeogeogr. Palaeoclimatol. Palaeoecol. 478, 103–120.
Marynowski, L., Simoneit, B.R., 2009. Widespread Upper Triassic to Lower Jurassic wildfire records from Poland: evidence from charcoal and pyrolytic polycyclic aromatic hydrocarbons. Palaios 24 (12), 785–798.
Marzoli, A., Renne, P.R., Piccirillo, E.M., Ernesto, M., Bellieni, G., De Min, A., 1999. Extensive 200-million-year-old continental flood basalts of the Central Atlantic Magmatic Province. Science 284 (5414), 616–618.
Marzoli, A., Bertrand, H., Knight, K.B., Cirilli, S., Buratti, N., Vérati, C., Nomade, S., Renne, P.R., Youbi, N., Martini, R., Allenbach, K., 2004. Synchrony of the Central Atlantic magmatic province and the Triassic–Jurassic boundary climatic and biotic crisis. Geology 32 (11), 973–976.
Marzoli, A., Callegaro, S., Dal Corso, J., Davies, J.H.F.L., Chiaradia, M., Youbi, N., Bertrand, H., Reisberg, L., Merle, R., Jourdan, F., 2018. The Central Atlantic Magmatic Province (CAMP): a review. In: Tanner, L.H. (Ed.), The Late Triassic World. Springer, Cham, Switzerland, pp. 91–126.
Mattioli, E., Pittet, B., Petitpierre, L., Mailliot, S., 2009. Dramatic decrease of pelagic carbonate production by nannoplankton across the Early Toarcian anoxic event (T-OAE). Glob. Planet. Chang. 65 (3–4), 134–145.

Maxwell, E.E., Vincent, P., 2016. Effects of the early Toarcian Oceanic Anoxic Event on ichthyosaur body size and faunal composition in the Southwest German Basin. Paleobiology 42 (1), 117–126.
Mazzini, A., Svensen, H., Leanza, H.A., Corfu, F., Planke, S., 2010. Early Jurassic shale chemostratigraphy and U–Pb ages from the Neuquen Basin (Argentina): Implications for the Toarcian oceanic anoxic event. Earth Planet. Sci. Lett. 297 (3-4), 633–645.
McArthur, J.M., 2019. Early Toarcian black shales: A response to an oceanic anoxic event or anoxia in marginal basins? Chem. Geol. 522, 71–83.
McArthur, J.M., Algeo, T.J., Van de Schootbrugge, B., Li, Q., Howarth, R.J., 2008. Basinal restriction, black shales, Re-Os dating, and the Early Toarcian (Jurassic) oceanic anoxic event. Paleoceanography 23 (4).
McElwain, J.C., Beerling, D.J., Woodward, F.I., 1999. Fossil plants and global warming at the Triassic–Jurassic boundary. Science 285 (5432), 1386–1390.
McElwain, J.C., Wade-Murphy, J., Hesselbo, S.P., 2005. Changes in carbon dioxide during an oceanic anoxic event linked to intrusion into Gondwana coals. Nature 435 (7041), 479–482.
McElwain, J.C., Popa, M.E., Hesselbo, S.P., Haworth, M., Surlyk, F., 2007. Macroecological responses of terrestrial vegetation to climatic and atmospheric change across the Triassic/Jurassic boundary in East Greenland. Paleobiology 33 (4), 547–573.
McElwain, J.C., Wagner, P.J., Hesselbo, S.P., 2009. Fossil plant relative abundances indicate sudden loss of Late Triassic biodiversity in East Greenland. Science 324 (5934), 1554–1556.
McHone, J.G., 2003. The Central Atlantic Magmatic Province: Insights from fragments of Pangea. Am. Geophys. Union, Geophysical Monograph 136, 1–13.
McPhee, B.W., Bordy, E.M., Sciscio, L., Choiniere, J.N., 2017. The sauropodomorph biostratigraphy of the Elliot Formation of southern Africa: Tracking the evolution of Sauropodomorpha across the Triassic–Jurassic boundary. Acta Palaeontol. Pol. 62 (3), 441–465.
McRoberts, C.A., Krystyn, L., Hautmann, M., 2012. Macrofaunal response to the end-Triassic mass extinction in the West-Tethyan Kössen Basin, Austria. Palaios 27 (9), 607–616.
Menini, A., Mattioli, E., Hesselbo, S.P., Ruhl, M., Suan, G., 2021. Primary v. carbonate production in the Toarcian, a case study from the Llanbedr (Mochras Farm) borehole, Wales. Geol. Soc. Lond., Spec. Publ. 514 (1), 59–81.
Miguez-Salas, O., Rodríguez-Tovar, F.J., Duarte, L.V., 2017. Selective incidence of the Toarcian oceanic anoxic event on macroinvertebrate marine communities: a case from the Lusitanian Basin, Portugal. Lethaia 50 (4), 548–560.
Montero-Serrano, J.C., Föllmi, K.B., Adatte, T., Spangenberg, J.E., Tribovillard, N., Fantasia, A., Suan, G., 2015. Continental weathering and redox conditions during the early Toarcian Oceanic Anoxic Event in the northwestern Tethys: insight from the Posidonia Shale section in the Swiss Jura Mountains. Palaeogeogr. Palaeoclimatol. Palaeoecol. 429, 83–99.
Morten, S.D., Twitchett, R.J., 2009. Fluctuations in the body size of marine invertebrates through the Pliensbachian-Toarcian extinction event. Palaeogeogr. Palaeoclimatol. Palaeoecol. 284, 29–38.
Moulin, M., Fluteau, F., Courtillot, V., Marsh, J., Delpech, G., Quidelleur, X., Gérard, M., 2017. Eruptive history of the Karoo lava flows and their impact on early Jurassic environmental change. J. Geophys. Res. Solid Earth 122 (2), 738–772.
Moulin, M., Fluteau, F., Courtillot, V., Marsh, J., Delpech, G., Quidelleur, X., Gérard, M., Jay, A.E., 2011. An attempt to constrain the age, duration, and eruptive history of the Karoo flood basalt: Naude's Nek section (South Africa). J. Geophys. Res. Solid Earth 116 (B7).
Müller, R.D., Dutkiewicz, A., Seton, M., Gaina, C., 2013. Seawater chemistry driven by supercontinent assembly, breakup, and dispersal. Geology 41 (8), 907–910.
Müller, T., Price, G.D., Bajnai, D., Nyerges, A., Kesjár, D., Raucsik, B., Varga, A., Judik, K., Fekete, J., May, Z., Pálfy, J., 2017. New multiproxy record of the Jenkyns Event (also known as the Toarcian Oceanic Anoxic Event) from the Mecsek Mountains (Hungary): Differences, duration and drivers. Sedimentology 64 (1), 66–86.
Müller, T., Karancz, S., Mattioli, E., Milovský, R., Pálfy, J., Schlögl, J., Segit, T., Šimo, V., Tomašových, A., 2020a. Assessing anoxia, recovery and carbonate production setback in a hemipelagic Tethyan basin during the Toarcian Oceanic Anoxic Event (Western Carpathians). Glob. Planet. Chang. 195, 103366.
Müller, T., Jurikova, H., Gutjahr, M., Tomašových, A., Schlögl, J., Liebetrau, V., Duarte, L.V., Milovský, R., Suan, G., Mattioli, E., Pittet, B., 2020b. Ocean acidification during the early Toarcian extinction event: Evidence from boron isotopes in brachiopods. Geology 48 (12), 1184–1188.
Muttoni, G., Kent, D.V., Olsen, P.E., Stefano, P.D., Lowrie, W., Bernasconi, S.M., Hernández, F.M., 2004. Tethyan magnetostratigraphy from Pizzo Mondello (Sicily) and correlation to the Late Triassic Newark astrochronological polarity time scale. GSA Bull. 116 (9-10), 1043–1058.
Muttoni, G., Kent, D.V., Jadoul, F., Olsen, P.E., Rigo, M., Galli, M.T., Nicora, A., 2010. Rhaetian magneto-biostratigraphy from the Southern Alps (Italy): constraints on Triassic chronology. Palaeogeogr. Palaeoclimatol. Palaeoecol. 285 (1-2), 1–16.
Muttoni, G., Mazza, M., Mosher, D., Katz, M.E., Kent, D.V., Balini, M., 2014. A Middle-Late Triassic (Ladinian–Rhaetian) carbon and oxygen isotope record from the Tethyan Ocean. Palaeogeogr. Palaeoclimatol. Palaeoecol. 399, 246–259.
Neumeister, S., Gratzer, R., Algeo, T.J., Bechtel, A., Gawlick, H.J., Newton, R.J., Sachsenhofer, R.F., 2015. Oceanic response to Pliensbachian and Toarcian magmatic events: implications from an organic-rich basinal succession in the NW Tethys. Glob. Planet. Chang. 126, 62–83.
Neumeister, S., Algeo, T.J., Bechtel, A., Gawlick, H.J., Gratzer, R., Sachsenhofer, R.F., 2016. Redox conditions and depositional environment of the Lower Jurassic Bächental bituminous marls (Tyrol, Austria). Austrian J. Earth Sci. 109 (2).
Neumeister, S., Misch, D., Algeo, T.J., Gawlick, H.J., Gratzer, R., Sachsenhofer, R.F., 2020. Early diagenesis of organic-rich marls under shifting suboxic to euxinic conditions: The lower Toarcian of the Bächental basin. Mar. Pet. Geol. 104513.
O'Dogherty, L., Carter, E.S., Goričan, Š., Dumitrica, P., 2010. Triassic radiolarian biostratigraphy. In: Lucas, S.G. (Ed.), Triassic Timescale, Geological Society of London Special Publication, 334, pp. 163–200.
Ogg, J.G., 2012. Triassic (chapter 25). In: Gradstein, F.M., Ogg, J.G., Schmitz, M.D., Ogg, G.M. (Eds.), The Geologic Time Scale 2012. Elsevier, Amsterdam, pp. 681–730.
Ogg, J.G., Hinnov, L.A., 2012. Jurassic (chapter 26). In: Gradstein, F.M., Ogg, J.G., Schmitz, M.D., Ogg, G.M. (Eds.), The Geologic Time Scale 2012. Elsevier, Amsterdam, pp. 731–791.
Ogg, J.G., Chen, Z.Q., Orchard, M.J., Jiang, H.S., 2020. The Triassic Period. In: Gradstein, F.M., Ogg, J.G., Schmitz, M.D., Ogg, G.M. (Eds.), Geologic Time Scale 2020. Elsevier, Amsterdam, pp. 903–953.
Olsen, P.E., Kent, D.V., Sues, H.D., Koeberl, C., Huber, H., Montanari, A., Rainforth, E.C., Fowell, S.J., Szajna, M.J., Hartline, B.W., 2002a. Ascent of dinosaurs linked to an iridium anomaly at the Triassic–Jurassic boundary. Science 296 (5571), 1305–1307.
Olsen, P.E., Kent, D.V., Whiteside, J.H., 2010. Implications of the Newark Supergroup-based astrochronology and geomagnetic polarity time scale (Newark-APTS) for the tempo and mode of the early diversification of the Dinosauria. Earth Environ. Sci. Trans. R. Soc. Edinb. 101 (3–4), 201–229.
Olsen, P.E., Koeberl, C., Huber, H., Montanari, A., Fowell, S.J., Et-Touhami, M., Kent, D. V., 2002b. Continental Triassic–Jurassic boundary in central Pangea: Recent progress and discussion of an Ir anomaly. In: Koeberl, C., MacLeod, K.G. (Eds.), Catastrophic Events and Mass Extinctions: Impacts and Beyond, Geological Society of America Special Paper, 356, pp. 505–522.
Olsen, P.E., Sha, J., Fang, Y., Clara Chang, C., Kinney, S., Sues, H.D., Kent, D., Whiteside, J.H., Schaller, M., Vajda, V., 2022. Arctic Ice and the Ecological Rise of the Dinosaurs. Science in press.
Onoue, T., Sato, H., Yamashita, D., Ikehara, M., Yasukawa, K., Fujinaga, K., Kato, Y., Matsuoka, A., 2016. Bolide impact triggered the Late Triassic extinction event in equatorial Panthalassa. Sci. Rep. 6, 29609.
Onoue, T., Hori, R.S., Kojima, S., 2017. Triassic and Jurassic radiolarian response to global catastrophic events in the Panthalassa Ocean, as recorded in the Mino Belt, central Japan. Sci. Rep. Niigata University (Geol.) 32, 29–69.
Pálfy, J., Smith, P.L., 2000. Synchrony between Early Jurassic extinction, oceanic anoxic event, and the Karoo-Ferrar flood basalt volcanism. Geology 28 (8), 747–750.
Pálfy, J., Demény, A., Haas, J., Hetényi, M., Orchard, M.J., Veto, I., 2001. Carbon isotope anomaly and other geochemical changes at the Triassic–Jurassic boundary from a marine section in Hungary. Geology 29 (11), 1047–1050.
Pálfy, J., Demény, A., Haas, J., Carter, E.S., Görög, Á., Halász, D., Oravecz-Scheffer, A., Hetényi, M., Márton, E., Orchard, M.J., Ozsvárt, P., 2007. Triassic–Jurassic boundary events inferred from integrated stratigraphy of the Csővár section, Hungary. Palaeogeogr. Palaeoclimatol. Palaeoecol. 244 (1-4), 11–33.
Palliani, R.B., Mattioli, E., Riding, J.B., 2002. The response of marine phytoplankton and sedimentary organic matter to the early Toarcian (Lower Jurassic) oceanic anoxic event in northern England. Mar. Micropaleontol. 46 (3–4), 223–245.
Panfili, G., Cirilli, S., Dal Corso, J., Bertrand, H., Medina, F., Youbi, N., Marzoli, A., 2019. New biostratigraphic constraints show rapid emplacement of the Central Atlantic Magmatic Province (CAMP) during the end-Triassic mass extinction interval. Glob. Planet. Chang. 172, 60–68.
Percival, L.M.E., Witt, M.L.I., Mather, T.A., Hermoso, M., Jenkyns, H.C., Hesselbo, S.P., Al-Suwaidi, A.H., Storm, M.S., Xu, W., Ruhl, M., 2015. Globally enhanced mercury deposition during the end-Pliensbachian extinction and Toarcian OAE: A link to the Karoo-Ferrar Large Igneous Province. Earth Planet. Sci. Lett. 428, 267–280.
Pearce, C.R., Cohen, A.S., Coe, A.L., Burton, K.W., 2008. Molybdenum isotope evidence for global ocean anoxia coupled with perturbations to the carbon cycle during the Early Jurassic. Geology 36 (3), 231–234.
Percival, L.M., Cohen, A.S., Davies, M.K., Dickson, A.J., Hesselbo, S.P., Jenkyns, H.C., Leng, M.J., Mather, T.A., Storm, M.S., Xu, W., 2016. Osmium isotope evidence for two pulses of increased continental weathering linked to Early Jurassic volcanism and climate change. Geology 44 (9), 759–762.
Percival, L.M., Ruhl, M., Hesselbo, S.P., Jenkyns, H.C., Mather, T.A., Whiteside, J.H., 2017. Mercury evidence for pulsed volcanism during the end-Triassic mass extinction. Proceed. Nat. Acad. Sci. (U.S.A.) *114* (30), 7929–7934.
Petersen, H.I., Lindström, S., 2012. Synchronous wildfire activity rise and mire deforestation at the Triassic–Jurassic boundary. PLoS One 7, e47236.
Peti, L., Thibault, N., 2017. Abundance and size changes in the calcareous nannofossil Schizosphaerella–relation to sea-level, the carbonate factory and palaeoenvironmental change from the Sinemurian to earliest Toarcian of the Paris Basin. Palaeogeogr. Palaeoclimatol. Palaeoecol. 485, 271–282.
Petryshyn, V.A., Greene, S.E., Farnsworth, A., Lunt, D.J., Kelley, A., Gammariello, R., Ibarra, Y., Bottjer, D.J., Tripati, A., Corsetti, F.A., 2021. The role of temperature in the initiation of the end-Triassic mass extinction. Earth Sci. Rev. 103266.
Piazza, V., Ullmann, C.V., Aberhan, M., 2020. temperature-related body size change of marine benthic macroinvertebrates across the Early Toarcian anoxic event. Sci. Rep. 10 (1), 1–13.
Pieńkowski, G., Hesselbo, S.P., Barbacka, M., Leng, M.J., 2021. Non-marine carbon-isotope stratigraphy of the Triassic–Jurassic transition in the Polish Basin and its relationships to organic carbon preservation, $pCO_2$ and palaeotemperature. Earth Sci. Rev. 103383.
Pittet, B., Suan, G., Lenoir, F., Duarte, L.V., Mattioli, E., 2014. Carbon isotope evidence for sedimentary discontinuities in the lower Toarcian of the Lusitanian Basin (Portugal): sea level change at the onset of the Oceanic Anoxic Event. Sediment. Geol. 303, 1–14.

Polgári, M., Philippe, M., Szábo-Drubina, M., Tóth, M., 2005. Manganese-impregnated wood from a Toarcian manganese ore deposit, Epleny mine, Bakony Mts., Transdanubia, Hungary. Neues Jahrbuch für Geologie und Paläontologie-Monatshefte 2005 (3), 175–192.
Prauss, M., Riegel, W., 1989. Evidence from phytoplankton associations for causes of black shale formation in epicontinental seas. Neues Jahrbuch für Geologie und Paläontologie-Monatshefte 671–682.
Preto, N., Kustatscher, E., Wignall, P.B., 2010. Triassic climates—state of the art and perspectives. Palaeogeogr. Palaeoclimatol. Palaeoecol. 290 (1-4), 1–10.
Quan, T.M., van de Schootbrugge, B., Field, M.P., Rosenthal, Y., Falkowski, P.G., 2008. Nitrogen isotope and trace metal analyses from the Mingolsheim core (Germany): Evidence for redox variations across the Triassic–Jurassic boundary. Glob. Biogeochem. Cycles 22, 002008.
Raucsik, B., Varga, A., 2008. Climato-environmental controls on clay mineralogy of the Hettangian–Bajocian successions of the Mecsek Mountains, Hungary: an evidence for extreme continental weathering during the early Toarcian oceanic anoxic event. Palaeogeogr. Palaeoclimatol. Palaeoecol. 265 (1–2), 1–13.
Raup, D.M., Sepkoski, J.J., 1982. Mass extinctions in the marine fossil record. Science 215, 1501–1503.
Remírez, M.N., Algeo, T.J., 2021a. Carbon-cycle changes during the Toarcian (Early Jurassic) and implications for regional versus global drivers of the Toarcian oceanic anoxic event. Earth Sci. Rev. 103283.
Remírez, M.N., Algeo, T.J., 2021b. Paleosalinity determination in ancient epicontinental seas: A case study of the T-OAE in the Cleveland Basin (UK). Earth Sci. Rev. 201, 103072.
Remírez, M.N., Algeo, T.J., 2021c. Reply to comment on "Remírez, MN and Algeo, TJ, 2021. Paleosalinity determination in ancient epicontinental seas: A case study of the T-OAE in the Cleveland Basin (UK). Earth-Science Reviews, 201, 103072" by Stephen P. Hesselbo, Crispin TS Little, Micha Ruhl, Nicolas Thibault, and Clemens V. Ullmann. Earth Sci. Rev. 103291.
Reolid, M., Molina, J.M., Nieto, L.M., Rodríguez-Tovar, F.J., 2018. The Toarcian Oceanic Anoxic Event in the South Iberian Palaeomargin. Springer, Dordrecht, 122 pp.
Reolid, M., Copestake, P., Johnson, B., 2019a. Foraminiferal assemblages, extinctions and appearances associated with the Early Toarcian Oceanic Anoxic Event in the Llanbedr (Mochras Farm) Borehole, Cardigan Bay Basin, United Kingdom. Palaeogeogr. Palaeoclimatol. Palaeoecol. 532, 109277.
Reolid, M., Duarte, L.V., Rita, P., 2019b. Changes in foraminiferal assemblages and environmental conditions during the T-OAE (Early Jurassic) in the northern Lusitanian Basin, Portugal. Palaeogeogr. Palaeoclimatol. Palaeoecol. 520, 30–43.
Reolid, M., Iwańczuk, J., Mattioli, E., Abad, I., 2020. Integration of gamma ray spectrometry, magnetic susceptibility and calcareous nannofossils for interpreting environmental perturbations: an example from the Jenkyns Event (lower Toarcian) from South Iberian Palaeomargin (Median Subbetic, SE Spain). Palaeogeogr. Palaeoclimatol. Palaeoecol. 560, 110031.
Retallack, G.J., 2001. A 300-million-year record of atmospheric carbon dioxide from fossil plant cuticles. Nature 411 (6835), 287–290.
Richoz, S., van de Schootbrugge, B., Pross, J., Puttmann, W., Quan, T.M., Lindström, S., Heunisch, C., Fiebig, J., Maquil, R., Schouten, S., Hauzenberger, C.A., Wignall, P.B., 2012. Hydrogen sulphide poisoning of shallow seas following the end-Triassic extinction. Nat. Geosci. 5, 662–667.
Rigo, M., Mazza, M., Karádi, V., Nicora, A., 2018. New Upper Triassic conodont biozonation of the Tethyan realm. In: Tanner, L.H. (Ed.), The Late Triassic World. Springer, Cham, Switzerland, pp. 189–236.
Rigo, M., Onoue, T., Tanner, L., Lucas, S.G., Godfrey, L., Katz, M.E., Zaffani, M., Grice, K., Cesar, J., Yamashita, D., Maron, M., 2020. The Late Triassic Extinction at the Norian/Rhaetian boundary: Biotic evidence and geochemical analysis. Earth Sci. Rev. 103180.
Ritterbush, K.A., Ibarra, Y., Bottjer, D.J., Corsetti, F.A., Rosas, S., West, A.J., Berelson, W. M., Yager, J.A., 2015. Marine ecological state-shifts following the Triassic–Jurassic mass extinction. Paleontol. Soc. Papers 21, 121–136.
Rodrigues, B., Silva, R.L., Reolid, M., Mendonça Filho, J.G., Duarte, L.V., 2019. Sedimentary organic matter and $\delta^{13}C_{Kerogen}$ variation on the southern Iberian palaeomargin (Betic Cordillera, SE Spain) during the latest Pliensbachian-Early Toarcian. Palaeogeogr. Palaeoclimatol. Palaeoecol. 534, 109342.
Rodríguez-Tovar, F.J., Miguez-Salas, O., Duarte, L.V., 2017. Toarcian Oceanic Anoxic Event induced unusual behaviour and palaeobiological changes in *Thalassinoides* tracemakers. Palaeogeogr. Palaeoclimatol. Palaeoecol. 485, 46–56.
Rodríguez-Tovar, F.J., Miguez-Salas, O., Dorador, J., Duarte, L.V., 2019. Opportunistic behaviour after the Toarcian Oceanic Anoxic Event: The trace fossil *Halimedides*. Palaeogeogr. Palaeoclimatol. Palaeoecol. 520, 240–250.
Röhl, H.J., Schmid-Röhl, A., Oschmann, W., Frimmel, A., Schwark, L., 2001. The Posidonia Shale (Lower Toarcian) of SW-Germany: an oxygen-depleted ecosystem controlled by sea level and palaeoclimate. Palaeogeogr. Palaeoclimatol. Palaeoecol. 165 (1–2), 27–52.
Rosales, I., Barnolas, A., Goy, A., Sevillano, A., Armendáriz, M., López-García, J.M., 2018. Isotope records (Co-Sr) of late Pliensbachian-early Toarcian environmental perturbations in the westernmost Tethys (Majorca Island, Spain). Palaeogeogr. Palaeoclimatol. Palaeoecol. 497, 168–185.
Rosales, I., Quesada, S., Robles, S., 2004. Paleotemperature variations of Early Jurassic seawater recorded in geochemical trends of belemnites from the Basque–Cantabrian basin, northern Spain. Palaeogeogr. Palaeoclimatol. Palaeoecol. 203 (3–4), 253–275.
Ros-Franch, S., Echevarría, J., Damborenea, S.E., Manceñido, M.O., Jenkyns, H.C., Al-Suwaidi, A., Hesselbo, S.P., Riccardi, A.C., 2019. Population response during an Oceanic Anoxic Event: The case of *Posidonotis* (Bivalvia) from the lower Jurassic of the Neuquén Basin, Argentina. Palaeogeogr. Palaeoclimatol. Palaeoecol. 525, 57–67.
Ruebsam, W., Müller, T., Kovács, J., Pálfy, J., Schwark, L., 2018. Environmental response to the early Toarcian carbon cycle and climate perturbations in the northeastern part of the West Tethys shelf. Gondwana Res. 59, 144–158.
Ruebsam, W., Mayer, B., Schwark, L., 2019. Cryosphere carbon dynamics control early Toarcian global warming and sea level evolution. Glob. Planet. Chang. 172, 440–453.
Ruebsam, W., Reolid, M., Sabatino, N., Masetti, D., Schwark, L., 2020. Molecular paleothermometry of the early Toarcian climate perturbation. Glob. Planet. Chang. 195, 103351.
Ruebsam, W., Münzberger, P., Schwark, L., 2014. Chronology of the early Toarcian environmental crisis in the Lorraine Sub-Basin (NE Paris Basin). Earth Planet. Sci. Lett. 404, 273–282.
Ruebsam, W., Reolid, M., Marok, A., Schwark, L., 2021. Drivers of benthic extinction during the early Toarcian (Early Jurassic) at the northern Gondwana paleomargin: Implications for paleoceanographic conditions. Earth Sci. Rev. 203, 103117.
Ruhl, M., Kürschner, W.M., 2011. Multiple phases of carbon cycle disturbance from large igneous province formation at the Triassic–Jurassic transition. Geology 39 (5), 431–434.
Ruhl, M., Kürschner, W.M., Krystyn, L., 2009. Triassic–Jurassic organic carbon isotope stratigraphy of key sections in the western Tethys realm (Austria). Earth Planet. Sci. Lett. 281 (3-4), 169–187.
Ruhl, M., Bonis, N.R., Reichart, G.-J., Sinninghe Damsté, J.S., Kürschner, W.M., 2011. Atmospheric carbon injection linked to End-Triassic mass extinction. Science 333, 430–434.
Ruhl, M., Hesselbo, S.P., Hinnov, L., Jenkyns, H.C., Xu, W., Riding, J.B., Storm, M.S., Minisini, D., Ullmann, C.V., Leng, M.J., 2016. Astronomical constraints on the duration of the Early Jurassic Pliensbachian Stage and global climatic fluctuations. Earth Planet. Sci. Lett. 455, 149–165.
Ruhl, M., Hesselbo, S.P., Al-Suwaidi, A., Jenkyns, H.C., Damborenea, S.E., Manceñido, M.O., Storm, M.S., Mather, T.A., Riccardi, A.C., 2021. On the onset of Central Atlantic Magmatic Province (CAMP) volcanism and environmental and carbon-cycle change at the Triassic–Jurassic transition (Neuquén Basin, Argentina). Earth Sci. Rev. 103229.
Ruvalcaba Baroni, I., Pohl, A., van Helmond, N.A., Papadomanolaki, N.M., Coe, A.L., Cohen, A.S., van de Schootbrugge, B., Donnadieu, Y., Slomp, C.P., 2018. Ocean circulation in the Toarcian (Early Jurassic): A key control on deoxygenation and carbon burial on the European shelf. Paleoceanogr. Paleoclimatol. 33 (9), 994–1012.
Salvador, A., 1987. Late Triassic–Jurassic paleogeography and origin of Gulf of Mexico basin. AAPG Bull. 71 (4), 419–451.
Schaller, M.F., Wright, J.D., Kent, D.V., 2011. Atmospheric $pCO_2$ perturbations associated with the Central Atlantic Magmatic Province. Science 331, 1404–1409.
Schaller, M.F., Wright, J.D., Kent, D.V., Olsen, P.E., 2012. Rapid emplacement of the Central Atlantic Magmatic Province as a net sink for $CO_2$. Earth Planet. Sci. Lett. 323-324, 27–39.
Schaller, M.F., Wright, J.D., Kent, D.V., 2015. A 30 myr record of Late Triassic atmospheric $pCO_2$ variation reflects a fundamental control of the carbon cycle by changes in continental weathering. GSA Bull. 127, 661–671.
Schmid-Röhl, A., Röhl, H.J., Oschmann, W., Frimmel, A., Schwark, L., 2002. Palaeoenvironmental reconstruction of Lower Toarcian epicontinental black shales (Posidonia Shale, SW Germany): global versus regional control. Geobios 35 (1), 13–20.
Schobben, M., Gravendyck, J., Mangels, F., Struck, U., Bussert, R., Kürschner, W.M., Korn, D., Sander, P.M., Aberhan, M., 2019. A comparative study of total organic carbon-$\delta^{13}C$ signatures in the Triassic–Jurassic transitional beds of the Central European Basin and western Tethys shelf seas. Newsl. Stratigr. 52 (4), 461–486.
Schoepfer, S.D., Algeo, T.J., Ward, P.D., Williford, K.H., Haggart, J.W., 2016. Testing the limits in a greenhouse ocean: Did low nitrogen availability limit marine productivity during the end-Triassic mass extinction? Earth Planet. Sci. Lett. 451, 138–148.
Schoepfer, S.D., Shen, J., Sano, H., Algeo, T.J., 2022. Onset of environmental disturbances in the Panthalassic Ocean over one million years prior to the Triassic-Jurassic boundary mass extinction. Earth Sci. Rev. 224, 103870.
Schöllhorn, I., Adatte, T., van de Schootbrugge, B., Houben, A., Charbonnier, G., Janssen, N., Föllmi, K.B., 2020. Climate and environmental response to the break-up of Pangea during the Early Jurassic (Hettangian-Pliensbachian); the Dorset coast (UK) revisited. Glob. Planet. Chang. 185, 103096.
Schouten, S., van Kaam-Peters, H.M., Rijpstra, W.I.C., Schoell, M., Damste, J.S.S., 2000. Effects of an oceanic anoxic event on the stable carbon isotopic composition of early Toarcian carbon. Ame. J. Sci. 300 (1), 1–22.
Sciscio, L., de Kock, M., Bordy, E., Knoll, F., 2017. Magnetostratigraphy across the Triassic–Jurassic boundary in the main Karoo Basin. Gondwana Res. 51, 177–192.
Sell, B., Ovtcharova, M., Guex, J., Bartolini, A., Jourdan, F., Spangenberg, J.E., Vicente, J.-C., Schaltegger, U., 2014. Evaluating the temporal link between the Karoo LIP and climatic–biologic events of the Toarcian Stage with high-precision U–Pb geochronology. Earth Planet. Sci. Lett. 408, 48–56.
Sepkoski, J.J., 1981. A factor analytic description of the Phanerozoic marine fossil record. Paleobiology 7 (1), 36–53.
Seton, M., Müller, R.D., Zahirovic, S., Gaina, C., Torsvik, T., Shephard, G., Talsma, A., Gurnis, M., Turner, M., Maus, S., Chandler, M., 2012. Global continental and oceanic basin reconstructions since 200 Ma. Earth Sci. Rev. 113, 212–270.
Shen, J., Algeo, T.J., Chen, J., Planavsky, N.J., Feng, Q., Yu, J., Liu, J., 2019. Mercury in marine Ordovician/Silurian boundary sections of South China is sulfide-hosted and non-volcanic in origin. Earth Planet. Sci. Lett. 511, 130–140.
Shen, J., Feng, Q., Algeo, T.J., Liu, J., Zhou, C., Wei, W., Liu, J., Them II, T.R., Gill, B.C., Chen, J., 2020. Sedimentary host phases of mercury (Hg) and implications for use of Hg as a volcanic proxy. Earth Planet. Sci. Lett. 543, 116333.

Silva, R.L., Duarte, L.V., 2015. Organic matter production and preservation in the Lusitanian Basin (Portugal) and Pliensbachian climatic hot snaps. Glob. Planet. Chang. 131, 24–34.
Silva, R.L., Ruhl, M., Barry, C., Reolid, M., Ruebsam, W., 2021. Pacing of late Pliensbachian and early Toarcian carbon cycle perturbations and environmental change in the westernmost Tethys (La Cerradura Section, Subbetic zone of the Betic Cordillera, Spain). Geol. Soc. Lond. Spec. Publ. 514 (1), 387–408.
Simms, M.J., 2003. Uniquely extensive seismite from the latest Triassic of the United Kingdom: Evidence for bolide impact? Geology 31 (6), 557–560.
Slater, S.M., Twitchett, R.J., Danise, S., Vajda, V., 2019. Substantial vegetation response to Early Jurassic global warming with impacts on oceanic anoxia. Nat. Geosci. 12 (6), 462–467.
Slodownik, M., Vajda, V., Steinthorsdottir, M., 2021. Fossil seed fern Lepidopteris ottonis from Sweden records increasing CO2 concentration during the end-Triassic extinction event. Palaeogeogr. Palaeoclimatol. Palaeoecol. 564, 110157.
Soh, W.K., Wright, I.J., Bacon, K.L., Lenz, T.I., Steinthorsdottir, M., Parnell, A.C., McElwain, J.C., 2017. Palaeo leaf economics reveal a shift in ecosystem function associated with the end-Triassic mass extinction event. Nat. Plants 3 (8), 1–8.
Song, Y., Algeo, T.J., Wu, W., Luo, G., Li, L., Wang, Y., Xie, S., 2021. Distribution of pyrolytic PAHs across the Triassic–Jurassic boundary in the Sichuan Basin, southwestern China: Evidence of wildfire outside the Central Atlantic Magmatic Province. Earth Sci. Rev. 201, 102970.
Song, J., Littke, R., Weniger, P., 2017. Organic geochemistry of the lower Toarcian Posidonia Shale in NW Europe. Org. Geochem. 106, 76–92.
Stanley, G.D., Shepherd, H.M., Robinson, A.J., 2018. Paleoecological response of corals to the end-Triassic mass extinction: an integrational analysis. J. Earth Sci. 29 (4), 879–885.
Steinthorsdottir, M., Jeram, A.J., McElwain, J.C., 2011. Extremely elevated $CO_2$ concentrations at the Triassic/Jurassic boundary. Palaeogeogr. Palaeoclimatol. Palaeoecol. 308 (3-4), 418–432.
Steinthorsdottir, M., Woodward, F.I., Surlyk, F., McElwain, J.C., 2012. Deep-time evidence of a link between elevated CO2 concentrations and perturbations in the hydrological cycle via drop in plant transpiration. Geology 40 (9), 815–818.
Steinthorsdottir, M., Elliott-Kingston, C., Bacon, K.L., 2018. Cuticle surfaces of fossil plants as a potential proxy for volcanic $SO_2$ emissions: observations from the Triassic–Jurassic transition of East Greenland. Palaeobiodiver. Palaeoenviron. 98 (1), 49–69.
Storm, M.S., Hesselbo, S.P., Jenkyns, H.C., Ruhl, M., Ullmann, C.V., Xu, W., Leng, M.J., Riding, J.B., Gorbanenko, O., 2020. Orbital pacing and secular evolution of the Early Jurassic carbon cycle. Proceed. Nat. Acad. Sci. (U.S.A.) *117* (8), 3974–3982.
Suan, G., Mattioli, E., Pittet, B., Mailliot, S., Lecuyer, C., 2008a. Evidence for major environmental perturbation prior to and during the Toarcian (Early Jurassic) oceanic anoxic event from the Lusitanian Basin, Portugal. Paleoceanography 23, PA1202.
Suan, G., Pittet, B., Bour, I., Mattioli, E., Duarte, L.V., Mailliot, S., 2008b. Duration of the Early Toarcian carbon isotope excursion deduced from spectral analysis: consequence for its possible causes. Earth Planet. Sci. Lett. 267 (3-4), 666–679.
Suan, G., Mattioli, E., Pittet, B., Lecuyer, C., Sucheras-Marx, B., Duarte, L.V., Philippe, M., Reggiani, L., Martineau, F., 2010. Secular environmental precursors to Early Toarcian (Jurassic) extreme climate changes. Earth Planet. Sci. Lett. 290, 448–458.
Suan, G., Van De Schootbrugge, B., Adatte, T., Fiebig, J., Oschmann, W., 2015. Calibrating the magnitude of the Toarcian carbon cycle perturbation. Paleoceanography 30 (5), 495–509.
Suan, G., Schöllhorn, I., Schlögl, J., Segit, T., Mattioli, E., Lécuyer, C., Fourel, F., 2018. Euxinic conditions and high sulfur burial near the European shelf margin (Pieniny Klippen Belt, Slovakia) during the Toarcian oceanic anoxic event. Glob. Planet. Chang. 170, 246–259.
Svensen, H., Planke, S., Chevallier, L., Malthe-Sørenssen, A., Corfu, F., Jamtveit, B., 2007. Hydrothermal venting of greenhouse gases triggering Early Jurassic global warming. Earth Planet. Sci. Lett. 256 (3-4), 554–566.
Svensen, H., Corfu, F., Polteau, S., Hammer, Ø., Planke, S., 2012. Rapid magma emplacement in the Karoo large igneous province. Earth Planet. Sci. Lett. 325, 1–9.
Tanner, L.H., 2018. Climates of the Late Triassic: Perspectives, proxies and problems. In: Tanner, L.H. (Ed.), The Late Triassic World. Springer, Cham, Switzerland, pp. 59–90.
Tanner, L.H., Hubert, J.F., Coffey, B.P., McInerney, D.P., 2001. Stability of atmospheric $CO_2$ levels across the Triassic/Jurassic boundary. Nature 411 (6838), 675–677.
Tanner, L.H., Lucas, S.G., Chapman, M.G., 2004. Assessing the record and causes of Late Triassic extinctions. Earth Sci. Rev. 65 (1-2), 103–139.
Tanner, L.H., Kyte, F.T., Walker, A.E., 2008. Multiple Ir anomalies in uppermost Triassic to Jurassic-age strata of the Blomidon Formation: Fundy basin, eastern Canada. Earth Planet. Sci. Lett. 274, 103–111.
Tanner, L.H., Kyte, F.T., Richoz, S., Krystyn, L., 2016. Distribution of iridium and associated geochemistry across the Triassic–Jurassic boundary in sections at Kuhjoch and Kendlbach, Northern Calcareous Alps, Austria. Palaeogeogr. Palaeoclimatol. Palaeoecol. 449, 13–26.
Tanner, L.H., Kyte, F.T., Puffer, J.H., 2020. Widespread elevated iridium in Upper Triassic-Lower Jurassic strata of the Newark Supergroup: implications for use as an extinction marker. Sci. Rep. 10 (1), 1–10.
Tegner, C., Marzoli, A., McDonald, I., Youbi, N., Lindström, S., 2020. Platinum-group elements link the end-Triassic mass extinction and the Central Atlantic Magmatic Province. Sci. Rep. 10, 3482.
Them, T.R., Gill, B.C., Caruthers, A.H., Gerhardt, A.M., Gröcke, D.R., Lyons, T.W., Marroquín, S.M., Nielsen, S.G., Alexandre, J.P.T., Owens, J.D., 2018. Thallium isotopes reveal protracted anoxia during the Toarcian (Early Jurassic) associated with volcanism, carbon burial, and mass extinction. Proceed. Nat. Acad. Sci. (U.S.A.) 115 (26), 6596–6601.
Them, T.R., Gill, B.C., Caruthers, A.H., Gröcke, D.R., Tulsky, E.T., Martindale, R.C., Poulton, T.P., Smith, P.L., 2017a. High-resolution carbon isotope records of the Toarcian Oceanic Anoxic Event (Early Jurassic) from North America and implications for the global drivers of the Toarcian carbon cycle. Earth Planet. Sci. Lett. 459, 118–126.
Them, T.R., Gill, B.C., Selby, D., Gröcke, D.R., Friedman, R.M., Owens, J.D., 2017b. Evidence for rapid weathering response to climatic warming during the Toarcian Oceanic Anoxic Event. Sci. Rep. 7 (1), 1–10.
Them, T.R., Jagoe, C.H., Caruthers, A.H., Gill, B.C., Grasby, S.E., Gröcke, D.R., Yin, R., Owens, J.D., 2019. Terrestrial sources as the primary delivery mechanism of mercury to the oceans across the Toarcian Oceanic Anoxic Event (Early Jurassic). Earth Planet. Sci. Lett. 507, 62–72.
Thibault, N., Ruhl, M., Ullmann, C.V., Korte, C., Kemp, D.B., Gröcke, D.R., Hesselbo, S.P., 2018. The wider context of the Lower Jurassic Toarcian oceanic anoxic event in Yorkshire coastal outcrops. UK. Proceed. Geol. Associat. 129 (3), 372–391.
Thibodeau, A.M., Ritterbush, K., Yager, J.A., West, A.J., Ibarra, Y., Bottjer, D.J., Berelson, W.M., Bergquist, B.A., Corsetti, F.A., 2016. Mercury anomalies and the timing of biotic recovery following the end-Triassic mass extinction. Nat. Commun. 7 (1), 1–8.
Thorne, P.M., Ruta, M., Benton, M.J., 2011. Resetting the evolution of marine reptiles at the Triassic–Jurassic boundary. Proceed. Nat. Acad. Sci. (U.S.A.) *108* (20), 8339–8344.
Todaro, S., Rigo, M., Randazzo, V., Di Stefano, P., 2018. The end-Triassic mass extinction: A new correlation between extinction events and $\delta^{13}C$ fluctuations from a Triassic–Jurassic peritidal succession in western Sicily. Sediment. Geol. 368, 105–113.
Trecalli, A., Spangenberg, J., Adatte, T., Föllmi, K.B., Parente, M., 2012. Carbonate platform evidence of ocean acidification at the onset of the early Toarcian oceanic anoxic event. Earth Planet. Sci. Lett. 357-358, 214–225.
Ullmann, C.V., Boyle, R., Duarte, L.V., Hesselbo, S.P., Kasemann, S.A., Klein, T., Lenton, T.M., Piazza, V., Aberhan, M., 2020. Warm afterglow from the Toarcian Oceanic Anoxic Event drives the success of deep-adapted brachiopods. Sci. Rep. 10 (1), 1–11.
van Acken, D., Tütken, T., Daly, J.S., Schmid-Röhl, A., Orr, P.J., 2019. Rhenium-osmium geochronology of the Toarcian Posidonia Shale, SW Germany. Palaeogeogr. Palaeoclimatol. Palaeoecol. 534, 109294.
van de Schootbrugge, B., Bailey, T.R., Rosenthal, Y., Katz, M.E., Wright, J.D., Miller, K.G., Feist-Burkhardt, S., Falkowski, P.G., 2005a. Early Jurassic climate change and the radiation of organic-walled phytoplankton in the Tethys Ocean. Paleobiology 31 (1), 73–97.
van de Schootbrugge, B., McArthur, J.M., Bailey, T.R., Rosenthal, Y., Wright, J.D., Miller, K.G., 2005b. Toarcian oceanic anoxic event: An assessment of global causes using belemnite C isotope records. Paleoceanography 20 (3).
van de Schootbrugge, B., Tremolada, F., Rosenthal, Y., Bailey, T.R., Feist-Burkhardt, S., Brinkhuis, H., Pross, J., Kent, D.V., Falkowski, P.G., 2007. End-Triassic calcification crisis and blooms of organic-walled 'disaster species'. Palaeogeogr. Palaeoclimatol. Palaeoecol. 244 (1-4), 126–141.
van de Schootbrugge, B., Payne, J.L., Tomasovych, A., Pross, J., Fiebig, J., Benbrahim, M., Föllmi, K.B., Quan, T.M., 2008. Carbon cycle perturbation and stabilization in the wake of the Triassic-Jurassic boundary mass-extinction event. Geochem. Geophys. Geosyst. 9 (4), 2007GC001914.
van de Schootbrugge, B., Quan, T.M., Lindström, S., Püttmann, W., Heunisch, C., Pross, J., Fiebig, J., Petschick, R., Röhling, H.G., Richoz, S., Rosenthal, Y., 2009. Floral changes across the Triassic/Jurassic boundary linked to flood basalt volcanism. Nat. Geosci. 2 (8), 589–594.
van de Schootbrugge, B., Bachan, A., Suan, G., Richoz, S., Payne, J.L., 2013. Microbes, mud and methane: cause and consequence of recurrent Early Jurassic anoxia following the end-Triassic mass extinction. Palaeontology 56 (4), 685–709.
van de Schootbrugge, B., Richoz, S., Pross, J., Luppold, F.W., Hunze, S., Wonik, T., Blau, J., Meister, C., Van der Weijst, C.M.H., Suan, G., Fraguas, A., 2019. The Schandelah Scientific Drilling Project: A 25-million year record of Early Jurassic palaeo-environmental change from northern Germany. Newsl. Stratigr. 52 (3), 249–296.
van de Schootbrugge, B., Houben, A.J.P., Ercan, F.E.Z., Verreussel, R., Kerstholt, S., Janssen, N.M.M., Nikitenko, B., Suan, G., 2020a. Enhanced Arctic-Tethys connectivity ended the Toarcian oceanic anoxic event in NW Europe. Geol. Mag. 157 (10), 1593–1611.
van de Schootbrugge, B., Mangerud, G., Galloway, J.M., Lindström, S., 2020b. The Mesozoic Arctic: warm, green, and highly diverse. Geol. Mag. 157 (10), 1543–1546.
van de Schootbrugge, B., van der Weijst, C.M.H., Hollaar, T.P., Vecoli, M., Strother, P.K., Kuhlmann, N., Thein, J., Visscher, H., van Konijnenburg-van Cittert, H., Schobben, M.A.N., Sluijs, A., 2021. Catastrophic soil loss associated with end-Triassic deforestation. Earth Sci. Rev. 103332.
van Eldijk, T.J., Wappler, T., Strother, P.K., van der Weijst, C.M., Rajaei, H., Visscher, H., van de Schootbrugge, B., 2018. A Triassic–Jurassic window into the evolution of Lepidoptera. Sci. Adv. 4 (1), e1701568.
Vasseur, R., Lathuilière, B., Lazăr, I., Martindale, R.C., Bodin, S., Durlet, C., 2021. Major coral extinctions during the early Toarcian global warming event. Glob. Planet. Chang. 207, 103647.
Verati, C., Rapaille, C., Féraud, G., Marzoli, A., Bertrand, H., Youbi, N., 2007. $^{40}Ar/^{39}Ar$ ages and duration of the Central Atlantic Magmatic Province volcanism in Morocco and Portugal and its relation to the Triassic–Jurassic boundary. Palaeogeogr. Palaeoclimatol. Palaeoecol. 244 (1-4), 308–325.
Vermeij, G.J., 1977. The Mesozoic marine revolution: evidence from snails, predators and grazers. Paleobiology 3, 245–258.

Vető, I., Demény, A., Hertelendi, E., Hetényi, M., 1997. Estimation of primary productivity in the Toarcian Tethys—a novel approach based on TOC, reduced sulphur and manganese contents. Palaeogeogr. Palaeoclimatol. Palaeoecol. 132 (1-4), 355–371.
von Hillebrandt, A., Kment, K., 2015. Psiloceratid ammonites from the Lower Hettangian of the Karwendel Mountains (Northern Calcareous Alps, Austria) and their biostratigraphic significance. Neues Jahrbuch für Geologie und Paläontologie-Abhandlungen 275–306.
von Hillebrandt, A., Krystyn, L., 2009. On the oldest Jurassic ammonites of Europe (Northern Calcareous Alps, Austria) and their global significance. N. Jb. Geol. Paläont. 253 (2-3), 163–195.
von Hillebrandt, A.V., Krystyn, L., Kürschner, W.M., 2007. A candidate GSSP for the base of the Jurassic in the Northern Calcareous Alps (Kuhjoch section, Karwendel Mountains, Tyrol, Austria). Int. Subcommission Jurassic Stratigr. Newsletter 34 (1), 2–20.
von Hillebrandt, A., Krystyn, L., Kürschner, W.M., Bonis, N.R., Ruhl, M., Richoz, S., Schobben, M.A.N., Urlichs, M., Bown, P.R., Kment, K., McRoberts, C.A., Simms, M., Tomasových, A., 2013. The Global Stratotype Sections and Point (GSSP) for the base of the Jurassic System at Kuhjoch (Karwendel Mountains, Northern Calcareous Alps, Tyrol, Austria). Episodes 36, 162–198.
Vörös, A., 2002. Victims of the Early Toarcian anoxic event: the radiation and extinction of Jurassic Koninckinidae (Brachiopoda). Lethaia 35 (4), 345–357.
Vörös, A., Kocsis, Á.T., Pálfy, J., 2016. Demise of the last two spire-bearing brachiopod orders (Spiriferinida and Athyridida) at the Toarcian (Early Jurassic) extinction event. Palaeogeogr. Palaeoclimatol. Palaeoecol. 457, 233–241.
Walkden, G., Parker, J., Kelley, S., 2002. A Late Triassic impact ejecta layer in southwestern Britain. Science 298 (5601), 2185–2188.
Ward, P.D., Haggart, J.W., Carter, E.S., Wilbur, D., Tipper, H.W., Evans, T., 2001. Sudden productivity collapse associated with the Triassic–Jurassic boundary mass extinction. Science 292 (5519), 1148–1151.
Ward, P.D., Garrison, G.H., Haggart, J.W., Kring, D.A., Beattie, M.J., 2004. Isotopic evidence bearing on Late Triassic extinction events, Queen Charlotte Islands, British Columbia, and implications for the duration and cause of the Triassic/Jurassic mass extinction. Earth Planet. Sci. Lett. 224 (3-4), 589–600.
Ward, P.D., Garrison, G.H., Williford, K.H., Kring, D.A., Goodwin, D., Beattie, M.J., McRoberts, C.A., 2007. The organic carbon isotopic and paleontological record across the Triassic–Jurassic boundary at the candidate GSSP section at Ferguson Hill, Muller Canyon, Nevada, USA. Palaeogeogr. Palaeoclimatol. Palaeoecol. 244 (1-4), 281–289.
Wei, W., Algeo, T.J., 2020. Elemental proxies for paleosalinity analysis of ancient shales and mudrocks. Geochim. Cosmochim. Acta 287, 341–366.
Whiteside, J.H., Ward, P.D., 2011. Ammonoid diversity and disparity track episodes of chaotic carbon cycling during the early Mesozoic. Geology 39 (2), 99–102.
Whiteside, J.H., Olsen, P.E., Kent, D.V., Fowell, S.J., Et-Touhami, M., 2007. Synchrony between the Central Atlantic magmatic province and the Triassic–Jurassic mass-extinction event? Palaeogeogr. Palaeoclimatol. Palaeoecol. 244 (1-4), 345–367.
Whiteside, J.H., Olsen, P.E., Eglinton, T., Brookfield, M.E., Sambrotto, R.N., 2010. Compound-specific carbon isotopes from Earth's largest flood basalt eruptions directly linked to the end-Triassic mass extinction. Proceed. Nat. Acad. Sci. (U.S.A.) *107* (15), 6721–6725.
Whiteside, J.H., Grogan, D.S., Olsen, P.E., Kent, D.V., 2011. Climatically driven biogeographic provinces of Late Triassic tropical Pangea. Proceed. Nat. Acad. Sci. (U.S.A.) *108* (22), 8972–8977.
Whiteside, J.H., Lindström, S., Irmis, R.B., Glasspool, I.J., Schaller, M.F., Dunlavey, M., Nesbitt, S.J., Smith, N.D., Turner, A.H., 2015. Extreme ecosystem instability suppressed tropical dinosaur dominance for 30 million years. Proc. Natl. Acad. Sci. 112 (26), 7909–7913.
Whiteside, J.H., Olsen, P.E., Et-Touhami, M., 2020. Platinum group element traces of CAMP volcanism associated with low latitude environmental and biological disruptions. In: Ernst, R.E., Dickson, A.J., Bekker, A. (Eds.), Large Igneous Provinces: A Driver of Global Environmental and Biotic Changes, AGU Geophysical Monograph, 255, pp. 263–304.
Wignall, P.B., 2015. The Worst of Times: How Life on Earth Survived Eighty Million Years of Extinctions. Princeton University Press, Princeton, New Jersey, p. 224.
Wignall, P.B., Atkinson, J.W., 2020. A two-phased end-Triassic mass extinction. Earth Sci. Rev. 208, 103282.
Wignall, P.B., Newton, R.J., Little, C.T., 2005. The timing of paleoenvironmental change and cause-and-effect relationships during the Early Jurassic mass extinction in Europe. Am. J. Sci. 305 (10), 1014–1032.
Williford, K.H., Ward, P.D., Garrison, G.H., Buick, R., 2007. An extended organic carbon-isotope record across the Triassic–Jurassic boundary in the Queen Charlotte Islands, British Columbia, Canada. Palaeogeogr. Palaeoclimatol. Palaeoecol. 244 (1-4), 290–296.
Williford, K.H., Grice, K., Holman, A., McElwain, J.C., 2014. An organic record of terrestrial ecosystem collapse and recovery at the Triassic–Jurassic boundary in East Greenland. Geochim. Cosmochim. Acta 127, 251–263.
Wotzlaw, J.F., Guex, J., Bartolini, A., Gallet, Y., Krystyn, L., McRoberts, C.A., Taylor, D., Schoene, B., Schaltegger, U., 2014. Towards accurate numerical calibration of the Late Triassic: High-precision U-Pb geochronology constraints on the duration of the Rhaetian. Geology 42 (7), 571–574.
Xu, W., Ruhl, M., Jenkyns, H.C., Hesselbo, S.P., Riding, J.B., Selby, D., Naafs, B.D.A., Weijers, J.W., Pancost, R.D., Tegelaar, E.W., Idiz, E.F., 2017. Carbon sequestration in an expanded lake system during the Toarcian oceanic anoxic event. Nat. Geosci. 10 (2), 129–134.
Xu, W., Mac Niocaill, C., Ruhl, M., Jenkyns, H.C., Riding, J.B., Hesselbo, S.P., 2018. Magnetostratigraphy of the Toarcian Stage (Lower Jurassic) of the Llanbedr (Mochras Farm) Borehole, Wales: basis for a global standard and implications for volcanic forcing of palaeoenvironmental change. J. Geol. Soc. Lond. 175 (4), 594–604.
Xu, W., Weijers, J.W., Ruhl, M., Idiz, E.F., Jenkyns, H.C., Riding, J.B., Gorbanenko, O., Hesselbo, S.P., 2021. Molecular and petrographical evidence for lacustrine environmental and biotic change in the palaeo-Sichuan mega-lake (China) during the Toarcian Oceanic Anoxic Event. Geol. Soc. Lond., Spec. Publ. 514 (1), 335–357.
Yager, J.A., West, A.J., Corsetti, F.A., Berelson, W.M., Rollins, N.E., Rosas, S., Bottjer, D. J., 2017. Duration of and decoupling between carbon isotope excursions during the end-Triassic mass extinction and Central Atlantic Magmatic Province emplacement. Earth Planet. Sci. Lett. 473, 227–236.
Yager, J.A., West, A.J., Thibodeau, A.M., Corsetti, F.A., Rigo, M., Berelson, W.M., Bottjer, D.J., Greene, S.E., Ibarra, Y., Jadoul, F., Ritterbush, K.A., Rollins, N.E., Rosas, S., Di Stefano, P., Sulca, D., Todaro, S., Wynn, P., Zimmerman, L., Bergquist, B., 2021. Mercury contents and isotope ratios from diverse depositional environments across the Triassic–Jurassic Boundary: Towards a more robust mercury proxy for large igneous province magmatism. Earth-Sci. Rev. 223, 103775.
Yiotis, C., Evans-FitzGerald, C., McElwain, J.C., 2017. Differences in the photosynthetic plasticity of ferns and *Ginkgo* grown in experimentally controlled low $[O_2]$:$[CO_2]$ atmospheres may explain their contrasting ecological fate across the Triassic–Jurassic mass extinction boundary. Ann. Bot. 119 (8), 1385–1395.
Zaffani, M., Jadoul, F., Rigo, M., 2018. A new Rhaetian $\delta^{13}C_{org}$ record: carbon cycle disturbances, volcanism, End-Triassic mass Extinction (ETE). Earth Sci. Rev. 178, 92–104.
Zhang, W., Grant-Mackie, J.A., 2001. Late Triassic-Early Jurassic palynofloral assemblages from Murihiku strata of New Zealand, and comparisons with China. J. R. Soc. N. Z. 31 (3), 575–683.
Zhang, J., Lenz, O.K., Hornung, J., Wang, P., Ebert, M., Hinderer, M., 2020. Palynology and the Eco-Plant model of peat-forming wetlands of the Upper Triassic Haojiagou Formation in the Junggar Basin, Xinjiang, NW China. Palaeogeogr. Palaeoclimatol. Palaeoecol. 556, 109888.

Shane D. Schoepfer[a,*], Thomas J. Algeo[b,c,d,**], Bas van de Schootbrugge[e], Jessica H. Whiteside[f]

[a] *Department of Geoscience and Natural Resources, Western Carolina University, Cullowhee, NC 28723, USA*

[b] *Department of Geology, University of Cincinnati, Cincinnati, OH 45221-0013, USA*

[c] *State Key Laboratory of Geological Processes and Mineral Resources, China University of Geosciences, Wuhan, Hubei, 430074, PR China*

[d] *State Key Laboratory of Biogeology and Environmental Geology, China University of Geosciences, Wuhan, Hubei, 430074, PR China*

[e] *Department of Earth Science, Utrecht University, Utrecht, The Netherlands*

[f] *School of Ocean and Earth Science, University of Southampton, National Oceanography Centre Southampton, Southampton SO14 3ZH, UK*

[*] Corresponding author.

[**] Corresponding author at: Department of Geology, University of Cincinnati, Cincinnati, OH 45221-0013, USA.

*E-mail addresses:* sschoepfer@email.wcu.edu (S.D. Schoepfer), Thomas.Algeo@uc.edu (T.J. Algeo), B.vanderSchootbrugge@uu.nl (B. van de Schootbrugge), J.Whiteside@soton.ac.uk (J.H. Whiteside).